Corrole Sensitized Solar Cells

Thesis by

Don Walker

In Partial Fulfillment of the Requirements for the

degree of

Doctor of Philosophy

California Institute of Technology

Pasadena, California

2011

(Defended September 13th, 2010)

Acknowledgements

In the beginning God created the heaven and the earth…….oh wait that was too early ☺. Where do I begin these acknowledgements? Who should I acknowledge? It's 1:57 a.m., I'm in a noffice with no room number, listening to Kanye West, and my mind is wrecked from writing this thesis. The truth is although I'm beaten and tired; the questions of "where do I begin these acknowledgements and who I should thank" are by far the easiest questions for me to answer. As far as where to begin, my journey to become a scientist began when I first met Dr. Edwin Walker. I was a sophomore at Southern University and A & M College in Baton Rouge, Louisiana. I had just got out of my organic chemistry class and was waiting in the chemistry library to tutor freshmen in general chemistry. As I waited, I began studying my organic chemistry notes and in walks this young guy who says "Whatcha doing?" I responded that I was waiting to tutor people. Then this professor says "Come here, I got something for you to do." So I got up and followed him to his lab where he told me to run a reaction. Being someone up for any challenge, I accepted. It was the first time I had run a reaction while not in a class setting. I found it challenging and rewarding. That was the start of my research career. From that point Dr. Walker proceeded to teach me the ins and outs of what it means to be a scientist. Dr. Walker truly inspired me to become a scientist. His mentorship gave me the knowledge and, more importantly, the confidence to pursue my doctorate degree. It was Dr. Walker who told me should go to grad school.   He had me apply to undergraduate research opportunities with the specific goal of working like a graduate student. He told me to apply to the best schools and work as hard as I possibly could. I applied and received an opportunity to work under Harry B. Gray and Elizabeth Libby

Mayo. Libby took the time to teach this young guy from a small town how to do research at Caltech. I never felt judged by Libby for being a guy who wasn't from one the big Ivy league or Tech schools. I always felt like she was confident in my ability. She made feel comfortable in the lab.   She always encouraged me and acknowledged my accomplishments.

My summer at Caltech inspired me to pursue a doctorate at Caltech. I must admit my tenure at Caltech has been extremely tough for me. I have had many ups and downs. The highs were HIGH, but the lows…..oh the lows. I had many lows. During the tough times there were a few people I could always turn to. First I would like to thank my brother in science, Anthony Gary Fitch. We came to Caltech the same year and we both joined the same groups. I remember in the beginning this guy thought I knew a lot about the lab because I spent a summer there. Boy was he wrong. Tony and I spent almost everyday talking science. Most of our conversations consisted of one of us asking "Do you know what this means," and one of us responding "I think #!@#%#$!$#^!#$^……ummm I don't know." Because both of us had an insatiable thirst for knowledge, we both would look up as much information we could and discuss what we learned. These scientific discussions eventually turned into conversations about sports and politics. I can honestly say I have learned a lot about life and science from Tony. Tony is one of the most responsible, dedicated, and intelligent people I have ever met. His friendship, both scientific and personal, has shaped me as a person and scientist. I can honestly say, if Tony was not here with me during my journey at Caltech, I don't know what I would have done. I would not be half the person or scientist I am today.

Next I would like to specifically thank Brian S. Leigh. He was the first person that I felt really welcomed me to Caltech. Brian has been an extremely dedicated friend and colleague. Although our projects never overlapped, he worked on a project similar to mine while pursuing his master's degree. Brian had a knack for explaining things to me in a way that was easy for me to understand. I cannot thank him enough for taking the time to explain things to me. I also learned a lot from Brian that I dare not put in this thesis, but I want Brian to know that I am extremely thankful for his friendship and scientific advice. I can publicly thank you for one thing and that is introducing me to Team Justice!

I would also like the thank Jay Winkler and Bruce Brunschwig for all their encouragement and guidance. Both Jay and Bruce's doors were always open. I must admit that when I first met Jay I was extremely intimidated. Lets be honest, Jay's a big guy and he doesn't smile. Throughout my graduate career I learned a lot from Jay. I never felt like he doubted my scientific ability and I felt like he respected me as a scientist. From Jay I learned that it's not all about how smart you are, but how hard you work. For that advice Jay, I thank you. Bruce has always had open ear to my personal troubles as well as my scientific troubles. I must admit that I have never felt like I fit in at Caltech, but Bruce and Jay always made feel like I was part of the team. Whether when they were kind to me or just plain mean, I always knew it was to push me to be a better scientist.

Harry has been an inspiration to me as a scientist. I remember the first time I met Harry. It was at a group meeting. I was sitting there watching a grad student give a talk and this old guy kept interrupting with jokes with no regard to the grad student. Don't

get me wrong, this old guy was hilarious, but I do remember thinking,g "Maybe no one tells this guy to shut up because he is old, or maybe he is crazy." Later the next day I was on the fourth floor of the BI making copies and I saw this old guy sitting in an office. I looked at the name placard and it said "Harry Gray." I was shocked. I never thought such a prolific scientist could be such an awesome guy! Through Harry's personality and scientific wisdom I feel as if I have all the tools necessary to pursue scientific interests outside of Caltech. Harry encouraged me to pursue my doctorate at Caltech while I was doing research with Libby. From the bottom of my heart I would like to thank Harry Gray for believing in me and being there for me through some of the best and worst times of my life. Harry has been extremely understanding and supportive throughout my graduate career.

I would especially like to thank Nate-dawg Lewis for being unofficial second advisor. Although I was never officially Nate's student, he always treated me like I was. He invited me to Lewis Group retreats, conferences, and meetings. He supported my research by allowing me to give several Lewis Group meetings. I was a member of his subgroups and he freely gave me advice. Heck, he even let me be in the group picture. I can honestly say Nate inspires me to fight the good fight for science. He has aggressively pursued scientific endeavors that can benefit the world, and he has also been unrelenting in letting any "false or shaky" science from harming honest and truthful scientific pursuits. Nate has been listed as one of the top 100 most influential people in the world by Rolling Stone and he debunked Cold Fusion. I kind of view Nate as a scientific superhero. A scientist to look up to and aspire to be. I'm glad I had the opportunity to work with Nate.

comic relief for me and I think of them as my own little brothers and I want them to excel at whatever they choose.

Finally I would like to thank my family. My parents, Son cha Walker and Wayne Walker, have supported me through all my endeavors. They sacrificed their lives for me. My mom and dad are truly amazing people. My dad and mom are both from completely different worlds. My dad is a black guy from Plaquemine, Louisiana and my mom is from South Korea. Although my parents are from two different worlds it's their inner selves and core principles that they share that have kept them together and married for almost 30 years. They are both extremely strong people. Neither of my parents went to college, but that never stopped them from pushing me to be the best at whatever I did. They have taught me how to be strong, a good man, and perseverance. I would also like to thank my twin brother, Ron. We both came to Caltech and went through this journey together, but I still don't know what he worked on here!!! He has been a rock and a metric for me. I could always look to my bro and say "Hey! If he can do that, then I should be able to do it as well!" During my time at Caltech my brother married his wife, Tammie Walker. Their relationship has shown me what true love is and how true love can get your through a place like Caltech. Tammie has been a sister to me. Her kindness and support throughout this process has been immense. I can't forget to thank one of the strongest women I have ever known, my little sister, Nicole Michelle Walker. For such young woman she has been through a lot. She has lost a son, and struggled to raise her daughter. But through it all she has managed to raise a lovely little woman, Harmony (age 4), and graduate from college with a bachelor's degree in psychology. Now she is

pursuing a master's degree in therapeutic recreation. She did all of this while having a full time job. My little sister is amazing and she inspires.

I know I did not thank everyone, and if I missed you I am truly sorry. But it's late, I'm tired, and I still have a little work left on this thesis. Thanks for everything.

Abstract

The performance of dye sensitized solar cells (DSSC) was investigated as a function of electrolyte composition and dye sensitizer. Electrolytes consisting of increasing concentrations of bromide and tri-bromide effectively increased the current of DSSCs while conserving an increase in open circuit voltage. Corroles were used to investigate their efficacy as light absorbers for DSSCs. Electronic spectroscopy of corroles demonstrated that the spectra of corroles could be red shifted through β-substitution. Also, the changes in the electronic spectra of corroles was not affected by adsorption to TiO_2. Electrochemical data concluded that the functionalization of the β-positions of the corroles did not significantly affect the corrole's redox potentials. FTIR spectroscopy confirmed that the corroles were chemically adsorbed onto TiO_2. Photoelectrochemical measurements concluded that the corroles are efficient sensitizers for DSSCs. A highly efficient corrole utilizing sulfonic acid binding groups was discovered. Also, a corrole with a malonic acid binding group was 70% as efficient as one of the best performing dye sensitizers in DSSCs.

Table of Contents

List of Figures

List of Tables

Chapter 1

Introduction

The need for inexpensive, clean energy is increasing everyday. As more and more countries develop and the world's population increases, the need to power the world increases. One of the most promising sources of energy for powering the planet is solar energy. Approximately 120,000 terawatts (TW) of solar energy strike the earth everyday. Considering that as of 2008 the current world energy consumption is approximately 15 TW, the sun is a huge, untapped resource. Currently, only 0.05% of the world's energy production is from solar energy.[1] This brings us to the question, "Why are we not using the sun to power the planet?" The basic fundamental answer to the question as to why the world isn't using solar energy is cost. Solar energy is relatively more expensive than conventional means of energy, such as coal and fossil fuels. According to the California levelized energy costs, in 2007 the cost of electricity produced by coal was 0.074-0.088 cents per kilowatt hour, and the cost of solar electricity was 0.116 − 0.312 cents per kilowatt hour.[2] Although these costs are for electricity production in California, the high cost of solar energy explains why 80 to 90 percent of the world's energy comes from fossil fuels.[3]

In order to overcome such high costs, solar cells must either be made from cheaper materials, or become more efficient. In order to be as efficient as possible a solar cell must be able to make efficient use of the solar spectrum (Figure 1.1). The region between 400 and 1100 has the highest photon density in the AM 1.5 solar spectrum. A material that can absorb sunlight between 400 and 1000nm would be the ideal absorber. Silicon solar cells accomplish this task, because silicon's bandgap is 1.1 eV. Silicon solar cells' small bandgap allows it to absorb light up to 1100nm. The most efficient solar cells to date, multijunction solar cells, absorb the solar spectrum using up to 3

different semiconductors that absorb three overlapping regions of the visible solar spectrum. Silicon solar cells have achieved efficiencies of ≈20%, and multijunction solar cells have achieved efficiencies of up to ≈40%.[4, 5] Although silicon and multijunction solar cells are very efficient at converting sunlight to electricity, their energy conversion efficiency doesn't reduce cost of the materials and construction in a such a way that they are competitive in price to fossil fuels.

Solar energy is expensive because the most promising and efficient devices are constructed from extremely pure materials. The most commonly available, efficient solar cells are based on silicon. Silicon is very abundant, making up 25.7 percent of the earth's crust by mass. Even though the element silicon is very abundant, a significant amount of refining is required for solar cell grade silicon. For silicon to be effectively used in solar cells it needs to be pure to parts per billion. To produce monocyrstalline silicon, raw silicon must be refined to metallurgical grade silicon, then refined to semiconductor grade silicon, and further refined by the Czochralski process, creating a large single crystal of silicon. Each process requires the silicon be heated to between 1000°C and 1900°C, depending on the process. Finally, once the silicon ingots are made they are cut into wafers and polished which destroys approximately 50% of the silicon. All these processes increase the cost of silicon solar cells. Multijunction solar cells can cost up to eight times as much as silicon solar cells. Multijunction solar cells' increased costs are due to their use of rare and hard to process materials such as gallium, indium, and germanium. They suffer from the same expensive processing as do silicon solar cells and the materials are not as abundant, which greatly increases the cost of multijunction solar

cells. In order to make solar energy more economically viable, efficient alternatives must be investigated.

A promising alternative to silicon and multijunction solar cells are dye sensitized solar cells (DSSC). DSSCs have the potential to be as efficient as silicon solar cells, but at a fraction of the cost of silicon and multijunction solar cells. Currently, the most efficient DSSC is 11.1% with a theoretical efficiency $\approx$31%.[6-8] DSSCs have the potential to be far cheaper than crystalline silicon and multijunction solar cells, primarily due to their abundant use of inexpensive materials. DSSCs are typically constructed with a glass counter electrode that is coated with a thin layer of platinum, a working electrode that is composed of anatase, nanocrystalline TiO_2 deposited on a fluorine doped SnO (F:SnO) glass slide, and a dye sensitizer (Figure 1.2). Because TiO_2 is a wide band gap semiconductor ($E_{bg} \approx$3.2eV), TiO_2 cannot efficiently absorb the solar spectrum.[9, 10] Dyes are attached to the surface of TiO_2 and serve as the light absorbers. The most efficient dyes are based on ruthenium polypyridyl compounds, but dyes ranging from porphyrins, organic, and other metal-based polypyridyl compounds have been used.[11-20] Dyes are chemisorbed to TiO_2 through the use of carboxylic, sulfonic, and phosphonic acid groups.[21-23] Because films of anatase nanocrystalline TiO_2 are used, an approximate 1000 fold increase in surface area is achieved when compared to a planar single crystal. Such an increase in surface area allows for a considerable amount of dye to be loaded onto a cell, which in turn makes for a thin and efficient solar cell. The basic principle of operation of DSSCs can be seen in Figure 1.2. In step 1 the dye molecule is excited by light. The electron in the ground state is excited to a higher energy state that is more negative in potential than the conduction band of the semiconductor nanoparticle. The
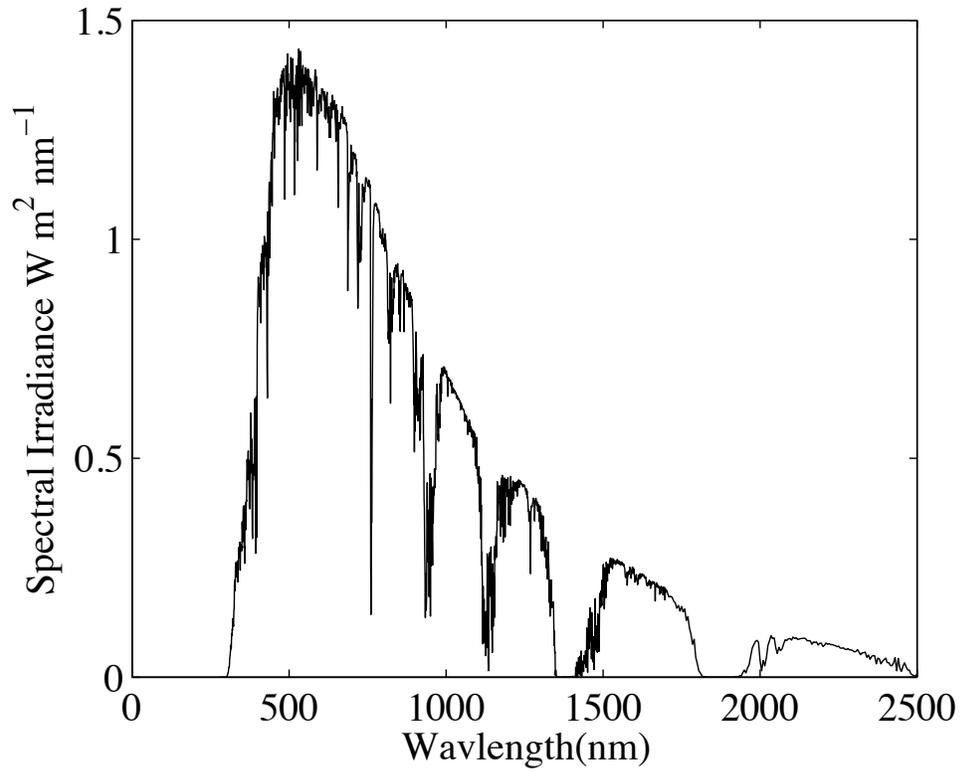
Figure 1.1. Spectral irradiance on the surface of Earth at air mass AM 1.5 conditions, which is the amount of solar radiation that strikes the Earth after passing through one and a half atmospheres. This corresponds to a solar zenith angle of 48.2°.

excited electron is then transferred to the semiconductor nanoparticle in step 2. Step 2 is known as electron injection, and the rate of injection typically occurs on the order of femtoseconds to picoseconds.[24-26] In dye sensitized solar cells there is also a redox couple that reduces the oxidized form of the dye after electron transfer to the TiO_2 nanoparticle. This process is known as regeneration and is step 3. Regeneration occurs on the order of nanoseconds. The rate is limited to the order of $<10^{-9}$s because redox couples in dye sensitized solar cells are in solution; therefore, the regeneration rate is diffusion limited at 10^{-9}s.[27,28] By reducing the dye in the regeneration step after injection, the positive charge, or hole, is now moved to the redox couple, which creates greater charge separation between the hole and electron. The counter electrode then reduces the redox couple in step 4. Finally, in step 5, the electron will travel through the nanoparticle interface to a conducting electrode, along the way doing work, and end is up on the counter electrode where the process repeats itself.

As the photogenerated electron travels through the DSSC, it can recombine with the photogenerated hole at several places along its path (Figure 1.3). The careful balance of forward, advantageous electron transfer processes with the reverse, deleterious electron transfer processes prevents the electron from recombining with the hole. The initial rate of light absorption (k_1) is extremely fast. After absorption the electron can deactivate (k_{-1}). The k_{-1} process is determined by the radiative and non-radiative decay of the excited electron. After k_1, electron injection (k_2) occurs on the order of femtoseconds to picoseconds. It has been determined in the highly efficient DSSC containing Ru(4,4'-dicarboxy-2,2'-bipyridine)$_2$(NCS)$_2$ or N3 dye that injection occurs from the excited, non-thermally relaxed, singlet state, and the thermally relaxed, triplet state.[25, 26] After k_2,

when the electron is in the conduction band of TiO_2, the electron can recombine with the chemisorbed dye sensitizer (k_3). In efficient DSSCs, the k_3 process is typically $>10^{-6}$s.[29,30] The k_3 process is in direct competition with the regeneration (k_5) process, which occurs at the diffusion limit of 10^{-9}s in the case of using I^- as the reducing agent. The electron can also recombine with redox species in solution (k_4). In the presence of the commonly used I^-/I_3^- electrolyte k_4 occurs on the order of $\approx 10^{-3}$s.[31] The careful control of these rates is one of the factors that leads to efficient dye sensitized solar cells.

Optimization of the kinetic factors ultimately leads to the increased currents in DSSCs. The efficiency (η) of a DSSC is determined by the ratio of the power of the DSSC (P_{DSSC}) to the power of the incident light (P_{in}) (Equation 1.1). The power of the DSSC is determined by the short circuit current density (J_{sc}), open circuit voltage (V_{oc}), and fill factor (ff). The short circuit current density is given by the current measured at short circuit conditions, or the current measured when there is zero applied voltage. The open circuit voltage is the voltage measured when the cell is at open circuit, or the voltage that is applied to produce zero current. The fill factor is simply the ratio of the measured power of the solar cell from the current-voltage curves to the maximal theoretical power of the solar cell. An ideal fill factor, or the measure of how similar the solar cell is to this theoretical maximum, would be 1. The fill factor is mostly determined by the kinetic factors of the solar cell. If recombination is high then the fill factor will be low, and if there is little to no recombination the ff will be near unity, but in efficient solar cells the ff is ≈ 0.6-0.8. Therefore, in kinetically optimized solar cells there is not much improvement in the fill factor. The ff is basically an indicator of whether the
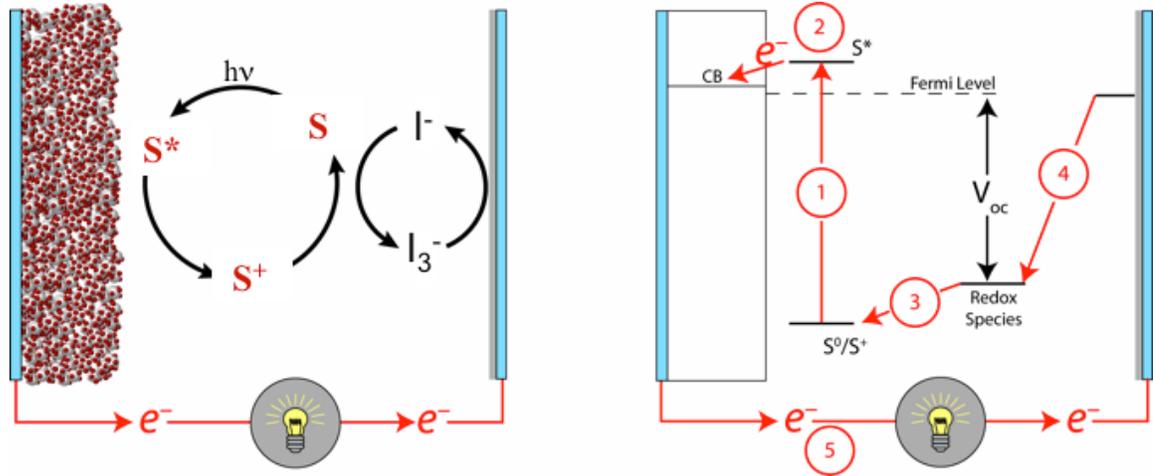
Figure 1.2. Schematic of a typical dye sensitized solar cell and its step-by-step operation.

kinetics of the solar cell are favorable. It can be concluded that by increasing the J_{sc}, V_{oc}, or ff one can increase the η.

$$\eta = \frac{P_{DSSC}}{P_{in}} = \frac{J_{sc} V_{oc} ff}{P_{in}}$$

Eq. 1.1

Short circuit current density is dependent on a given dye's efficiency to convert photons to electrons in DSSCs as well as the overlap of the dye sensitizer's absorption spectrum with the solar spectrum (Figure 1.3). In order for a dye to efficiently convert light to electricity in DSSCs, several thermodynamic and kinetic requirements must be met (Figure 1.4). First, the excited state potential, or lowest unoccupied molecular orbital (LUMO), must be more negative in potential than the conduction band edge (E_{cb}) of TiO_2. This makes the injection process thermodynamically favorable. Also, the dye must be in good electrical and chemical contact with the TiO_2 to allow for efficient injection of photogenerated electrons. In addition to proper matching of the LUMO of a dye with E_{cb} of TiO_2, the ground state potential, or highest occupied molecular orbital (HOMO), of the dye sensitized must be more positive than the potential of the redox species. This allows regeneration of the oxidized dye to be thermodynamically favorable. Finally, the band gap of the dye, or HOMO-LUMO gap, must be as small as possible, while still maintaining a LUMO that is more negative than the E_{cb} and HOMO that is more positive than the redox species. When the thermodynamics are well balanced to allow for favorable kinetics, optimal current can be obtained. The HOMO-LUMO gap of the dye sensitizer determines spectral range of light that it can absorb. By decreasing the HOMO-LUMO gap, the dye can absorb more red photons, thus increasing its spectral overlap. One example of demonstrating increased current and efficiency in DSSCs through increased spectral overlap is the "Black Dye," or [tris(isothiocyanato)-

ruthenium(II)-2,2':6',2"-terpyridine-4,4',4"-tricarboxylic acid].   The photocurrent action

spectra, or external quantum yield, displayed in Figure 1.5 demonstrates that both the N3

and Black Dye have close to ≈80% efficient conversion of incident light from 420nm to

about 650nm, but the Black Dye has significantly higher light conversion affiances above

650nm than the N3 dye. Because of the increased spectral overlap of the Black Dye, the

efficiency increased from 10% in the N3 sample to 10.4% in the Black Dye. The

increased efficiency is attributed to the Black Dye having 3mA/cm^2 more short circuit

current than the N3. Although the increase in efficiency and current is small, the Black

Dye demonstrates that increasing the spectral overlap of a dye molecule with the solar

spectrum can increase efficiency of DSSCs.

The open circuit voltage (V_{oc}) of DSSCs is determined by the difference in

potential between the redox couple and the conduction band edge of TiO_2.   The

theoretical maximum between V_{oc} is ≈1.1V, but in the most efficient DSSCs the most

photovoltage that has been obtained is ≈0.72V.[32,33] There are two methods for increasing

the open circuit voltage: 1.) Make the conduction band edge of TiO_2 more negative, and

2.) use alternative redox couples with more positive potentials. In order to move the

conduction band edge of TiO_2 more negative, one must be careful not to make the

conduction band edge more negative than the excited state potential of the adsorbed dye

as this would prevent injection of photoexcited electrons. One method that can be used to

move the conduction band edge of TiO_2 to more negative potentials is by

using the Nernstian dependence of the conduction band edge potential on the electrolyte

proton concentration in aqueous solutions.[34-36] Since most DSSCs are in non-aqueous

environments it is difficult to assign a pH to the solution to quantifiably control the
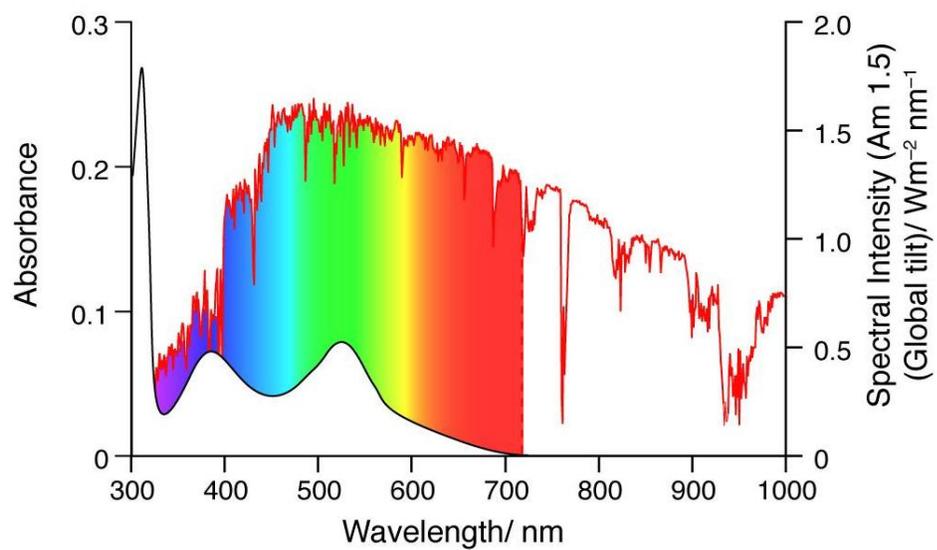
Figure 1.3. Absorption spectrum of N3 dye overlapped with the AM 1.5 solar spectrum.

- k_1: Absorption
- k_{-1}: Deactivation
- k_2: Injection
- k_3: Recombination
- k_4: Escape
- k_5: Regeneration
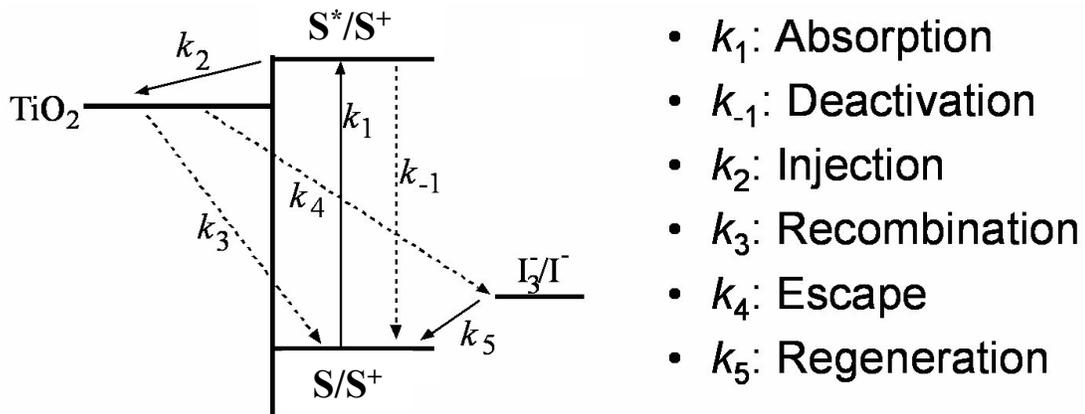
Figure 1.4. Diagram illustrating the rate constants involved in electron transport in DSSCs. The solid lines are favorable processes and the dashed lines are deleterious processes. S is any dye sensitizer. TiO2, dye HOMO/LUMO gap, and I^-/I_3^- energy levels are all positioned in relative potentials to one another in a working DSSC.
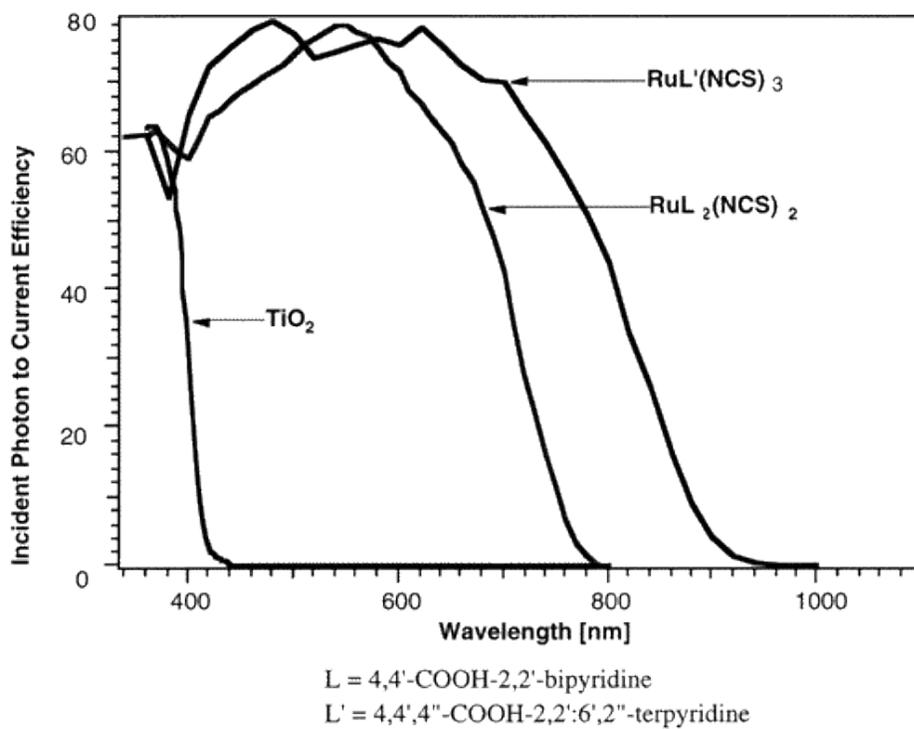
Figure 1.5. Incident photon to current efficiency of N3 [RuL$_2$(NCS)$_2$] and Black Dye [RuL'(NCS)$_3$].

energy of the TiO_2 conduction band edge . A variety of nitrogen containing heterocycles, of varying pKa, have been used in DSSCs to varying success in DSSCs to increase open circuit voltages. The most significant improvements in V_{oc} have been made by the use of the nitrogen containing heterocycle 4-tert-butlypyridine (TBP). TBP has improved the efficiency of the N3 and coumarin dyes in DSSCs by increasing the V_{oc} without any significant decreases in the J_{sc}.[11, 37] By using IMVS, Frank *et al.* were able to determine that TBP makes the conduction band of TiO_2 more negative, which results in a larger photovoltage.[38] Since the discovery of the effect that nitrogen containing heterocycles have on the V_{oc} of DSSCs, several studies have been conducted to compare the effects of several nitrogen containing heterocycles on the V_{oc}, J_{sc}, ff, and η (Figure 1.6).[39] Even though these studies show that nitrogen containing heterocycles affect the V_{oc}, J_{sc}, ff, and η, it is still not completely clear if the changes in the V_{oc}, J_{sc}, ff, and η are due to the nitrogen containing heterocycles adsorbing to the surface, which could affect the recombination and escape rates, or if the increases and decreases in the V_{oc}, J_{sc}, ff, and η are simply due to moving the conduction band edge. Also, because the system is in a non-aqueous environment, it makes it even more difficult to predict the effects of these additives on the conduction band energy of TiO_2.

Changing the redox couple to one that is more positive in potential can also modify open circuit voltage. There have been many unsuccessful attempts at using alternative redox couples of varying potentials.[40-43] It is not enough to have a redox couple that is more positive in potential to increase the open circuit voltage. The redox couple cannot be more positive than the ground state redox potential of the adsorbed dye. Being more positive than the ground state redox potential of the adsorbed dye is not
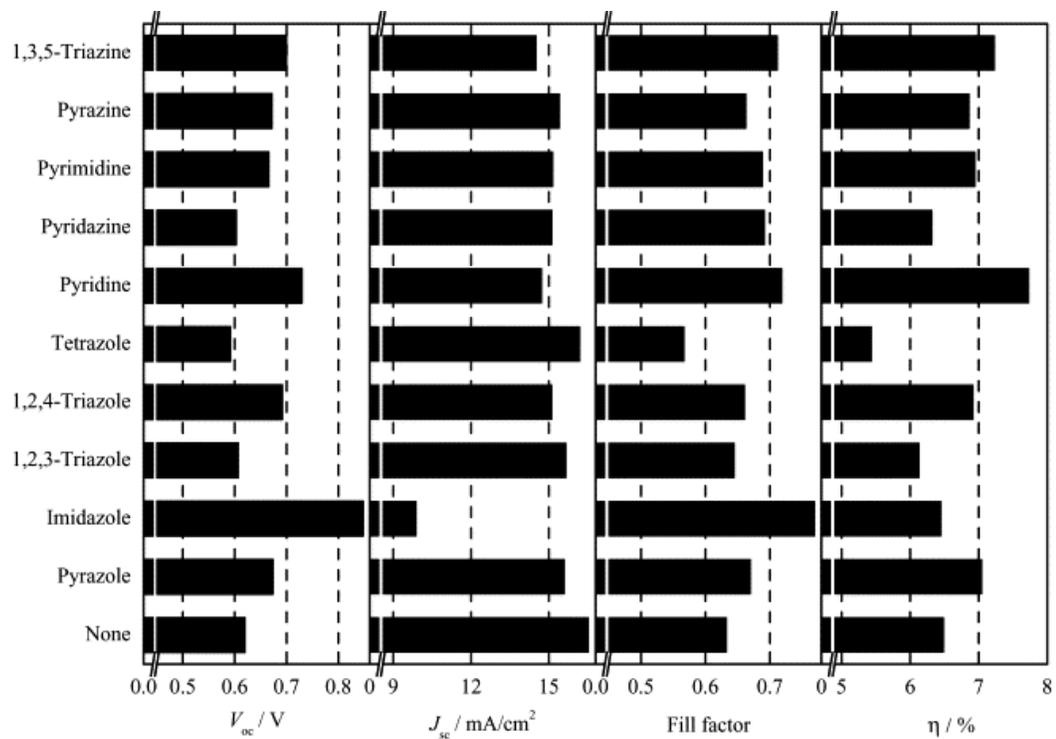
Figure 1.6. The effects of various nitrogen containing heterocycles on the V_{oc}, J_{sc}, ff, and

η. The Black Dye was used in these studies.

thermodynamically favorable and efficient regeneration of the oxidized will not occur. Also, in order for the redox to operate efficiently, the electron transfer kinetics must be favorable. The redox couple must have slow electron transfer rates with TiO_2 surface and fast electron transfer rates with the oxidized dye. In I^-/I_3^- electrolytes the electron transfer between the TiO_2 surface and the redox couple is slow, but for a redox couple such as ferrocene/ferrocennium the electron transfer with the TiO_2 surface is much faster.[41] Also, the regeneration rate must be at or near the diffusion limit to prevent recombination. An efficient redox couple must effectively kill two birds with one stone.

Since the development of an efficient dye sensitized TiO_2 solar cell pioneered by O'Regan and Grätzel, the most efficient dyes have been the well-known N3 dye, which obtained an efficiency of 10% in 1993.[11, 27] There has only been a 1.1% improvement in the efficiency of dye sensitized solar cells. In order to further improve DSSCs, a greater understanding of the fundamental parameters are needed to improve the performance of DSSCs. Careful experimentation and demonstration of the factors that can improve solar cell performance, such as alternate redox couples and spectral overlap, are the central focus of this thesis. Through optimization of alternative redox couples greater currents and open circuit voltages can be obtained. Also, by using a different class of dye molecules spectral overlap can be increased to improve currents and ultimately efficiencies in DSSCs.

Chapter 2

Bromide/Tri-Bromide Electrolytes

Introduction

The most efficient DSSCs to date operate in a liquid electrolyte containing I^-/I_3^- redox couple. The I^-/I_3^- redox couple is extremely important in DSSCs as can be seen in Figure 1.2. The I^-/I_3^- redox couple is directly involved in several processes, such as regeneration, recombination, escape, and shuttling the hole to the counter electrode. The I^-/I_3^- redox couple is used in the most efficient DSSCs, because it provides a unique platform to control four separate processes. The I^-/I_3^- redox couple provides a key kinetic and thermodynamic balance to DSSCs. There have been many efforts to try and better optimize the regeneration, recombination, escape, and hole transport to the counter electrode through the use of several organic and inorganic redox couples.[42-47] When outer sphere redox couples, such as ferrocene/ferricinium, are used, low photovoltages and photocurrents are observed. This is due to an increase in the recombination rate. When k_4 approaches k_5, photovoltages and photocurrents decrease, because the injected electrons now start to recombine from the TiO_2 to the redox couple, instead of perchalating to the back F:SnO contact and performing work.

The I^-/I_3^- redox couple works efficiently in DSSCs for several reasons. For one, two electrons are required to reduce I_3^- to I^-. The reduction can happen at the TiO_2 surface and the back platinum counter electrode. The I^-/I_3^- redox couple works so well in TiO_2 systems because the two-electron reduction at TiO_2 surface is orders of magnitude slower than the same two-electron reduction of tri-iodide at the back platinum counter electrode. The fast kinetics of tri-iodide with the back counter electrode is believed to be due to electrocatalysis via dissociative chemisorption of I_2. Also, the strong adsorption of iodide and tri-iodide on the platinum counter electrode provides protection against any

contaminant.[48] Fast outer sphere redox couples and the many other organic and inorganic redox couples may not adsorb as well to platinum as the I^-/I_3^- redox couple, which reduces the rate of reduction of the redox couple. Also, the rate of reduction of redox couples other than the I^-/I_3^- redox couple may have been faster with the TiO_2 than platinum. In order for a redox couple to properly mediate the electron transfer processes in DSSCs, the redox couple must sufficiently retard the escape process, but still facilitate fast electron transfer between the platinum counter electrode and the adsorbed dye sensitizer.

Only two redox couples over almost 20 years of research have showed any results close to the I^-/I_3^- redox couple: A 5-mercapto-1-methyltetrazole ion with the dimmer of 5-mercapto-1-methyltetrazole ion (T^-/T_2) and a tris(4,4'-di-*tert*-butyl-2,2'-dipyridyl)cobalt(II/III) perchlorate (Co^{II}/Co^{III}).[48, 49] These two redox couples have yielded efficient DSSCs. Both of the redox couples essentially accomplish this by retarding the k_4 better than the I^-/I_3^- redox couple. Due to the reduction in k_4 an increase in current was observed in DSSCs containing these electrolytes electrolyte. Improvements were minimal and at best the redox couples only matched the efficiency of DSSCs with an I^-/I_3^- redox couple. Although the currents were increased the photovoltages were generally lower for the Co^{II}/Co^{III} redox couple. The Co^{II}/Co^{III} redox couple is 0.331V vs. NHE and is close to the redox potential of the I^-/I_3^- redox couple, which is approximately 0.350V vs. NHE.[40, 50] Although the redox potential of the Co^{II}/Co^{III} redox couple and the I^-/I_3^- redox couple are close, there is a 200mV difference in the V_{oc} produced in DSSCs. Such a difference implies that the kinetics of the Co^{II}/Co^{III} redox couple are vastly different in DSSCs with Co^{II}/Co^{III} redox couple when

compared to DSSCs with an I^-/I_3^- redox couple. The V_{oc} of the T^-/T_2 redox couple was similar to that of the I^-/I_3^- redox couple. The J_{sc} in the T^-/T_2 redox couple was about 20% higher but the ff was 25% lower when compared to the control cell containing an I^-/I_3^- redox couple. The differences in the J_{sc} can possibly be attributed more to the electrolyte composition than the redox couple. In the DSSC with a T^-/T_2 redox couple lithium was used and in the control cell with I^-/I_3^- redox couple, 1,3-dimethylimidazolium iodide (DMII) was used with no lithium. The addition of lithium is known have significant effects on the performance of DSSCs. Such a difference in the electrolyte composition could explain the increased photocurrent in T^-/T_2 redox couple. The decreased fill factor is most likely due to increased recombination of electrons in the TiO_2 with the T^-/T_2 redox couple. The Co^{II}/Co^{III} and T^-/T_2 redox couple have provided the field of DSSCs with potential alternative redox couples but no significant increases in efficiencies have been noted due the use of these redox couples.

Most alternative redox couples fail because they do not possess the unique electron transfer properties as observed in the I^-/I_3^- redox couple. The reduction of the dye by iodide is extremely fast in DSSCs and approaches the solution diffusion limit of 10^{-9}s, but this regeneration process is in competition with the reduction of tri-iodide by the electrons in the conduction band. Reduction of the tri-iodide is generally accepted to occur according to Equation 2. The net reaction in Equation 2.1 can occur either by a second or

$$2e^- + I_3^- \rightarrow 3I^- \qquad \qquad \text{Eq. 2.1}$$
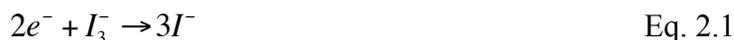
first order mechanism in respect to I_2. The second order mechanism is believed to proceed as expressed in Equations 2.2 to 2.4.[51] In Eq. 2.2 tri-iodide can equilibrate to

iodide and iodine with a rate constant of $\approx 10^{-7}$ mol dm^{-3}.[52] Iodine then can accept an electron from the conduction band of TiO$_2$ or from the platinum electron to form $I_2^{-\bullet}$. If Eq. 2.3 is in equilibrium the net reaction will be first or second order in I$_2$ depending on if 5a or 5b is dominant. If Eq. 4 is the rate-determining step then the net reaction is first order in the electron and first order in I$_2$.

$$I_3^- \Leftrightarrow I_2 + I^- \qquad \text{Eq. 2.2}$$
$$I_2 + e^- \Leftrightarrow I_2^{-\bullet} \qquad \text{Eq. 2.3}$$
$$I_2^{-\bullet} \rightarrow I_3^- + I^- \qquad \text{Eq. 2.4a}$$
$$I_2^{-\bullet} + e^- \rightarrow 2I^- \qquad \text{Eq. 2.4b}$$

Equations 2.5 and 2.6 express another possible first order mechanism by which the reduction of tri-iodide can occur. In Eq. 2.5 the electron for either the conduction band or platinum counter electrode causes the I$_2$ to dissociate, which leaves an adsorbed iodide (I_{ads}) on either the platinum or TiO$_2$. This I_{ads} can then rapidly accept an electron to produce another I$^-$. The two pathways on which tri-iodide can proceed have been investigated rigorously in the literature and there is still much debate on the specific pathway that the net reaction in Eq. 2.1 proceeds upon. But it can be concluded that the pathway that the reduction of tri-iodide takes is very slow, due to its two-electron reduction, and this is one of the reasons why the I$^-$/I$_3^-$ redox couple is the gold standard in efficient DSSCs.

$$I_3^- \Leftrightarrow I_2 + I^- \qquad \text{Eq. 2.2}$$
$$I_2 + e^- \Leftrightarrow I_{ads} + I^- \qquad \text{Eq. 2.5}$$
$$I_2 + e^- \rightarrow I^- \qquad \text{Eq. 2.6}$$

The low photovoltages produced in DSSCs has been attributed to the I$^-$/I$_3^-$ redox couple. Its redox potential is fixed and does not lend itself to manipulation. Changing the redox

couple to one that has the same two-electron reduction pathway and equilibrium constant would be a reasonable place to start. One such redox couple is the bromide/tri-bromide redox couple. The Br^-/Br_3^- redox couple should have the same kinetics as the I^-/I_3^- redox couple, but with a much larger redox potential (≈ 0.420V). Such a large redox potential should increase the V_{oc} considerably while still maintaining excellent regeneration kinetics and retarded k_4 rates (Figure 2.1). The Br^-/Br_3^- redox couple has been shown to increase the V_{oc} of an eosin Y and several ruthenium polypyridyl dyes significantly enough to increase the efficiency of these cells when compared to similar cells in the presence of an I^-/I_3^- redox couple.[53, 54] The results of a series of dyes tested by Elizabeth Mayo are summarized in Table 2.1. For the DSSCs in a Br^-/Br_3^- electrolyte with $[Os(H_2L^{'})_2(CN)_2]^{2+}$ and $[Os(H_2L')L_2]^{2+}$ (L' = 4,4'-dicarboxylic acid-2,2'-bipyridine, and L = 2,2'-bypridine) dyes, the efficiencies were less than the comparable I^-/I_3^- electrolyte. The DSSCs with $[Ru(H_2L^{'})_2(CN)_2]^{2+}$ as the adsorbed sensitizer demonstrated the same efficiency as comparable cells with I^-/I_3^- electrolyte. The dyes $[Os(H_2L^{'})_2(CN)_2]^{2+}$, $[Os(H_2L')L_2]^{2+}$, and $[Ru(H_2L^{'})_2(CN)_2]^{2+}$ all had increased photovoltages, but they all had reduced photocurrents. The data for N3 in a Br^-/Br_3^- electrolyte is not reported because it did not produce any photocurrent or photovoltage. The reason for this is that the N3 ground state redox potential (0.68V) is too close in potential to the redox potential of the Br^-/Br_3^- redox couple (0.44V). Although there is a 0.240V over-potential it is not enough to drive the reduction of the oxidized N3. The amount of over-potential may explain the reduced photocurrents seen in the $[Os(H_2L^{'})_2(CN)_2]^{2+}$, $[Os(H_2L')L_2]^{2+}$, and $[Ru(H_2L^{'})_2(CN)_2]^{2+}$ dyes, because their ground state redox potentials are less than the two dyes that demonstrated increased efficiencies.

The two dyes $[Ru(H_2L')L_2]^{2+}$ and $[Ru(H_2L')_3]^{2+}$ demonstrated increased efficiencies, 24hrs under vacuum. Iodine (Sigma-Aldrich, ≥99.8%, solid, ACS reagent) was sublimed because not only was the V_{oc} significantly increased but also the J_{sc} was maintained at or near the same levels as in comparable DSSCs with an I^-/I_3^- electrolyte. The decreased currents in $[Os(H_2L')_2(CN)_2]^{2+}$, $[Os(H_2L')L_2]^{2+}$, and $[Ru(H_2L')_2(CN)_2]^{2+}$ can possibly be increased with the introduction of more bromide. Because the rate of reduction of oxidized dye is first order, increasing the concentration of bromide will increase the rate of reduction of oxidized dye. Also, if the ratio of bromide to tri-bromide is maintained, the V_{oc} should remain constant. The experiments conducted in this chapter seek to improve photocurrents in DSSCs containing a Br^-/Br_3^- electrolyte.

Experimental

Materials

Acetonitrile (Sigma-Aldrich, 99.8% anhydrous), ethanol (Decon Laboratories, Inc., 200 proof), lithium bromide (Sigma-Aldrich, 99.9% anhydrous beads), bromine (Aldrich, 99.99%), titanium tetrachloride (Fluka, ≥99.8%), lithium iodide (99.9% anhydrous beads), and pyridine (Sigma-Aldrich, 99.8% anhydrous) were all used as received. Lithium perchlorate (Sigma-Aldrich, ≥95.0%) was dried by fusing at $240^{\circ}C$ over a sand bath and under vacuum. Pyridinium trifluoroacetate (Sigma-Aldrich, 98%) was purified by dissolving and supersaturating it in acetonitrile. The pyridinium trifluoroacetate salt was precipitated by addition diethyl ether. The precipitate was then filtered through a medium-porosity glass frit, rinsed with diethyl ether, and dried at $40^{\circ}C$. $Os(H_2L')L_2(PF_6)_2$ was synthesized as reported in the literature.[20] $Ru(H_2L')_2(CN)_2$ was purchased from Solaronix under the label Ruthenizer 505 and used

$$S^+/S^*$$

$$TiO_2$$

$$V_{oc}$$

$$I_3^-/I^-$$ 0.04V

0.44V

$$Br_3^-/Br^-$$

$$S/S^+$$
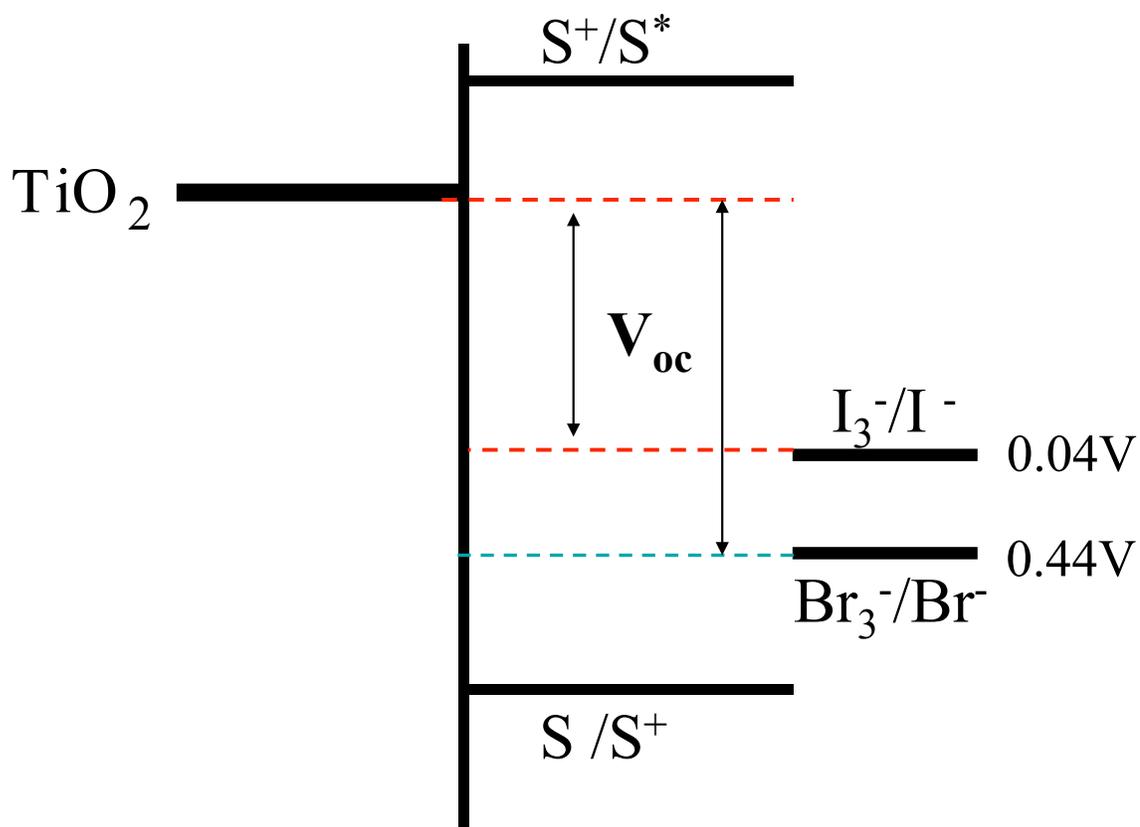
Figure 2.1. Energy diagram demonstrating the theoretical increase in V_{oc} due to using a redox couple that is significantly more positive in potential than I^-/I_3^- and is still capable of thermodynamically reducing the oxidized sensitizer (S).

	$[Os(H_2L')_2(CN)_2]^{2+}$		$[Os(H_2L')L_2]^{2+}$		$[Ru(H_2L')_2(CN)_2]^{2+}$		$[Ru(H_2L')L_2]^{2+}$		$[Ru(H_2L')_3]^{2+}$	
$E^{\circ'}$	0.72 V vs. SCE		0.81 V vs. SCE		1.08 V vs. SCE		1.23 V vs. SCE		1.4 V vs. SCE	
X	I	Br	I	Br	I	Br	I	Br	I	Br
V_{dark}[b]	-325	-680	-290	-570	-380	-770	-325	-650	-375	-740
V_{oc} (mV)[c]	-460	-540	-440	-670	-495	-815	-400	-670	-495	-795
J_{sc} (mA)[d]	14.1	0.2	7.1	3	8.2	4.4	3.3	3.4	6.7	5.9
ff[e]	0.64	0.58	0.64	0.56	0.58	0.67	0.64	0.61	0.64	0.81
Efficiency[f]	4.2	0.1	2.0	1.1	2.4	2.4	0.8	1.7	2.2	3.6

a: The electrolyte was acetonitrile containing 0.50 M LiX, 0.040 M X_2, 0.020 M pyridine and 0.020 M pyridinium triflate, where X=I or Br.

b: Potential required to drive a cathodic current density of 0.5 mA cm^{-2} in the dark. Standard deviations over many trials are ±0.05 V

c: Standard deviations over many trials are ±0.01 V.

d: Standard deviations over many trials are ±0.2 mA cm^{-2}.

e: The fill factor (ff) is calculated as $P_{max}/(J_{sc} \times V_{oc})$, where P_{max} is the most negative value of $J \times V$.

f: Calculated as $(J_{sc} \times V_{oc} \times ff \times 100\%)/I_{light}$, where $I_{light} = 100$ mW cm^{-2}.

Table 2.1. Compiled results comparing I^-/I_3^- and Br^-/Br_3^- electrolytes for a series of dyes. L' = 4,4'-dicarboxylic acid-2,2'-bipyridine, and L = 2,2'-bypridine.

as received. All materials were stored under a nitrogen atmosphere in a dry box with the exception of I_2, ethanol, $Os(H_2L')L_2(PF_6)_2$ and $Ru(H_2L')_2(CN)_2$. TiO_2 screen-printing paste was purchased from Solaronix under the product name Ti-Nanoxide HT/SP ($\approx$9nm sized particles) and used as received. Fluorine doped SnO glass slides (4in x 1in) with a resistivity of 15 Ω cm^{-2} were purchased from Hartford Glass Co., Inc.

Dye Coated Electrodes

Fluorine doped SnO glass slides were first cleaned in soapy water and rinsed with 18 MΩ water. The slides were subsequently rinsed with acetone, 200 proof absolute ethanol, and dried under nitrogen. Special care was taken to assure no residue was left on the slides in the form or spotting or other blemishes. TiO_2 screen printing paste was deposited on the F:SnO slides by screen printing with an AMI Inc. HC-53 screen printer with a 156 mesh polyester screen and 10.2 μm of MX emulsion (Sefar Printing). The printed films were covered to prevent dust from settling on top of the slides and left at room temperature for 1hr. The slides were then dried in a furnace at 80°C for 1hr before being sintered at 450°C for 30 minutes in air. The thickness of the TiO_2 layer on F:SnO was measured by a Dektak 3030 profilometer and determined to be $\approx$5 μm thick.

TiO_2 slides for photoelectrochemical experiments were prepared by cutting the 4in x 1in slides into 0.5in x 1in electrodes. TiO_2 electrodes were cleaned by rinsing with 18 MΩ water and 200 proof absolute ethanol. The TiO_2 electrodes were then dried under nitrogen and the surface of the TiO_2 of the electrodes was covered with 3-4 drops of 0.2M $TiCl_4$ and allowed to soak for eight hours. 0.2M $TiCl_4$ is not very air stable as it was prepared from a stable stock solution of 2M $TiCl_4$.[55] After soaking for eight hours in 0.2M $TiCl_4$, the electrodes were rinsed with 18 MΩ water and 200 proof absolute ethanol

then dried under nitrogen. The slides were sintered at 450°C for thirty minutes and allowed to cool to 120°C over two hours. The 120°C TiO_2 electrodes were immersed in 200 proof absolute ethanolic solutions of approximately 1 x 10^{-4}M $Os(H_2L')L_2(PF_6)_2$ or $Ru(H_2L')_2(CN)_2$. The slides were immersed while still hot and allowed to soak in the dye solution for 12-24 hours in the dark.

Electrolyte

Electrolyte solutions of 1.0M LiBr/ 0.08M Br_2, 0.75M LiBr/ 0.06M Br_2, 0.5M LiBr/ 0.04M Br_2, and 0.25M LiBr/ 0.02M Br_2, 0.5M LiI/ 0.04M I_2 were all prepared with a 20mM pyridine and 20mM pyridinium trifluoroacetate buffer. The 20mM pyridine and 20mM pyridinium trifluoroacetate buffer was used to prevent dye desorption and buffer the proton activity of the TiO_2 to stabilize the conduction band edge of the TiO_2. $LiClO_4$ was added to electrolyte solutions of 0.75M LiBr/ 0.06M Br_2, 0.05M LiBr/ 0.04M Br_2, and 0.25M LiBr/ 0.2M Br_2 to maintain a 1.0M concentration of lithium in all the electrolyte solutions used for increasing concentration studies. All solutions were prepared and stored in a nitrogen atmosphere. Electrolyte solutions were either prepared the day before or day of experimentation and used within three days of the experiment. Special care was taken to assure that all powdered reagents were completely dissolved in the electrolyte.

Photoelectrochemistry

A custom, three electrode, electrochemical cell was used in all photoelectrochemistry experiments (Figure 2.2). The three electrodes were a platinum gauze counter electrode, platinum wire reference electrode (referenced to the solution potential), and a dye coated TiO_2 slide was the working electrode. The distance between

To Reference Pt Wire

To Counter Pt gauze

Electrolyte:
0.50 M LiI
0.04 M I_2
Acetonitrile
20 mM Pyridine
20 mM Pyridinium
Triflate

Distance between WE and CE: 2 mm;
Surface area illuminated: 0.25 cm²
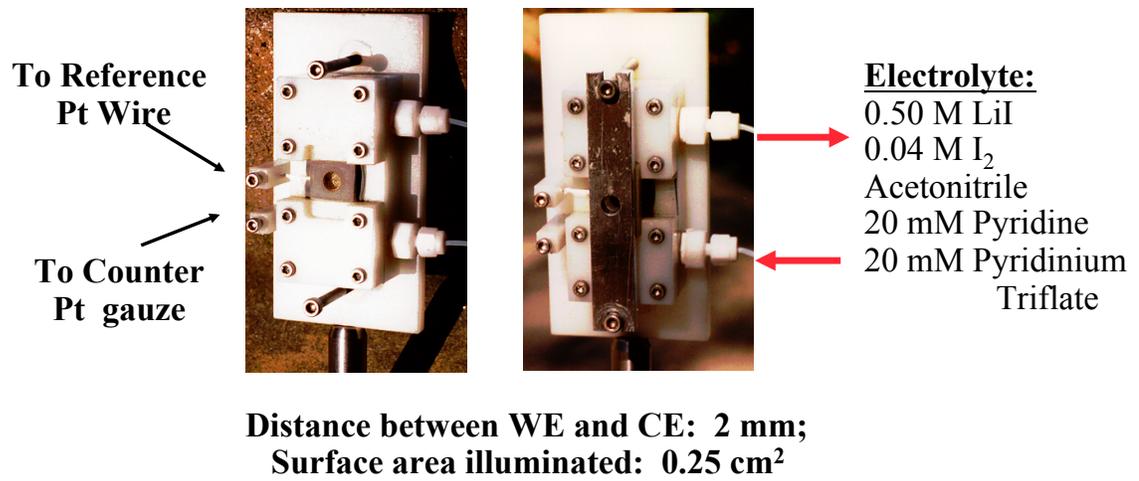
Figure 2.2. Custom three-electrode photoelectrochemical cell used to test I-V behavior in DSSCs.

the working and counter electrodes was 2mm, which was determined by a silicon rubber

spacer. Light from a 150 Xe lamp in an Oriel Lamp Research housing was used to

illuminate the photoelectrochemical cell from the backside of the TiO_2. Light first passed

through the glass, then the $F:SnO_2$, and finally illuminated the dye coated TiO_2. The light

from the xenon lamp was filtered with a long pass 385nm filter to prevent direct

excitation of TiO_2. An AM 1.5 and AM 0 filter were used to perfectly match the solar

spectrum at AM 1.5. A Solarex, Inc. diode was used to calibrate the light intensity to

$100mW/cm^2$. The photoelectrochemical cell was placed an appropriate distance from the

lamp that allowed for measurements to be taken at a light intensity of $100mW/cm^2$.

Electrolyte was introduced into the custom photoelectrochemical cell from the lower port.

Special care was taken to remove any air bubbles in the cell by tapping and flushing the

cell while monitoring the top exit port for bubbles. During experimentation the least

concentrated electrolyte was first added and the following electrolytes were added in

order of increasing concentration. A BAS 100B potentiostat was used to apply a

scanning potential of 20mV s^{-1}. Scans were performed from 200mV to 600mV or

-800mV depending on the dye and electrolyte used. Current was measured every 2mV.

Scans always began at 0V. Cell resistances were measured with the BAS 100B

potentiostat and were determined to be 50Ω. The final current potential (I-V) curves

were corrected for cell resistance.

Results and Discussion

$[Os(H_2L')L_2]^{2+}$ and $[Ru(H_2L')_2(CN)_2]^{2+}$ DSSC with a Bromide/tri-Bromide Electrolyte

The dyes, $[Os(H_2L')L_2]^{2+}$ and $[Ru(H_2L')_2(CN)_2]^{2+}$, were studied in four Br^-/Br_3^-

electrolytes of increasing concentrations. $[Os(H_2L')L_2]^{2+}$ and $[Ru(H_2L')_2(CN)_2]^{2+}$ were

chosen as the dyes to study, because $[Os(H_2L')L_2]^{2+}$ and $[Ru(H_2L')_2(CN)_2]^{2+}$ both exhibited low photocurrents as seen in Table 2.1. By increasing the electrolyte concentration, an increase in photocurrent can be achieved while still maintaining the increased photovoltage for the $[Os(H_2L')L_2]^{2+}$ as seen in Figure 2.3 and Table 2.2. The open circuit voltage of DSSCs with $[Os(H_2L')L_2]^{2+}$ and the electrolytes 0.25M LiBr/ 0.2M Br$_2$, 0.5M LiBr/ 0.4M Br$_2$, 0.75M LiBr/ 0.6M Br$_2$, and 1.0M LiBr/ 0.8M Br$_2$ all had open circuit voltages within 3% of each electrolyte. The open circuit voltages were -782mV, 763mV, 770mv, and 760mV in order of increasing electrolyte concentration. The open circuit voltages remained relatively constant. The short circuit currents showed a remarkable increase with increasing electrolyte concentration. The short circuit current increased from 1.12 mA cm^{-2} for $[Os(H_2L')L_2]^{2+}$ in the electrolyte 0.25M LiBr/ 0.2M Br$_2$, to 1.91 mA cm^{-2} for the electrolyte containing 0.75M LiBr/ 0.6M Br$_2$. This correlates to a 70.5% increase in short circuit current density. The short circuit current density also increased when increasing the electrolyte concentration from 0.25M LiBr/ 0.2M Br$_2$ to 0.5M LiBr/ 0.4M Br$_2$. The increase in current from 0.25M LiBr/ 0.2M Br$_2$ to 0.5M LiBr/ 0.4M Br$_2$ was only 17% which was not as great an increase in current from the electrolyte 0.5M LiBr/ 0.4M Br$_2$ to the electrolyte 0.75M LiBr/ 0.6M Br$_2$. The increase in short circuit current from the 0.5M LiBr/ 0.4M Br$_2$ electrolyte to the 0.75M LiBr/ 0.6M Br$_2$ electrolyte was 46%. The short circuit current density for $[Os(H_2L')L_2]^{2+}$ in the 0.75M LiBr/ 0.6M Br$_2$ electrolyte decreased by 9% when going to the 1.0M LiBr/ 0.8M Br$_2$ electrolyte. The decrease in current is most likely due to the insolubility of such a high concentration of LiBr. Over time, the 1.0M LiBr would eventually crystallize out of the solution in high concentrations. On occasion the LiBr would
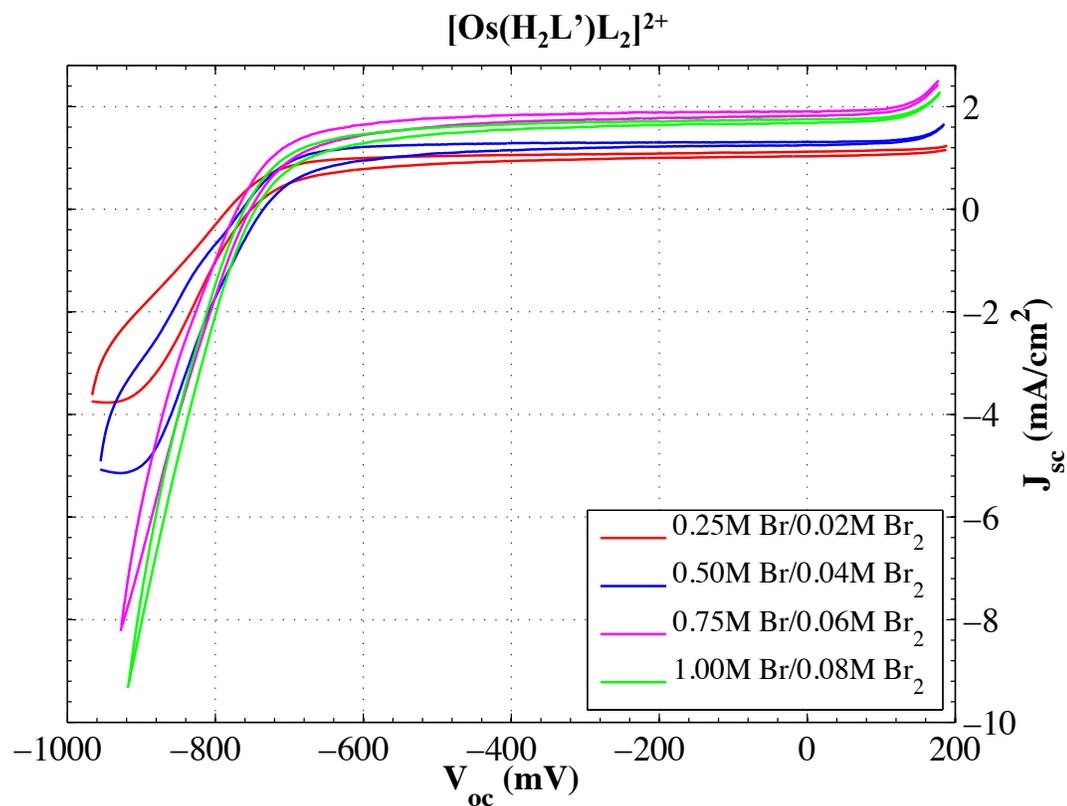
$[Os(H_2L')L_2]^{2+}$

Figure 2.3. Current versus potential characteristics of $[Os(H_2L')L_2]^{2+}$ in the presence of increasing Br/Br_3^- concentrations under AM 1.5 solar simulated conditions. All electrolytes contained 1.0M Li^+, 20mM pyridine, and 20mM pyridinium trifluoroacetate.

	[Os(H$_2$L')L$_2$]$^{2+}$			
	0.25M Br /0.02M Br$_3^-$	0.50M Br/ 0.04M Br$_3^-$	0.75M Br/ 0.06M Br$_3^-$	1.00M Br/ 0.08M Br$_3^-$
V$_{oc}$ (mV)	-782	-764	-770	-760
J$_{sc}$ (mA)	1.12	1.31	1.91	1.75
ff	0.71	0.74	0.68	0.66
Efficiency (η%)	0.62	0.74	1.00	0.88

Table 2.2. All electrolytes contained 1.0M Li$^+$, 20mM pyridine, and 20mM pyridinium trifluoroacetate.

remain in solution and not crystallize out of solution. Such behavior could be due to changes in ambient temperature in the laboratory, seeding points on the inside of the Schlenk vessel, or slight variations in electrolyte solution. Because LiBr would only recrystallize some of the time, the electrolyte 1.0M LiBr/ 0.8M Br_2 was believed to be supersaturated. The supersaturated nature of the electrolyte could have contributed to the 9% decrease in short circuit current density seen in the $[Os(H_2L')L_2]^{2+}$ DSSC with a 1.0M LiBr/ 0.8M Br_2 electrolyte. Fill factors for the $[Os(H_2L')L_2]^{2+}$ DSSCs remained relatively constant for increasing Br^-/Br_3^- electrolyte concentrations. The fill factors were at most within 10% of each other. The efficiencies of the $[Os(H_2L')L_2]^{2+}$ DSSCs showed a 70% percent increase from the 0.25M LiBr/ 0.2M Br_2 electrolyte to the 0.75M LiBr/ 0.6M Br_2 electrolyte. There was also a 17% increase in efficiency from the electrolyte concentration of 0.25M LiBr/ 0.2M Br_2 to 0.5M LiBr/ 0.4M Br_2. A 12% decrease in efficiency occurred when going from the 0.75M LiBr/ 0.6M Br_2 to the 1.0M LiBr/ 0.8M Br_2. The increase and decrease in efficiency is due to the changes seen in the photocurrent as a function of electrolyte concentration. As seen in Equation 1.1, a change in short circuit current would generate a proportional change in the efficiency. The changes in efficiency follow the changes in current with a significant increase in efficiency from the 0.25M LiBr/ 0.2M Br_2 electrolyte to the 0.75M LiBr/ 0.6M Br_2 electrolyte, which directly correlates to the large increase in photocurrent from the different electrolyte concentrations. Also, a decrease in efficiency from the 0.75M LiBr/ 0.6M Br_2 electrolyte to the 1.0M LiBr/ 0.8M Br_2 electrolyte was observed. This trend also followed the trend in short circuit current. The increase in short circuit current was the only significant change that occurred when increasing the electrolyte concentration.

Because the fill factors and open circuit voltages remained relatively constant for all concentrations of Br⁻/Br₃⁻ electrolyte and the short circuit currents increased with increasing concentrations of Br⁻/Br₃⁻ electrolyte, the efficiency of the $[Os(H_2L')L_2]^{2+}$ DSSCs increased.

$[Ru(H_2L')_2(CN)_2]^{2+}$ exhibited similar trends as $[Os(H_2L')L_2]^{2+}$, but the changes in short circuit current and efficiency were not as significant (Figure 2.4 and Table 2.3). The open circuit voltages of $[Ru(H_2L')_2(CN)_2]^{2+}$ DSSCs in Br⁻/Br₃⁻ electrolytes were within 7% percent of each other and did not show any trends in the slight increases and decreases in open circuit voltages for the Br⁻/Br₃⁻ electrolytes. The fill factors of $[Ru(H_2L')_2(CN)_2]^{2+}$ DSSCs exhibited values that were within 6% of each other. The increasing concentrations of Br⁻/Br₃⁻ electrolytes did not affect the fill factor characteristics of $[Ru(H_2L')_2(CN)_2]^{2+}$ DSSCs. The short circuit currents of $[Ru(H_2L')_2(CN)_2]^{2+}$ DSSCs increased with increasing concentrations of Br⁻/Br₃⁻ electrolyte. The increase in short circuit current from the 0.25M LiBr/ 0.2M Br₂ electrolyte to the 0.75M LiBr/ 0.6M Br₂ electrolyte increased by 66%, which is a similar increase to that in the $[Os(H_2L')L_2]^{2+}$ DSSCs of 70%. The increase in current from the 0.25M LiBr/ 0.2M Br₂ electrolyte to the 0.50M LiBr/ 0.4M Br₂ electrolyte in $[Ru(H_2L')_2(CN)_2]^{2+}$ DSSCs was 38%. The increase in current from 0.25M LiBr/ 0.2M Br₂ electrolyte to the 0.50M LiBr/ 0.4M Br₂ electrolyte for $[Os(H_2L')L_2]^{2+}$ DSSCs was significantly less at 17% when compared to $[Ru(H_2L')_2(CN)_2]^{2+}$ DSSCs. A similar decrease in current was observed when going from the 0.75M LiBr/ 0.6M Br₂ electrolyte to the 1.0M LiBr/ 0.8M Br₂ electrolyte in $[Ru(H_2L')_2(CN)_2]^{2+}$ DSSCs. The decrease in current for $[Ru(H_2L')_2(CN)_2]^{2+}$ DSSCs from 0.75M LiBr/ 0.6M Br₂ to the 1.0M LiBr/

[Ru(H₂L')₂(CN)₂]²⁺
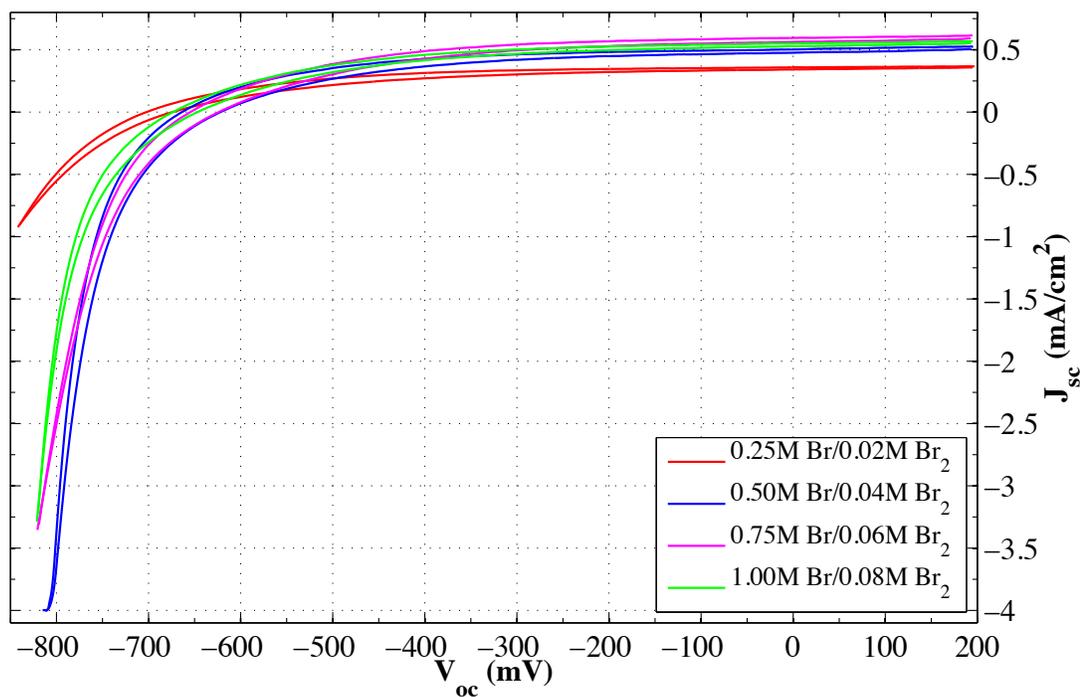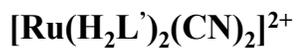
Figure 2.4. Current versus potential characteristics of $[Os(H_2L')L_2]^{2+}$ in the presence of increasing Br/Br_3^- concentrations under AM 1.5 solar simulated conditions. All electrolytes contained 1.0M Li^+, 20mM pyridine, and 20mM pyridinium trifluoroacetate.

	[Ru(H$_2$L')$_2$(CN)$_2$]$^{2+}$			
	0.25M Br /0.02M Br$_3^-$	0.50M Br/ 0.04M Br$_3^-$	0.75M Br/ 0.06M Br$_3^-$	1.00M Br/ 0.08M Br$_3^-$
V$_{oc}$ (mV)	702	664	654	674
J$_{sc}$ (mA)	0.36	0.50	0.60	0.55
ff	0.54	0.54	0.51	0.51
Efficiency (η%)	0.14	0.18	0.20	0.19

Table 2.3. All electrolytes contained 1.0M Li$^+$, 20mM pyridine, and 20mM pyridinium trifluoroacetate.

0.8M Br_2 electrolyte was 9% which is the same percent change seen in $[Os(H_2L')L_2]^{2+}$ DSSCs of the same electrolytes.

$[Os(H_2L')L_2]^{2+}$ and $[Ru(H_2L')_2(CN)_2]^{2+}$ DSSC Equilibration

The $[Os(H_2L')L_2]^{2+}$ and $[Ru(H_2L')_2(CN)_2]^{2+}$ DSSCs both required a certain amount of time to equilibrate to their maximum values. In the case of DSSCs with the dye $[Os(H_2L')L_2]^{2+}$ and a 0.5M LiBr/ 0.4M Br_2 electrolyte it took 80 minutes before the dye reached its maximal values (Figures 2.5 and 2.6). Over the 80-minute duration of the experiment the open circuit voltages and fill factors did not vary significantly and they did not increase over time. The open circuit voltages stayed within 4mV of each other and the fill factors were within 4 percent of each other. The short circuit currents in $[Os(H_2L')L_2]^{2+}$ DSSCs increased significantly from the beginning of the experiment to the end. The current approximately quadrupled from time zero to 80 minutes, going from 0.37 mA cm^{-2} to 1.31 mA cm^{-2}. This increase in current also increased the efficiency of the cells significantly from 0.21% to 0.74%. The increase in efficiency was approximately the same as the increase in current. Similar results were seen in the $[Ru(H_2L')_2(CN)_2]^{2+}$ DSSCs in the same electrolyte of 0.5M LiBr/ 0.4M Br_2, but the increases in current and efficiency were not as significant (Figures 2.7 and 2.8). Also, the time needed to reach maximal values was less for $[Ru(H_2L')_2(CN)_2]^{2+}$ DSSCs than for $[Os(H_2L')L_2]^{2+}$ DSSCs. It took 50 minutes to reach maximal values as opposed to 80 minutes for $[Os(H_2L')L_2]^{2+}$ DSSCs. The open circuit voltages in $[Ru(H_2L')_2(CN)_2]^{2+}$ DSSCs were more varied when compared to $[Os(H_2L')L_2]^{2+}$ DSSCs. The open circuit voltage decreased 32mV over 50 minutes, but this was only a 5% change and can be considered negligible. The fill factors slightly increased but only by about 5% which is
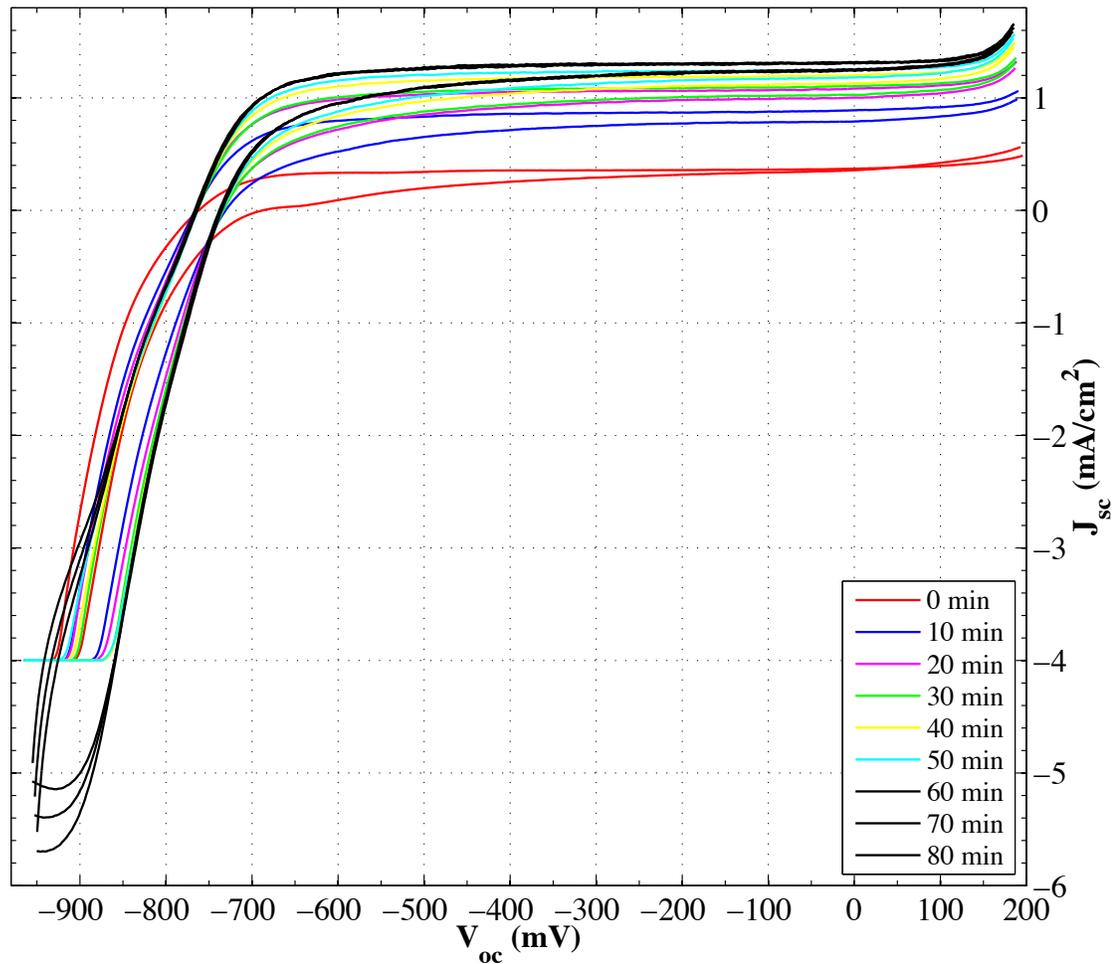
$[Os(H_2L')L_2]^{2+}$

Figure 2.5. Current versus potential curves of $[Os(H_2L')L_2]^{2+}$ taken over time until the cell equilibrated. The electrolyte used was 0.5M LiBr, 0.04M Br_2, 0.5M $LiClO_4$, 20mM pyridine, and 20mM pyridinium trifluoroacetate in acetonitrile.
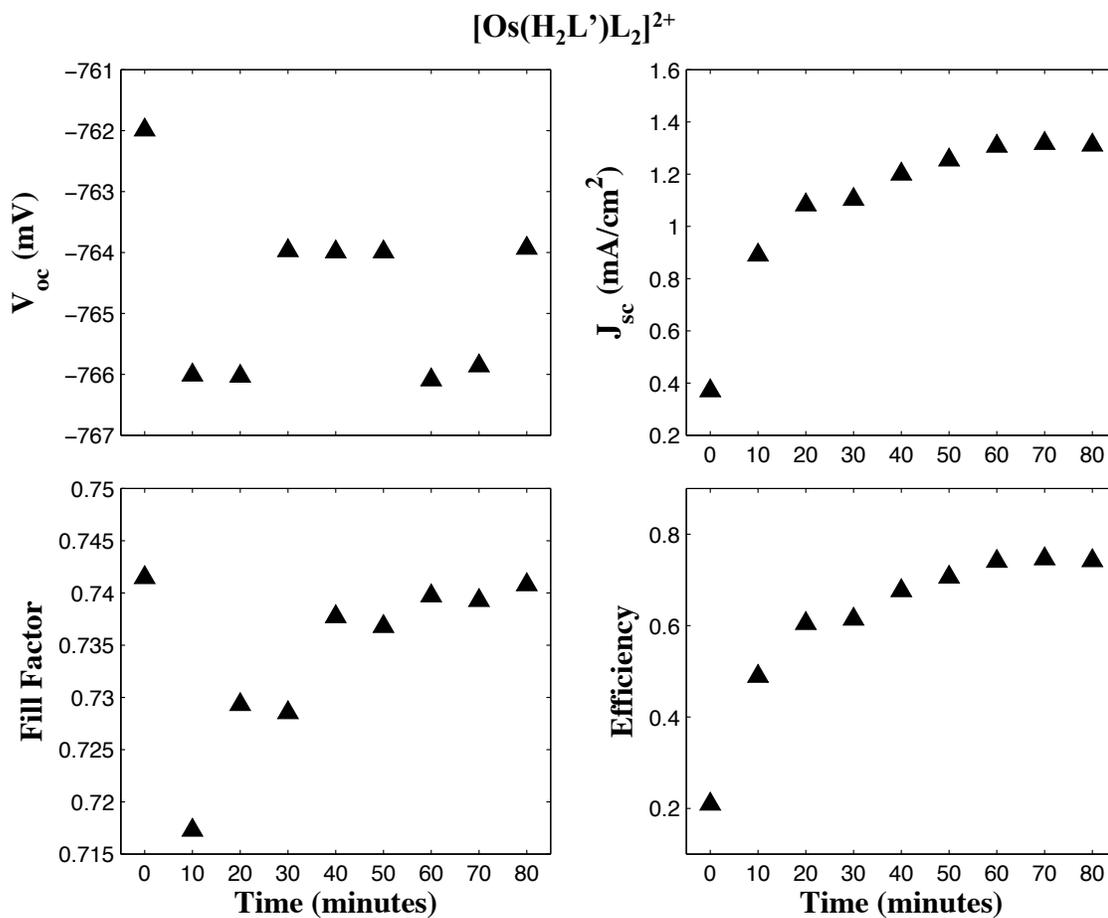
$[Os(H_2L')L_2]^{2+}$

Figure 2.6. Plot of short circuit current, open circuit voltage, fill factor, and efficiency versus time for $[Os(H_2L')L_2]^{2+}$. The electrolyte used was 0.5M LiBr, 0.04M Br_2, 0.5M $LiClO_4$, 20mM pyridine, and 20mM pyridinium trifluoroacetate in acetonitrile.
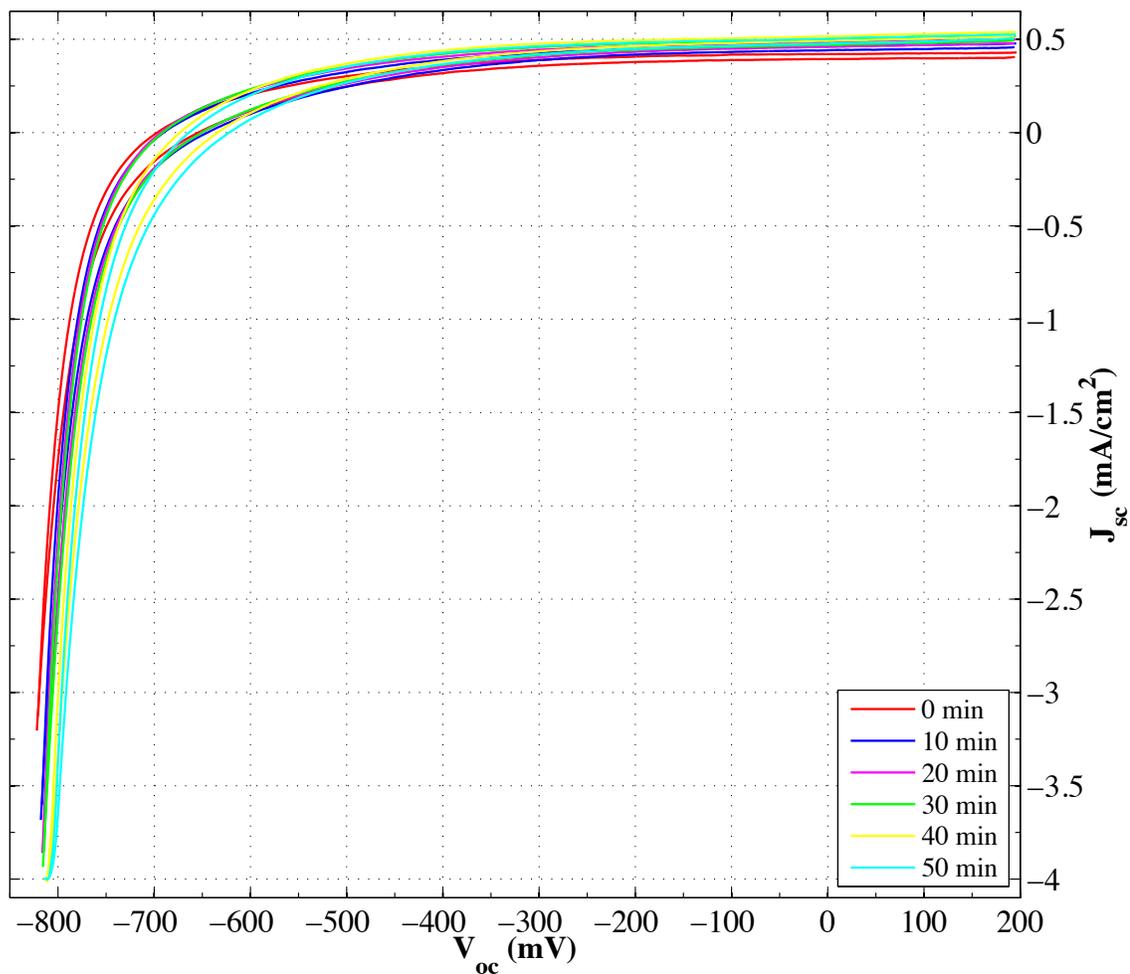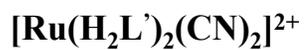
$[Ru(H_2L')_2(CN)_2]^{2+}$

Figure 2.7. Current versus potential curves of $[Ru(H_2L')_2(CN)_2]^{2+}$ taken over time until the cell equilibrated. The electrolyte used was 0.5M LiBr, 0.04M Br_2, 0.5M $LiClO_4$, 20mM pyridine, and 20mM pyridinium trifluoroacetate in acetonitrile.
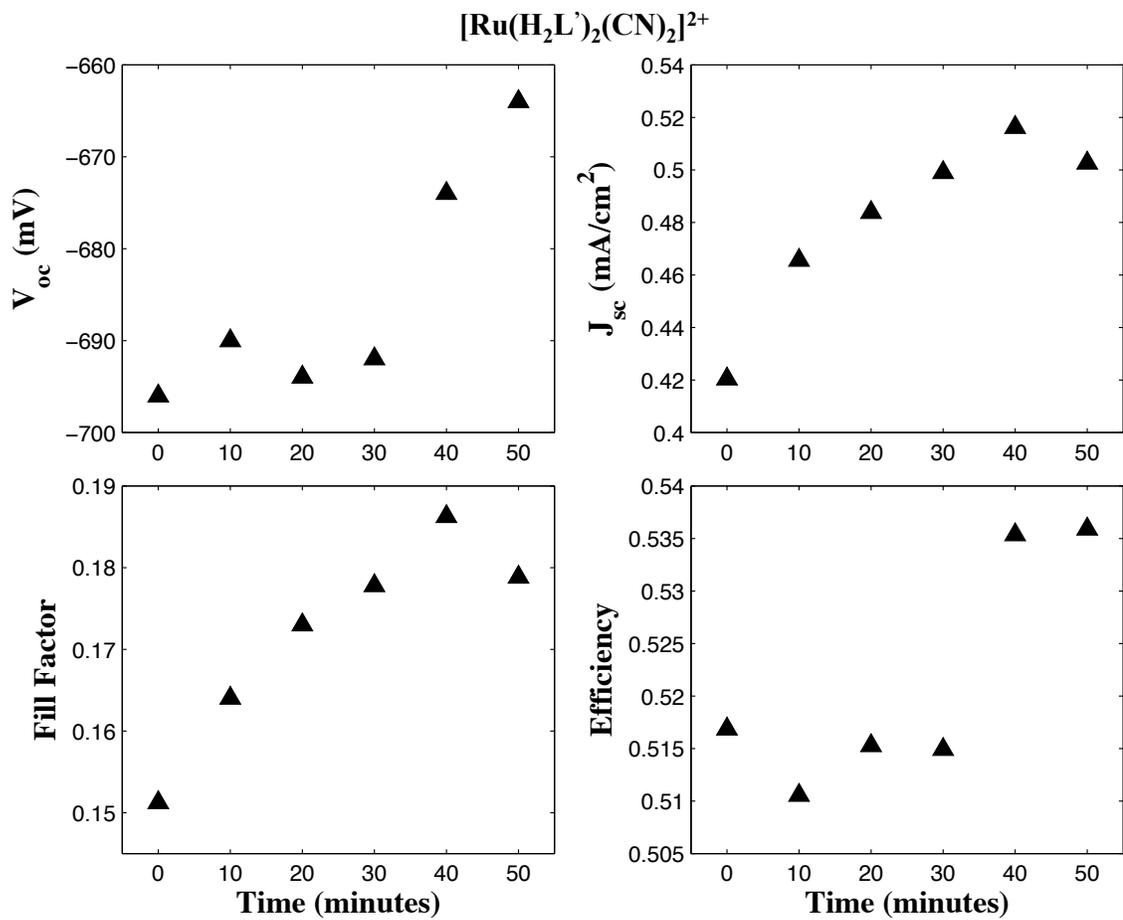
$$[Ru(H_2L')_2(CN)_2]^{2+}$$

Figure 2.8. Plot of short circuit current, open circuit voltage, fill factor, and efficiency versus time for $[Ru(H_2L')_2(CN)_2]^{2+}$. The electrolyte used was 0.5M LiBr, 0.04M Br$_2$, 0.5M LiClO$_4$, 20mM pyridine, and 20mM pyridinium trifluoroacetate in acetonitrile.

negligible as well. The short circuit current increased by 19% over the 50-minute experiment. While this increase was not as significant as that seen in the $[Os(H_2L')L_2]^{2+}$ DSSCs it is still considerable. The increase in current and negligible changes in fill factors and open circuit voltages led to a similar ≈20% increase in efficiency over 50 minutes. Similar increases in currents and efficiencies were observed in all electrolytes to varying degrees. The most significant changes over time observed for the two test dyes in the 0.5M LiBr/ 0.4M Br_2 electrolyte was in the short circuit current. Such changes over time indicate that an equilibrium must be achieved in order to achieve maximal values. It is possible that intercalation and adsorption of the lithium cations as well as the subsequent adsorption of the bromide anion require a certain amount of time to equilibrate and facilitate efficient operation of DSSCs. There are no reports in the literature of such equilibration, but reports as to the effect of cations on the regeneration and recombination of oxidized dye with iodide indicate that cation intercalation and adsorption facilitate faster regeneration rates and slower recombination.[56,57]

Bromide vs. Iodide Electrolytes

When comparing $[Os(H_2L')L_2]^{2+}$ and $[Ru(H_2L')_2(CN)_2]^{2+}$ DSSCs in the presence of 0.5M Li^+/0.5M I^-/0.04M I_2 and 0.5M Li^+/0.5M Br^-/0.04M Br_2 some notable differences are observed (Table 2.4). In $[Os(H_2L')L_2]^{2+}$ DSSCs the short circuit current, fill factor, and efficiency are significantly decreased, but the open circuit voltage increased by 80mV from 400mV when going from a 0.5M Li^+/0.5M I^-/0.04M I_2 electrolyte to a 0.5M Li^+/0.5M Br^-/0.04M Br_2 electrolyte. DSSCs containing $[Ru(H_2L')_2(CN)_2]^{2+}$ as the light absorber showed a significant decrease in current and efficiency, but the fill factors remained the same when going from a 0.5M Li^+/0.5M I^-

/0.04M I_2 electrolyte to a 0.5M Li^+/0.5M Br^-/0.04M Br_2 electrolyte. The open circuit voltage in the $[Ru(H_2L^{'})_2(CN)_2]^{2+}$ DSSC increased significantly by approximately 200mV.

A Careful note must be taken to clarify the differences in the results reported in this work when compared to the results reported by Elizabeth Mayo. The primary differences from the work in this thesis and Elizabeth Mayo's thesis is the thickness of the TiO_2 layer and the size of the nanoparticles. The TiO_2 slides by Elizabeth Mayo were 10μm thick with nanoparticles that were 15nm in diameter. The TiO_2 slides used in this work were 5μm thick with a nanoparticle diameter of 9nm. Several publications have studied the effects of film thickness and particle size in DSSCs.[58-60] In general, smaller particles increase the surface area and allow for more dye to be absorbed, but light scattering effects are decreased and the diffusion lengths are smaller. Less light scattering usually leads to less to current because light that wasn't absorbed cannot be redirected to be absorbed. Smaller diffusion lengths typically lead to more recombination. Increasing

film thickness leads to an increase in current because by increasing the film more dye can be absorbed. In the results reported in this thesis and that of Elizabeth Mayo's thesis there was a 2x difference in film thickness. The currents reported for $[Os(H_2L^{'})L_2]^{2+}$ and $[Ru(H_2L^{'})_2(CN)_2]^{2+}$ DSSCs for this work were less when compared to Elizabeth Mayo's work for both iodide and bromide based electrolytes. The open circuit voltages of this work and Elizabeth Mayo's work were also less, which was also mostly due to the lower currents. Only in the $[Ru(H_2L^{'})_2(CN)_2]^{2+}$ DSSCs with 0.5M Li^+/0.5M I^-/0.04M I_2 was the open circuit voltage large but it was not a significant increase in voltage.

	$[Os(H_2L')L_2]^{2+}$		$[Ru(H_2L')_2(CN)_2]^{2+}$	
	I	**Br**	**I**	**Br**
V_{oc} **(mV)**	-415	-502	-548	-748
J_{sc} **(mA)**	6.17	0.81	6.62	1.23
ff	0.70	0.50	0.66	0.62
Efficiency (η%)	1.80	0.20	2.39	0.56

Table 2.4. All electrolytes contained 20mM pyridine and 20mM pyridinium triflouroacetate. The I^-/I_3^- electrolyte contained 0.5M LiI and 0.04M I_2 and the Br^-/Br_3^- electrolyte contained 0.5M LiBr and 0.04Br$_2$.

Effect of Lithium Concentration

When $[Os(H_2L')L_2]^{2+}$ and $[Ru(H_2L')_2(CN)_2]^{2+}$ DSSCs with an electrolyte concentration with a 1.0M Li^+/0.5M Br^-/0.04M Br_2 electrolyte are compared to data collected in a 0.5M Li^+/0.5M Br^-/0.04M Br_2 electrolyte some striking differences are observed. In the $[Os(H_2L')L_2]^{2+}$ DSSC with a 1.0M Li^+/0.5M Br^-/0.04M Br_2 electrolyte the short circuit current and open circuit voltages were all larger than the $[Os(H_2L')L_2]^{2+}$ DSSC with a 0.5M Li^+/0.5M Br^-/0.04M Br_2. The large open circuit voltage can simply be explained by the almost double increase in short circuit current. The increase in current with an increase in lithium concentration is not as clear. It is well accepted that lithium intercalates and adsorbs to the surface of TiO_2.[56,61-63] Lithium intercalation has been shown to effectively move the flatband potential of the TiO_2 conduction band edge to more positive potentials, thus increasing injection, electron hole pair separation, and photocurrent. While this seems to explain the increased photocurrent and subsequent photovoltage in $[Os(H_2L')L_2]^{2+}$ DSSCs, a significant decrease in photocurrent is observed when comparing $[Ru(H_2L')_2(CN)_2]^{2+}$ DSSCs in 0.5M Li^+/0.5M Br^-/0.04M Br_2 electrolyte to a 1.0M Li^+/0.5M Br^-/0.04M Br_2 electrolyte. Such a decrease in photocurrent can possibly be explained by the formation of a dye^+-Br^- adduct. Such dye^+-I^- adducts have been observed for $[Ru(H_2L')_2(diethyldithiocarbamate)_2]^{2+}$, $[Ru(H_2L')_2(CN)_2]^{2+}$, $[Ru(H_2L')_2(Cl)_2]^{2+}$, and $[Ru(H_2L')_2(NCS)_2]^{2+}$.[64, 65] The I^- has been shown to form an adduct with the aforementioned dyes by either bonding, ion pairing, or specific π interaction through the diethyldithiocarbamate, CN, Cl, and NCS ligands. It is believed that this dye^+-I^- adduct helps facilitate regeneration of the oxidized dyes. It is possible that if an adduct is formed with Br^-, it prevents or slows down regeneration in

$[Ru(H_2L^{'})_2(CN)_2]^{2+}$ DSSCs. It may be possible that lithium intercalation and absorption may facilitate the formation of more or longer-lived dye^+-Br^- adducts that retard regeneration and accelerate recombination, but there is no literature evidence for cation interaction with dye adduct. What is known is that cations facilitate the adsorption of anions such as iodide. By doing so it is possible that the iodide ions are closer to the surface bound dye to produce adducts. More studies would need to be conducted to conclude such interactions of the dye with the redox couple and thier affect on DSSC performance. The aforementioned explanation is only based on the limited and recently discovered adduct.

Conclusions

Increasing the concentration of bromide in $[Os(H_2L^{'})L_2]^{2+}$ and $[Ru(H_2L^{'})_2(CN)_2]^{2+}$ DSSCs effectively increased the short circuit current, while maintaining a consistent voltage that was substantially increased when compared to iodide based electrolytes. The fill factors and voltages remained largely unaffected by the increasing concentrations of electrolyte. The short circuit currents increased with increasing concentrations of electrolyte and consequently increased the efficiency of the $[Os(H_2L^{'})L_2]^{2+}$ and $[Ru(H_2L^{'})_2(CN)_2]^{2+}$ DSSCs. Although the efficiencies increased with increasing Br^-/Br_3^- concentration the efficiencies were still not greater than $[Os(H_2L^{'})L_2]^{2+}$ and $[Ru(H_2L^{'})_2(CN)_2]^{2+}$ DSSCs in an I^-/I_3^- electrolyte. Equilibration of the $[Os(H_2L^{'})L_2]^{2+}$ and $[Ru(H_2L^{'})_2(CN)_2]^{2+}$ DSSCs was required to obtain maximal efficiency of the cells. Equilibration of the cell in $[Os(H_2L^{'})L_2]^{2+}$ DSSCs was longer than in $[Ru(H_2L^{'})_2(CN)_2]^{2+}$ DSSCs, and the changes in photocurrent were larger in $[Os(H_2L^{'})L_2]^{2+}$ DSSCs than $[Ru(H_2L^{'})_2(CN)_2]^{2+}$ DSSCs. The concentration of lithium

significantly affects the performance of DSSCs. In $[Os(H_2L')L_2]^{2+}$ DSSCs the short circuit currents were increased, but in the $[Ru(H_2L')_2(CN)_2]^{2+}$ DSSCs short circuit currents were decreased. In conclusion, increasing the concentration of bromide and bromine in the electrolyte increased the current while maintaining a high open circuit voltage. Use of a bromide and bromine electrolyte increased the open circuit voltage of DSSCs when compared to DSSCs with an iodide and iodine electrolyte. The effects of lithium would indicate there may be a specific concentration range that works best. This could be achieved by using a specified amount of lithium bromide or lithium percholrate to achieve the desired lithium concentration and using a tetrabutlyammonium bromide salt (tetrabutlyammonium does not intercalate or adsorb to TiO_2) to increase the bromide concentration.

Chapter 3

Characterization of Corroles

Introduction

Several dye sensitizers have been used since the discovery of an efficient DSSC by O'Reagan and Grätzel.[66] Dye sensitizers for DSSCs should ideally absorb across the entire visible spectrum (Figure1.3), have a suitable redox potentials for regeneration and injection, and have a binding group to bind to TiO_2. An exciting class of molecules that meet these requirements are porphyrins. Porphyrins have been identified as potential candidates for dye sensitizers in DSSCs because of their well known strong absorbances in the 400-450nm region, known as the Soret of B band, and the 500-700nm region, known as the Q band. Their large extinction coefficients and broad spectral overlap make porphyrins prime light absorbers for photosynthesis, which lends to their efficacy in DSSCs. Several porphyrins have the appropriate LUMO and HOMO to allow for efficient injection and regenereration.[67-69] Also porphyrins have been functionalized with several binding groups such as phosphonic acid, carboxylic acid, and sulfonic acid groups.[70, 71] Currently, porphyrins have reached a record efficiency of 7.1%.[72]

Many porphyrins have been used in DSSCs to varying degrees of success. Zinc and free-base porphyrins based on meso-benzoic acid substituted porphyrins (TCPP) were some of the first used to sensitize TiO_2. Zn-TCPP was reported to have a very low efficiency of 1.1%, but the TCPP had a slightly higher efficiency of 3.5%.[73, 74] In addition to TCPP a derivative with sulfonic acid binding groups (TSPP) in place of the carboxylic acid binding groups has been used in DSSCs. Ma *et al*. were seeking to investigate the effect of the functional groups on DSSC performance by comparing TCPP, TSPP, and TPP (5,10,15,20-tetraphenyl-porphyrin). Their studies showed that TCPP was nine times more efficient than TSPP and TPP gave negligible efficiencies because it had no binding

groups. There are several reasons why the aforementioned porphyrins have had such limited success. Some reasons include that the porphyrins readily aggregate, but it has been demonstrated that the low efficiencies are more likely due to the binding groups being located in the meso positions of the porphyrins.[75] In porphyrins where the binding groups are on meso substituted phenyl rings, conjugation from the macrocycle to the binding group is not possible.[76] It is possible for conjugation to occur to a styryl from a β-pyrrolic linker. Also, studies of electron transfer in porphyrin-quinone donor-acceptor systems show that oxidation of the porphyrin is easier in β-substituted porphyrins than for meso-substituted porphyrins.[77] β-substituted porphyrins have demonstrated higher efficiencies in DSSCs than those with meso-substituted binding groups with the most efficient porphyrin to date being a β-substituted porphyrin.

In addition to β-substitution, the amount of conjugation and nature of the linker to the binding group has a profound effect on the electronic absorption characteristics of porphyrins. By functionalizing a porphyrin at the β-position with extended π systems, enhancement of the red-absorbing Q-bands is achieved.[78, 79] Enhancement of the Q-bands is caused by the splitting of the four frontier molecular orbitals of the Gouterman's four-orbital model.[80] By enhancing the Q-band absorption β-substituted porphyrins with extended π systems can absorb more of the visible spectrum, which has lead to more and more efficient porphyrins.[72,81,82] In contrast to the effect that β-substitution has on the electron absorption properties, aryl groups located at the meso-positions have no effect on the absorption spectra of β-substituted corroles.[72] Some of the most promising alternatives to potentially expensive ruthenium polypyridyl dye sensitizers have been

porphyrins. Through β-substitution the absorption spectra can be red shifted allowing for better spectral overlap with the visible spectrum.

Because porphyrins have been shown to be efficient sensitizers, it is possible for similar molecules to be as good or possibly better than the existing porphyrins used to sensitize TiO_2. Corroles are molecules that are very similar to porphyrins (Figure 3.1). They have the same tetrapyrrolic construction and their spectra consist of the characteristic B and Q bands. Although similar to porphyrins corroles have distinct differences from their porphyrin brethren. Corroles lack one meso-carbon. Instead of this meso-carbon two of the four pyrroles are directly bonded to one another. Another key difference between corroles and porphyrins is that inner pocket is tri-basic unlike the porphyrins bis-basic pocket. Finally corroles typically have higher quantum yields of fluorescence when compared to similar porphyrins.[83]

Corroles have not been readily investigated until recently. The first report of a corrole synthesis was by Johnson and Kay in 1965.[84] The synthesis proceeded in low yields and was very difficult. Because of the long, difficult synthesis, much work in the field was very limited. This was remedied by the almost simultaneous discovery of two facile synthetic methods for the preparation of 5,10,15-triarylcorroles by Gross and Paolesse in 1999.[85, 86] Since the discovery of these facile syntheses a boom in corrole research has occurred. A quick search of the literature shows that 85% of all publications associated with corroles are after 1999 (Figure 3.2). Very little is known about the fundamental properties of corroles as they compare to porphyrins. Even less is known about how corroles compare to porphyrins in similar applications such as cancer diagnosis, treatment, and DSSCs.[87] This chapter seeks to investigate the effects on
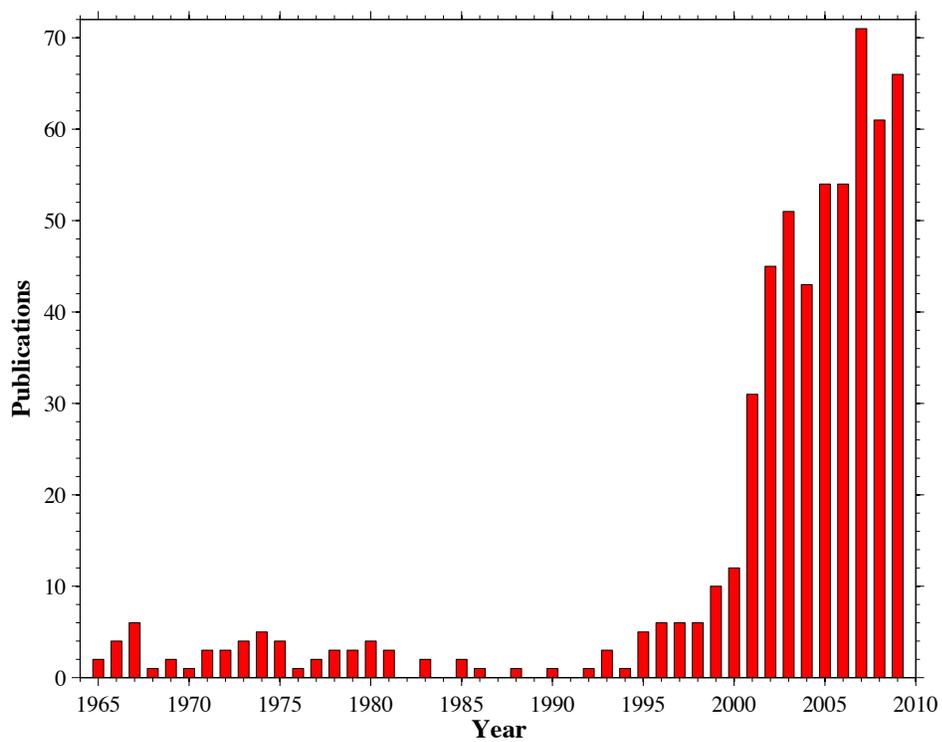
Figure 3.1.   Analysis of corrole publication history since the first corrole synthesis publication in 1965.   In 1999 Gross and Paolesse developed a more facile corrole synthesis, which is the reason behind the boom in corrole publications after 1999.

corrole β-substituted linkers and binding groups on the visible absorption spectra, IR spectra, and redox potentials of corroles for applications in DSSCs.

Experimental

Synthesis

The corroles tpfc-(SO₃H)₂, Ga-tpfc-(SO₃H)₂, Ga-tpfc-(CN-COOH), and Al-tpfc-CN-COOH are depicted in Figure 3.3 and were synthesized and characterized according to literature procedures.[88-90] The corroles Ga-tpfc-COOH, Ga-tpfc-(COOH)₂, Ga-tpfc-(CN-COOH)₂, Ga-tpfc-C(COOH)₂, Al-tpfc-SO₃H, Al-tpfc-(COOH, and Al-tpfc-C(COOH)₂ were used as received from Zeev Gross.

Electronic Spectroscopy

UV-Vis spectra were collected using an Agilent 8453A diode array spectrometer. All corrole spectra were taken in acetonitrile (Sigma-Aldrich, 99.8% anhydrous). Starna 4 sided quartz cuvettes were used for unbound dyes in solution. Spectra of corroles bound to TiO_2 were taken in air. Corroles were bound to TiO_2 in the same manner as described in Chapter 2 of this thesis.

IR spectroscopy

All IR spectra were taken on a Nicolet 6700 FTIR. Corrole samples were prepared in powdered form and pressed into pellets. Corroles were bound to TiO_2 in the same manner as described in Chapter 2. Once the dyes were bound to TiO_2, they were placed in individual aluminum foil wrapped vials. The slide containing vials were placed in a vacuum desiccator overnight. To prepare corrole-TiO_2 samples for IR, the corrole-TiO_2 was carefully scraped off approximately 3 slides using a new razor blade. Pellets of corrole dyed TiO_2 were then pressed. Spectra were taken with a $0.5cm^{-1}$

resolution in transmission mode. All spectra were baseline corrected. For TiO_2 baseline correction below $1200cm^{-1}$ was difficult due to the absorbance in the IR by TiO_2 and carried out as best as possible. The spectra were normalized to the CN stretch for N3 dye and the $1522cm^{-1}$ stretch for the corroles.

Electrochemistry

A standard three-electrode cell was used to conduct cyclic and differential pulse voltammetry. The electrodes consisted of a platinum working electrode, platinum counter electrode, and a non-aqueous silver/silver nitrate reference electrode. The reference electrode was prepared first by cleaning a silver wire in aqua regia (1:4 parts by volume of nitric acid in hydrochloric acid). A saturated solution of silver nitrate was prepared in acetonitrile (BakerDry 99.5% anhydrous). The electrolyte used consisted of 0.1M tetrabutlyammonium hexafluorophosphate ($TBAPF_6$) in acetonitrile (BakerDry 99.5% anhydrous). $TBAPF_6$ was purified by recrystallization in a water/ethanol mixture. Five parts ethanol in one part water was warmed and saturated with $TBAPF_6$. The solution was then placed in an ice bath and allowed to cool at which point crystals of $TBAPF_6$ formed. The crystals were filtered using a coarse glass frit, rinsed with cold 5:1 ethanol:water mixture, and finally rinsed with ether. The recrystallized $TBAPF_6$ was dried over a mineral oil bath at $80^{\circ}C$ under vacuum. A BAS 100B scanning potentiostat was used to collect cyclic and differential pulse voltammetry data. Between each sample and scan all three electrodes were rinsed, cleaned, and tested for abnormalities by scanning them in a 0.1M $TBAPF_6$ electrolyte.

tpfc-(SO₃H)

Sn-tpfc-(SO₃H)

Ga-tpfc-(SO₃H)

Al-tpfc-(SO₃H)

Al-tpfc-COOH

Al-tpfc-CN-COOH

Al-tpfc-CH-(COOH)₂

Ga-tpfc-CH-(COOH)₂

Ga-tpfc-COOH

Ga-tpfc-(COOH)₂

Ga-tpfc-CN-COOH

Ga-tpfc-(CN-COOH)₂
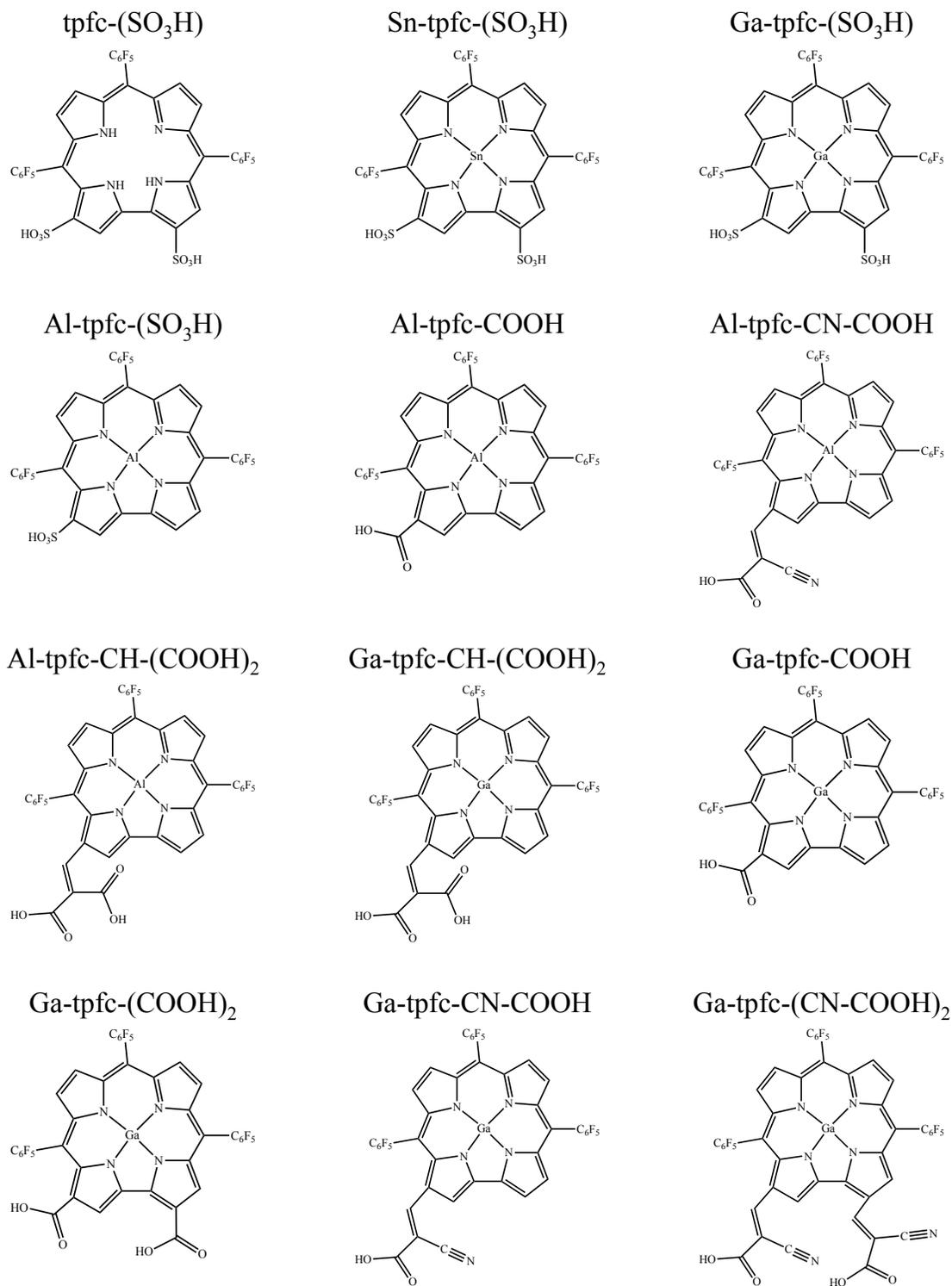
Figure 3.2. Structures of all corroles used in this study.

Results and Discussion

Electronic spectroscopy

The electronic spectra of the corroles in acetonitrile indicated significant differences and similarities that can be attributed to several factors. Similarities are noted in spectra that contain sulfonic acid groups in the β-positions (Figure 3.4). Corroles with sulfonic acid groups in the β-position all have Soret Bands that are at or near 430nm. Also, the Q-bands for the corroles with sulfonic acids groups in the β-position exhibit two bands between 550nm and 650nm. When comparing the effect of the metal on the electronic spectra of the corroles with sulfonic acids in the β-position, it can be seen that the gallium and aluminum spectra are red shifted by approximately 40nm to 50nm when compared to the Sn-tpfc-(SO$_3$H)$_2$. The free base sulfonated corrole's electronic spectra is relatively broad when compared to the spectra of metallated corroles. Metallation of corroles seems to make the Q-bands more defined when compared to free base corrole. Adding carboxylic acid binding groups to the β-position of the corroles does not affect the electronic spectra of caboxylated corroles compared to their sulfonic acid analogues (Figures 3.5 and 3.6). In contrast to direct carboxylation and sulfonation of the β-position of corroles, the addition of electron withdrawing π linkers red shifted the spectra of the gallium and aluminum corroles. The degree of the red shift increased in order of electron withdrawing character of the linkers for aluminum and gallium corroles. The bis-CN-COOH was the most red shifted in the series of β-substituted gallium corroles followed by the mono-CN-COOH. The gallium corrole with the malonic acid group was only slightly more red shifted than its caboxylated and sulfonated analogues. In the series of β-substituted aluminum corroles, the highest red shift was observed in the

mono-CN-COOH, followed by the aluminum corrole with a malonic acid group. The Al-tpfc-CH-(COOH)$_2$ was more red shifted than its carboxylated and sulfonated analogues. The degree of red shift seen in the Al-tpfc-CH-(COOH)$_2$, when compared to its carboxylated and sulfonated counterparts, is greater than the degree of red shift seen in Ga-tpfc-CH-(COOH)$_2$, when compared to its carboxylated and sulfonated counterparts. Another interesting aspect that the linkers and binding groups have on the electronic spectra other than red shifting the spectra is that they increase the epsilon values. When comparing corroles with aluminum and gallium corroles with analogous functional groups, corroles with gallium were more red shifted than analogous aluminum corroles (Figures 3.7 - 3.9). The addition of a nitrile group in conjunction with a π-conjugated linker nearly doubles the epsilon values of the gallium and aluminum corroles with-CN-COOH moieties when compared to their sulfonated and carboxylated analogues. The increased red shift and epsilon values due to the electron withdrawing character of π-conjugated linkers on the β-position of the corroles has also been observed by Chen *et al.* in nickel tetraphenylporphyrins.[78] By increasing the electron withdrawing character of β-substituted linkers they also observed increased red shifts and epsilon values.

Chemisorption of the corroles on TiO$_2$ has unique effects on the electronic spectra of the corroles (Figures 3.10 - 3.12). Chemisorption effectively deprotonates the corroles which is the primary cause of the shifts in spectra between bound and unbound corroles. It is difficult to quantitate the shifts, because the light scattering caused by the TiO$_2$ destroys some of the finer splitting in the Q and Soret bands. The pH can also have a large effect the electronic characteristics of the corroles causing shifts in the intensities of

the different bands in the Q-band region as well as the Soret.[91] Shifts to the red and blue have also been seen between bound, unbound, protonated, and deprotonated ruthenium polypyridyl dyes.[92] Binding to TiO_2 effectively deprotonates the corroles causing shifts in the spectra when compared to unbound corrole dyes in acetonitrile. The spectra of corroles bound to TiO_2 indicated that they are chemisorbed to TiO_2. Also, a considerable amount of corrole dye is absorbed onto the TiO_2. The gallium dyes seem to be more readily absorbed onto TiO_2. This can be seen by the fact the Q bands of the gallium dyes absorb approximately 80% of the incident light. Corroles that chemisorbed to TiO_2 show differences in their spectra when compared to their solution spectra. Some of the finer splitting in the Q and Soret bands is lost due to the increased scattering caused by the TiO_2 particles and it is difficult to make specific peak maxima assignments. Although small shifts in the electronic spectra of corroles did occor, the order of red shifting did not change and was conserved. Also, an important thing to note is that the region between the Q and Soret bands absorbs 20% of the incident light. When the corroles are absorbed to TiO_2 the red shifts for the corroles with π-conjugated linkers are conserved for aluminum and gallium corroles. The adsorption of corroles onto TiO_2 also does not affect the red shift caused by gallium when compared to analogous corroles with aluminum (Figures 3.13 - 3.15). The similarities of corroles in solution and bound to TiO_2 indicate that the benefits of increased red absorbance achieved through the addition of β-substituted π-conjugated linkers is conserved and could prove to be advantageous in DSSCs.
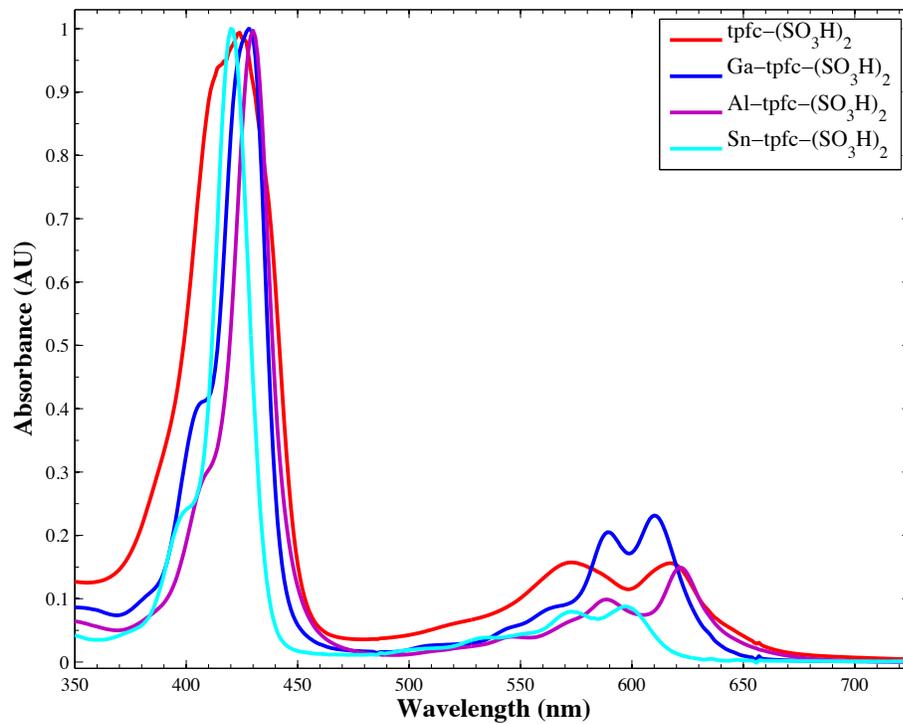
Figure 3.3. Absorbance spectra of sulfonated corroles in acetonitrile. Spectra were normalized at the Soret band.
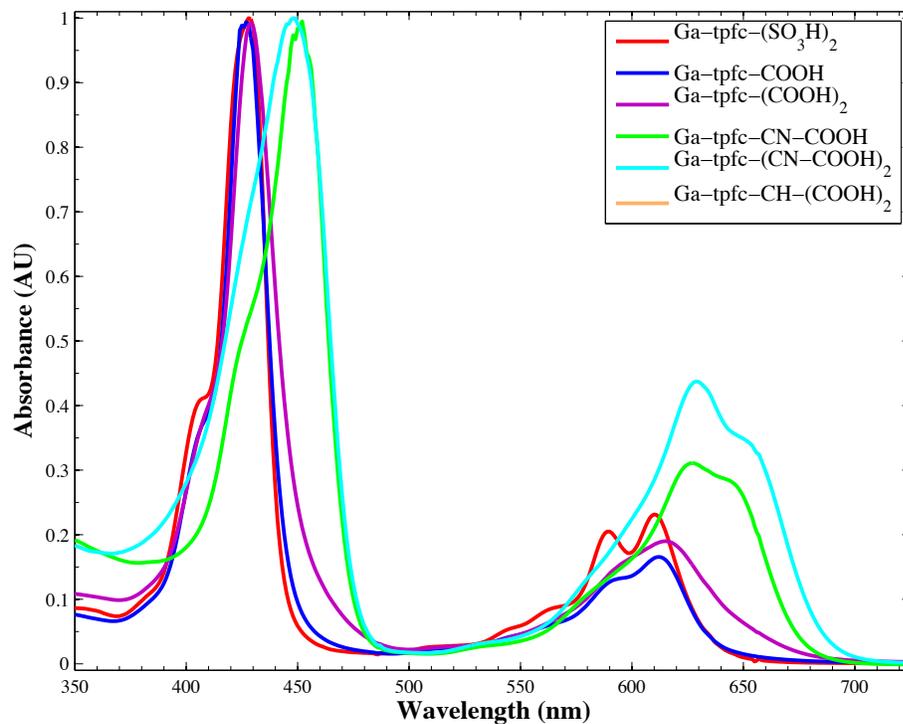
Figure 3.4. Absorbance spectra of gallium corroles in acetonitrile. Spectra were normalized at the Soret band.
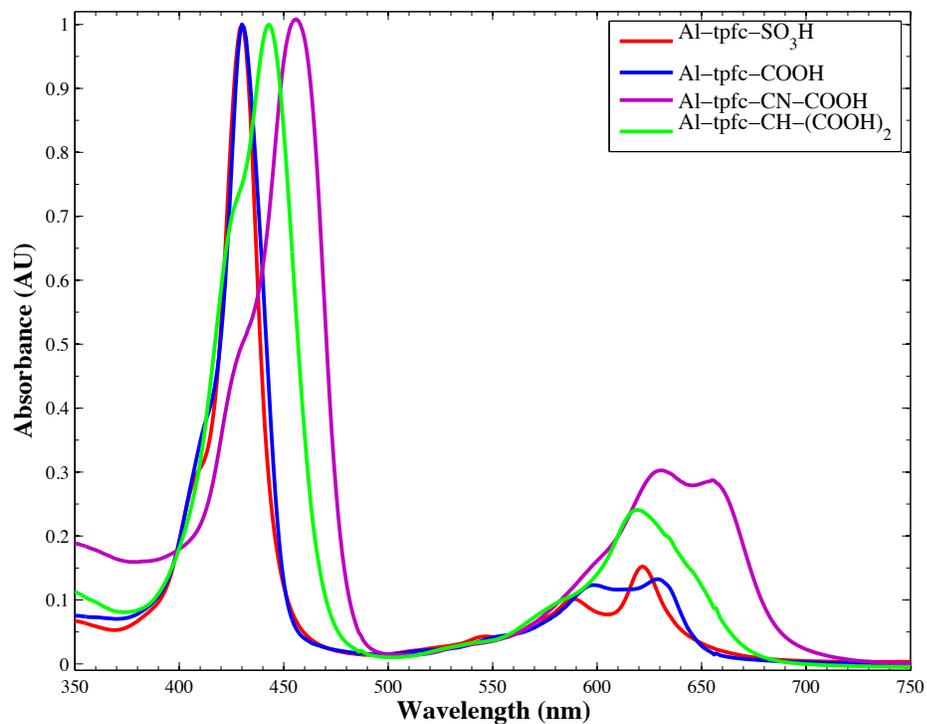
Figure 3.5. Absorbance spectra of aluminum corroles in acetonitrile. Spectra were normalized at the Soret band.
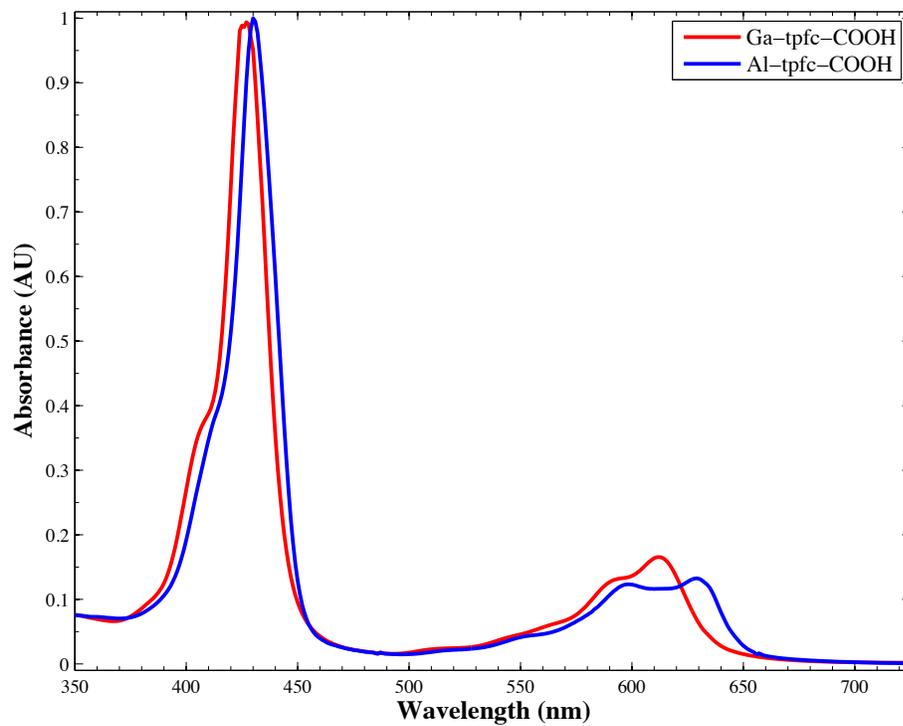
Figure 3.6. Absorbance spectra comparing the effect of aluminum and gallium for mono-COOH substituted tpfc. Spectra were taken in acetonitrile and normalized at the Soret band.
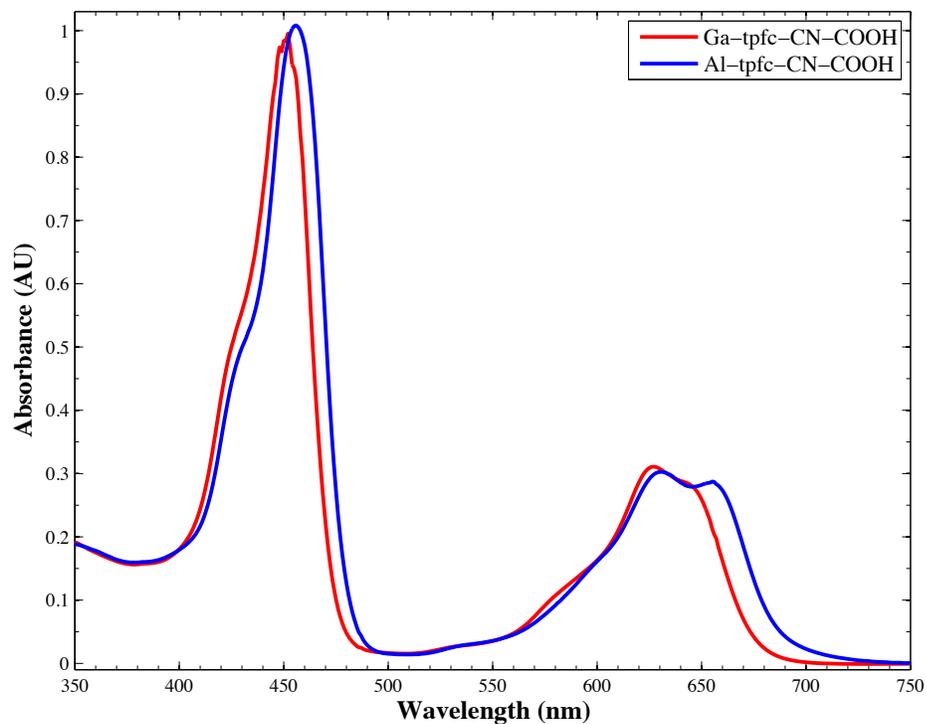
Figure 3.7. Absorbance spectra comparing the effect of aluminum and gallium for mono-CN-COOH substituted tpfc. Spectra were taken in acetonitrile and normalized at the Soret band.
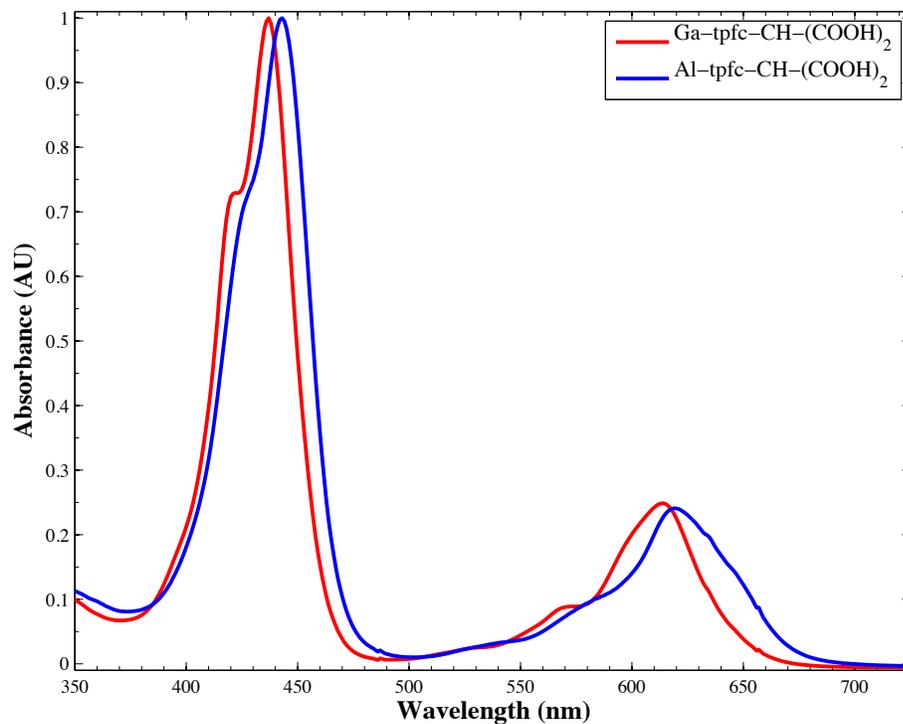
Figure 3.8. Absorbance spectra comparing the effect of aluminum and gallium for mono-CH-(COOH)$_2$ substituted tpfc. Spectra were taken in acetonitrile and normalized at the Soret band.
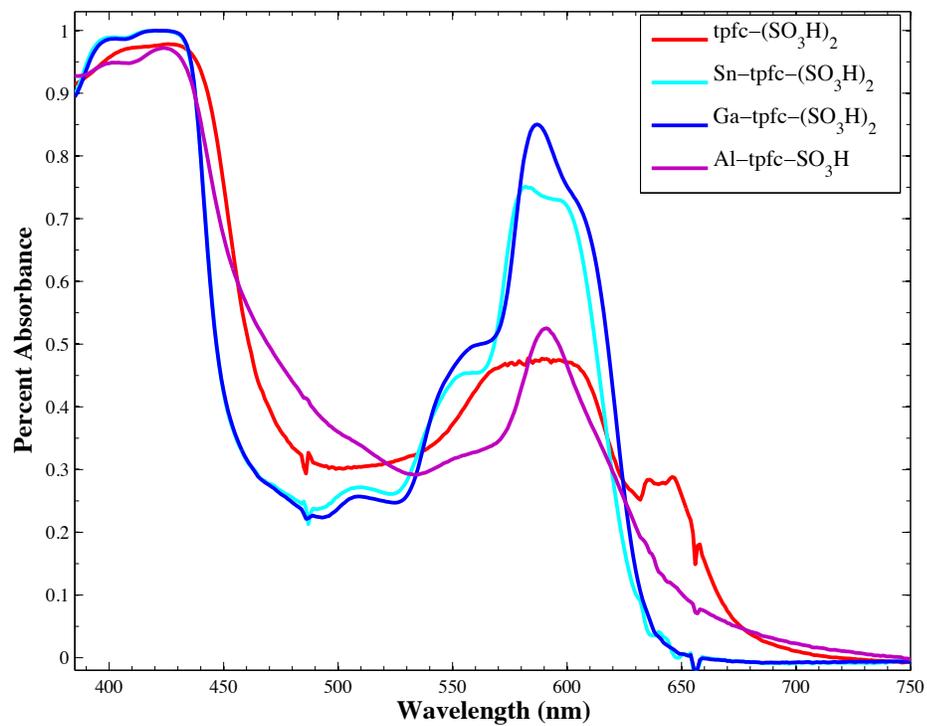
Figure 3.9. Absorbance spectra of sulfonated corroles adsorbed on TiO_2. Spectra were in air and normalized at the Soret band.
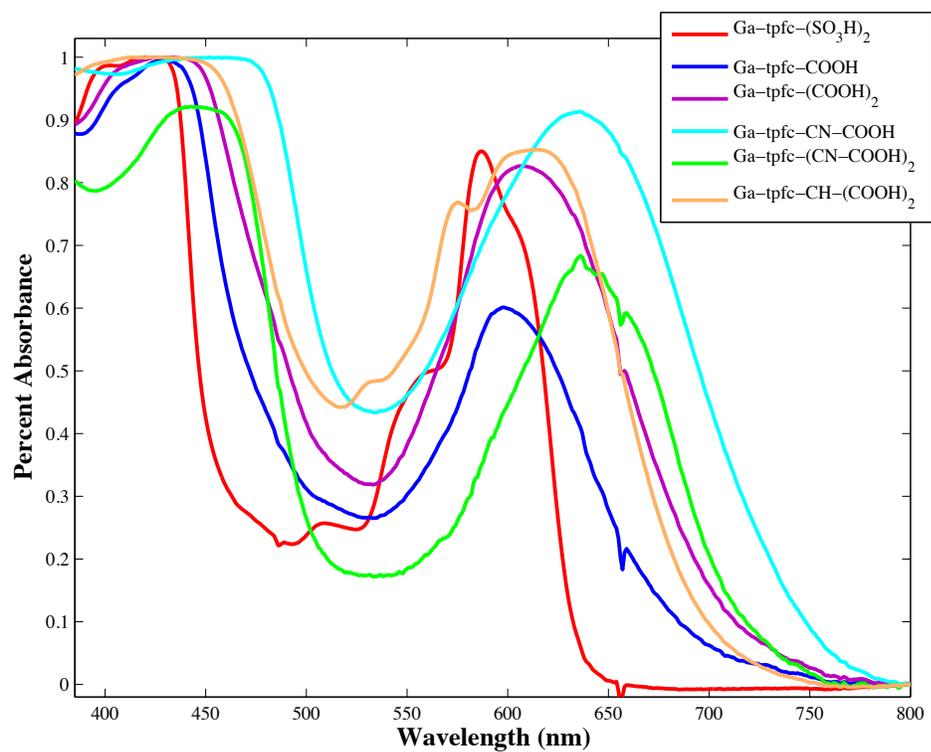
Figure 3.10. Absorbance spectra of gallium corroles adsorbed on TiO_2. Spectra were in air and normalized at the Soret band.
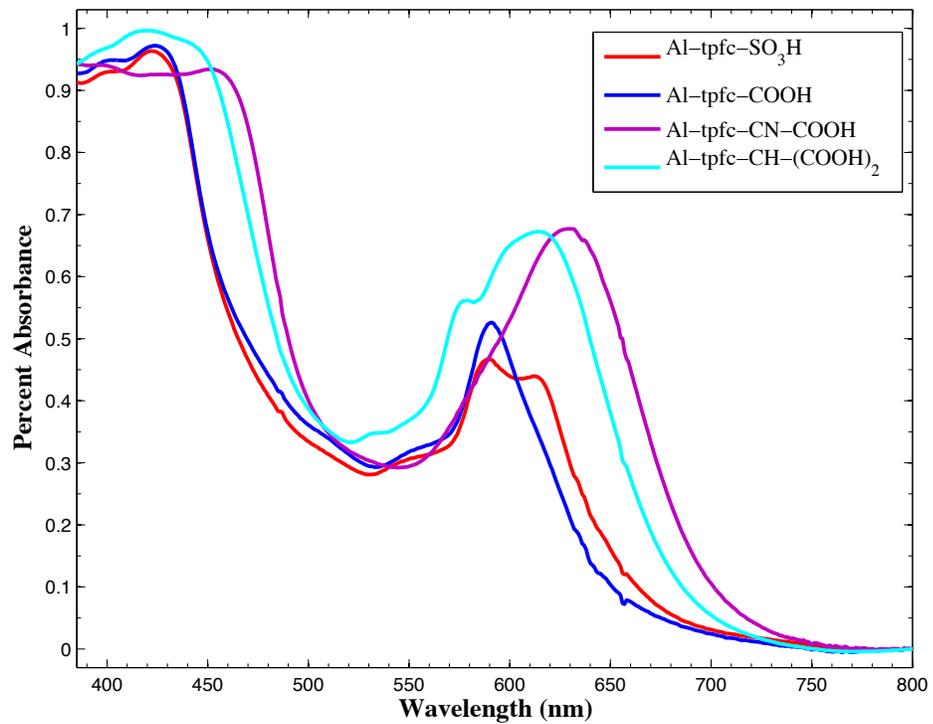
Figure 3.11. Absorbance spectra of aluminum corroles adsorbed on TiO_2. Spectra were in air and normalized at the Soret band.
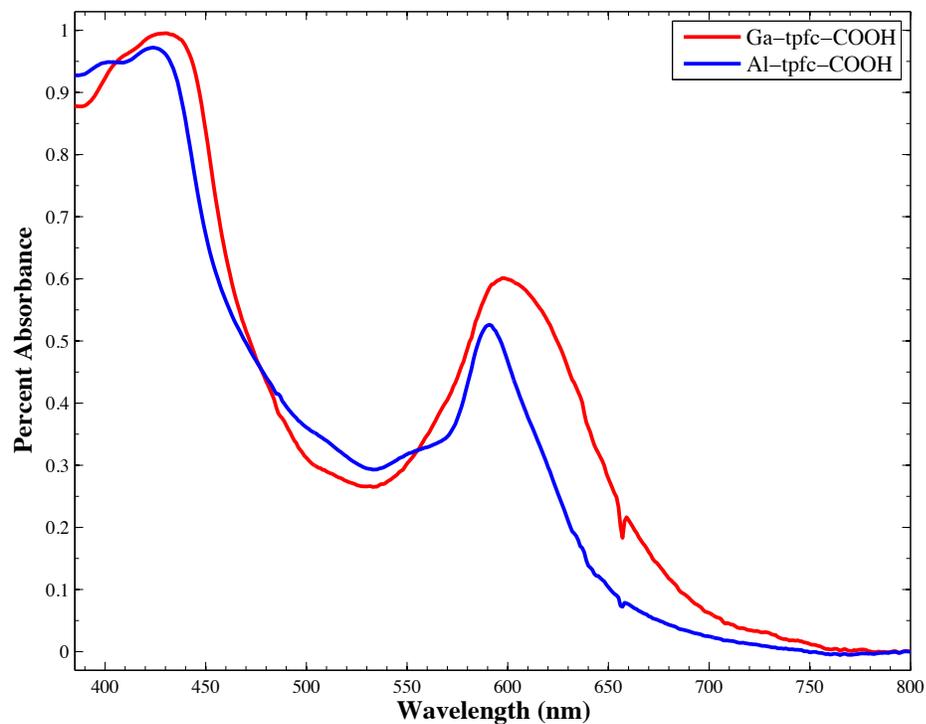
Figure 3.12. Absorbance spectra comparing the effect of aluminum and gallium for mono-COOH substituted tpfc. Spectra were taken in air and normalized at the Soret band.
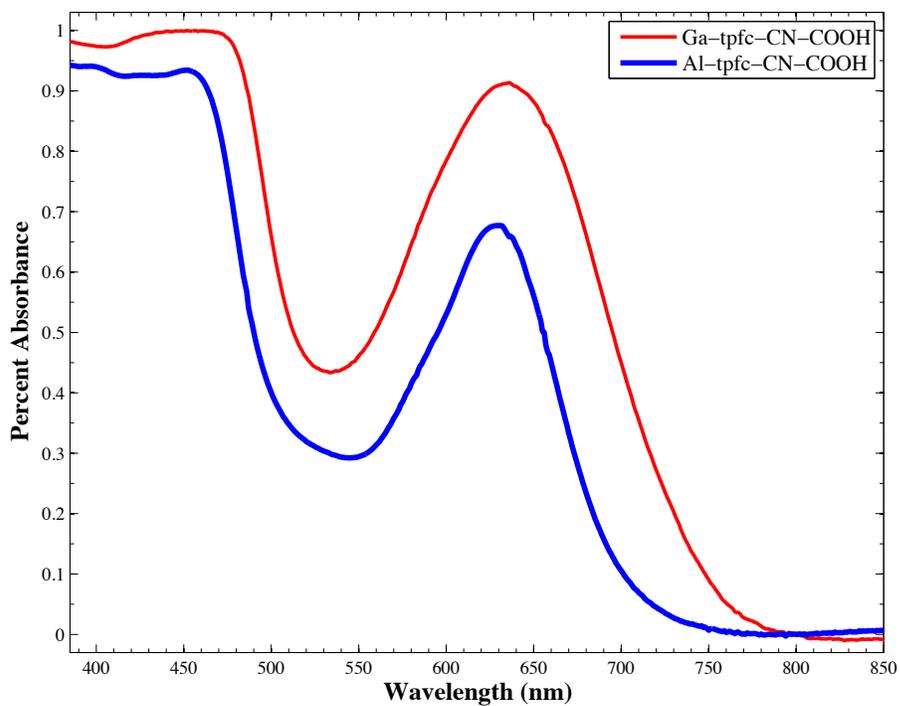
Figure 3.13. Absorbance spectra comparing the effect of aluminum and gallium for mono-CN-COOH substituted tpfc. Spectra were taken in air and normalized at the Soret band.
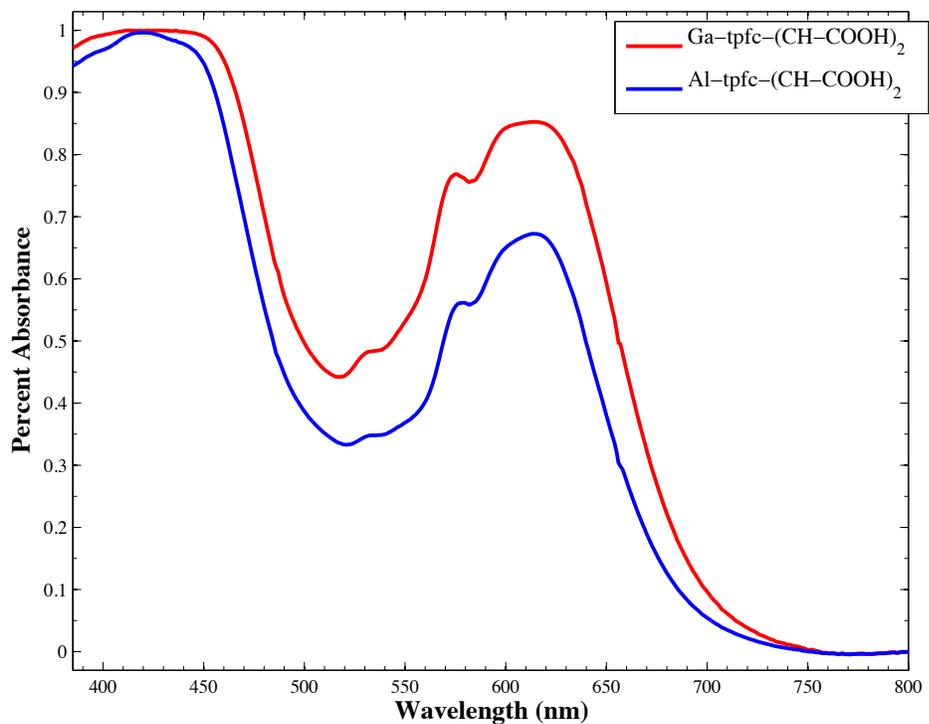
Figure 3.14. Absorbance spectra comparing the effect of aluminum and gallium for mono-CH-(COOH)$_2$ substituted tpfc. Spectra were taken in acetonitrile and normalized at the Soret band.

IR Spectroscopy

The IR spectra of corroles bound to TiO_2 can give insight into the nature of binding of corroles to TiO_2.[92-94] The N3 dye and Ga-CN-COOH corrole both had a strong band at $2100cm^{-1}$ for the –CN stretch of the N3 dye and $2200cm^{-1}$ for the –CN stretch of the Ga-CN-COOH corrole (Figures 3.16 and 3.17). For N3 and Ga-CN-COOH the-CN stretch did not change when comparing bound and unbound spectra which indicated that the dyes did not bind to TiO_2 by using the CN groups as in $Fe^{II}(CN)_6^{4-}$ sensitized TiO_2.[95] The IR spectra of N3 was normalized to the strong -CN band at approximately $2100cm^{-1}$. In the IR spectra of unbound N3 dye, a strong peak is observed at $1700cm^{-1}$, which is where free carboxylic acid groups appear. In the spectra of N3 bound to TiO_2, peaks at $1614cm^{-1}$ and $1384cm^{-1}$ appear. These peaks are due to the asymmetric and symmetric stretching of the bound carboxylic acid.[92, 94] The peak at $1700cm^{-1}$ can also still be seen in the bound spectra indicating there is still some free carboxylic acid present. Because the stretch at $1700cm^{-1}$ is still present, this indicates that N3 dye is bound in either a bidentate or bridging mode.[92]

All corrole IR spectra exhibited very similar spectra to one another as well as porphyrins (Figures 3.17 – 3.21). All corrole spectra showed the same stretches between $2800cm^{-1}$ and $3000cm^{-1}$ that were assigned to the porphyrin aromatic C-H stretching. The spectra for all the corroles were similar to each other and porphyrins between $1550cm^{-1}$ and $900cm^{-1}$ with slight variations due to the missing meso carbon and various β-substituents. This study focused primarily on the investigation of binding of gallium corroles to TiO_2. All corroles that were not bound to TiO_2 with carboxylic acid groups displayed small bands near $1700cm^{-1}$ that belonged to the free carboxylic acids. When

the corroles with carboxylic acids are bound to TiO_2 they all displayed new bands appearing at approximately $1610cm^{-1}$ for the asymmetric carboxylic stretch and $1370cm^{-1}$ symmetric carboxylic stretch. Unlike the spectra of bound and unbound N3 dye the corroles exhibited stronger asymmetric stretching than symmetric stretching. The ratio of asymmetric to symmetric stretching for N3 was approximately 1:1, but for the corroles the ratio of asymmetric to symmetric stretching was approximately 3:1. One interesting note was the increase of free carboxylic stretch of the Ga-tpfc-$(COOH)_2$ when compared to the Ga-tpfc-(COOH). Also, the sulfonic acid presented a unique binding spectra due to its β-substituted sulfonic acid. In the unbound spectra the absorptions in between $1750cm^{-1}$ to $1550cm^{-1}$ were due to the free sulfonic acid groups and were similar absorptions to carboxylic acids. Sulfonic acid binding was observed on spectra of Ga-tpfc-$(SO_3H)_2$ by the appearance of a sulfoxide peak at $1049cm^{-1}$. All corroles indicated that bound to TiO_2 through either carboxylic acid groups or sulfonic acid groups.

N3
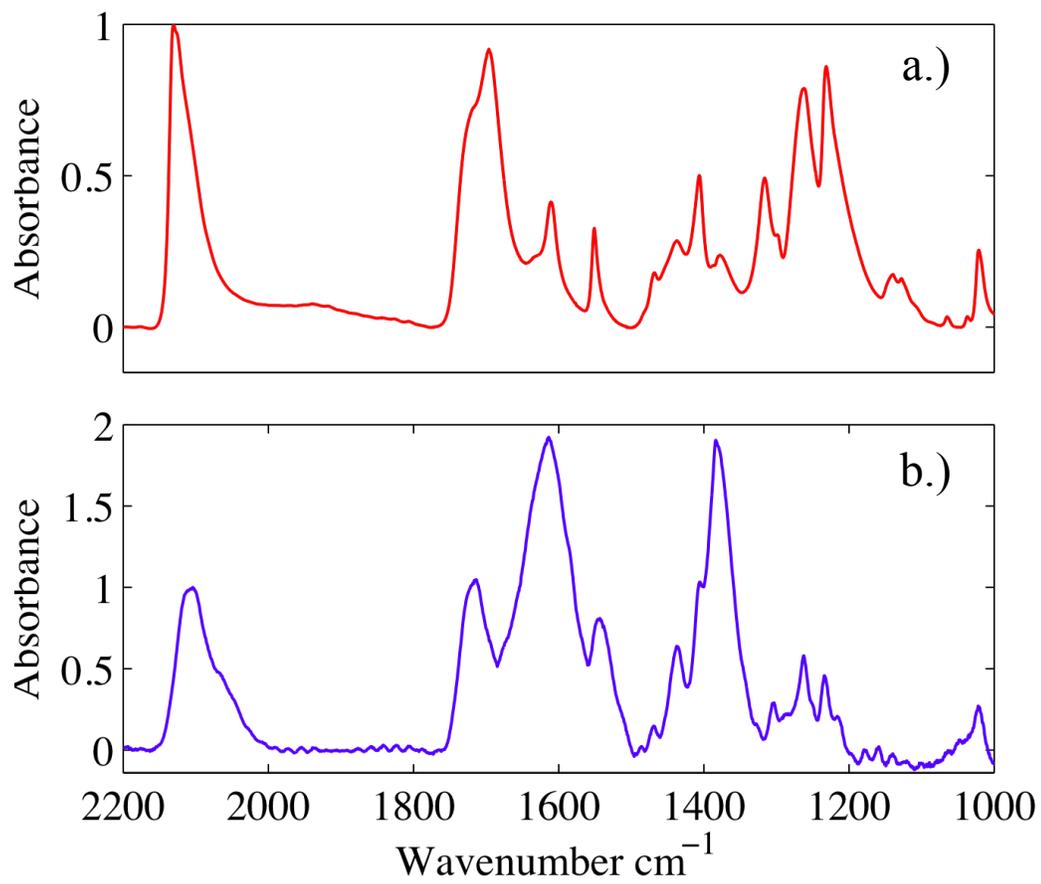
Figure 3.15. FT-IR spectra of N3 dye a.) in dry, powdered form, and b.) adsorbed onto TiO$_2$.
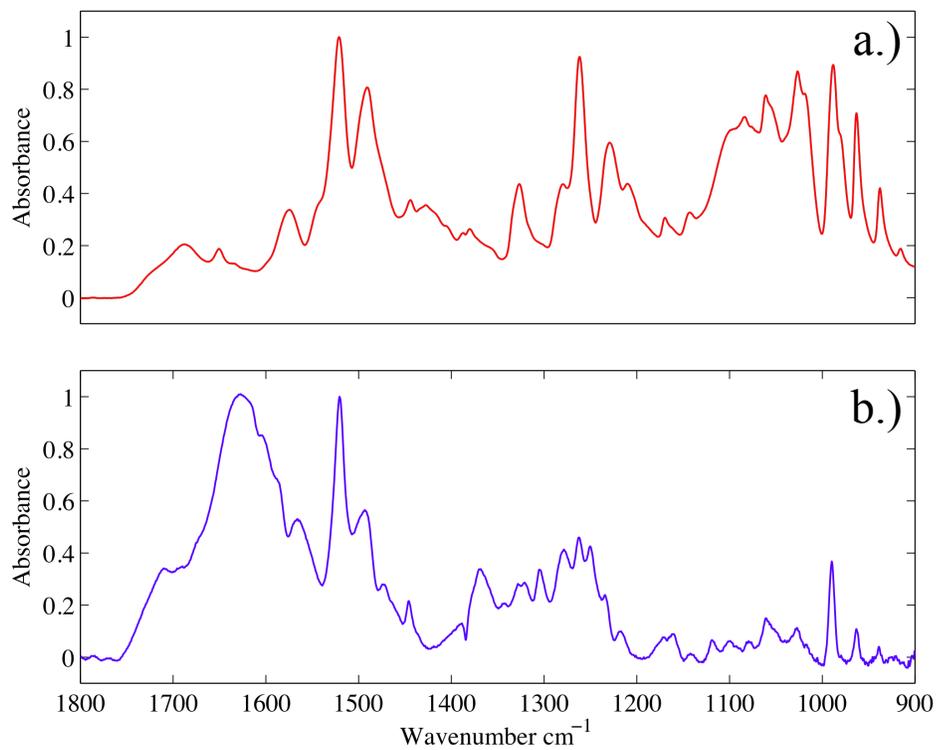
Figure 3.16. FT-IR spectra of Ga-CN-COOH dye a.) in dry, powdered form, and b.) adsorbed onto TiO$_2$.
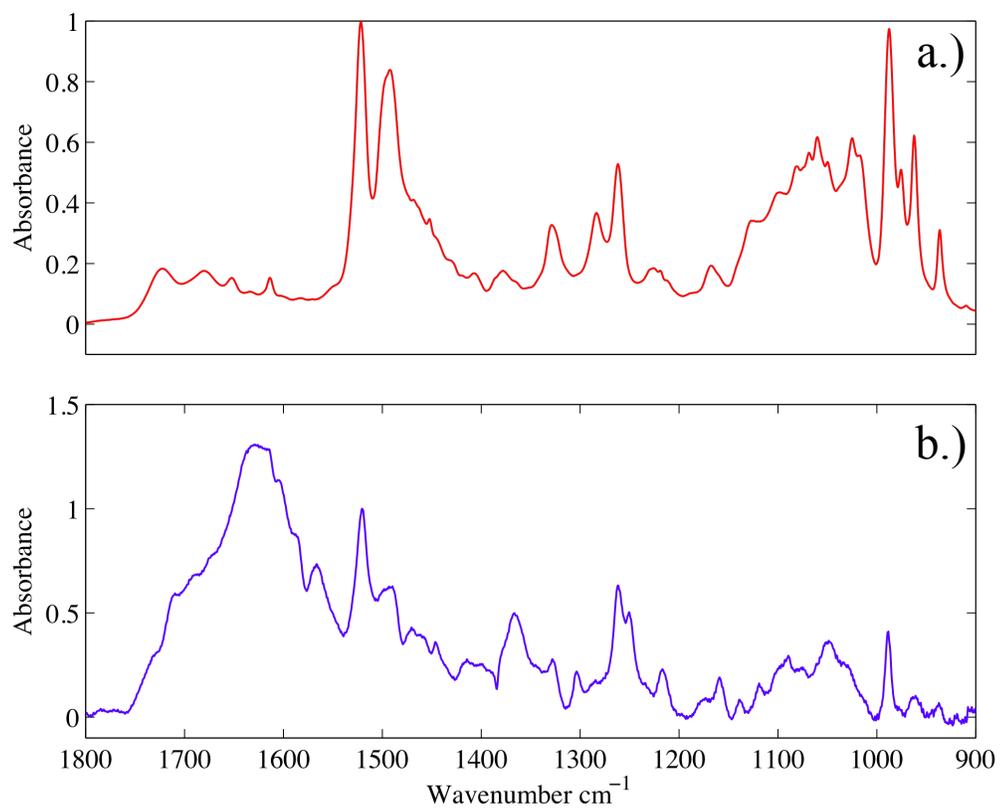
Ga-tpfc-COOH

Figure 3.17. FT-IR spectra of Ga-tpfc-COOH a.) in dry, powdered form, and b.) adsorbed onto TiO_2.

Ga-tpfc-(COOH)$_2$
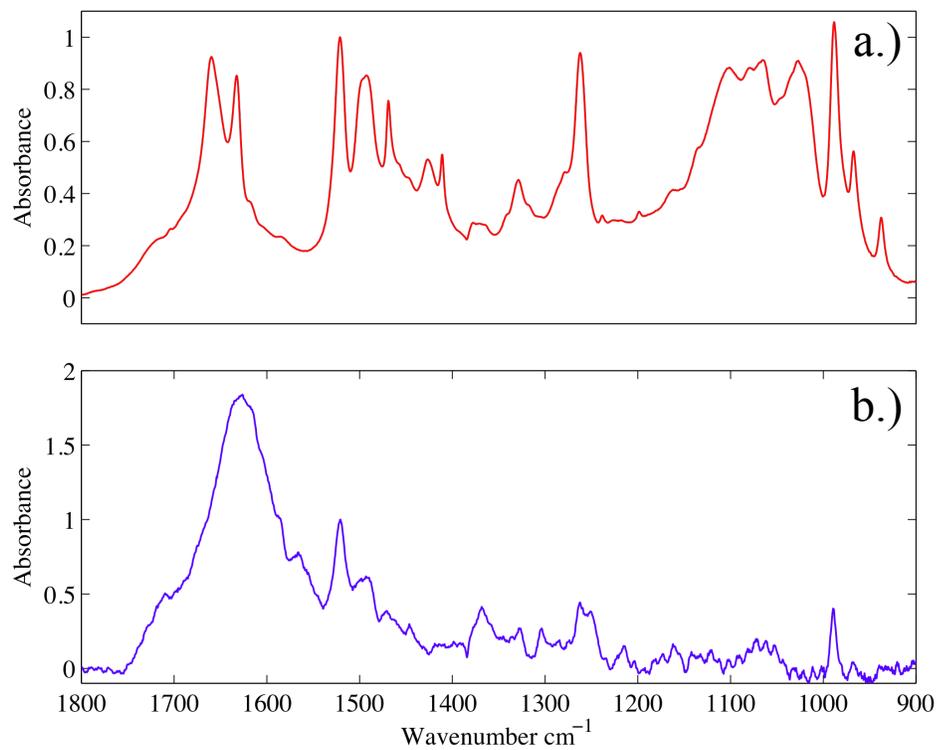
Figure 3.18. FT-IR spectra of Ga-tpfc-(COOH)$_2$ a.) in dry, powdered form, and b.) adsorbed onto TiO$_2$.

Ga-tpfc-CH-(COOH)$_2$
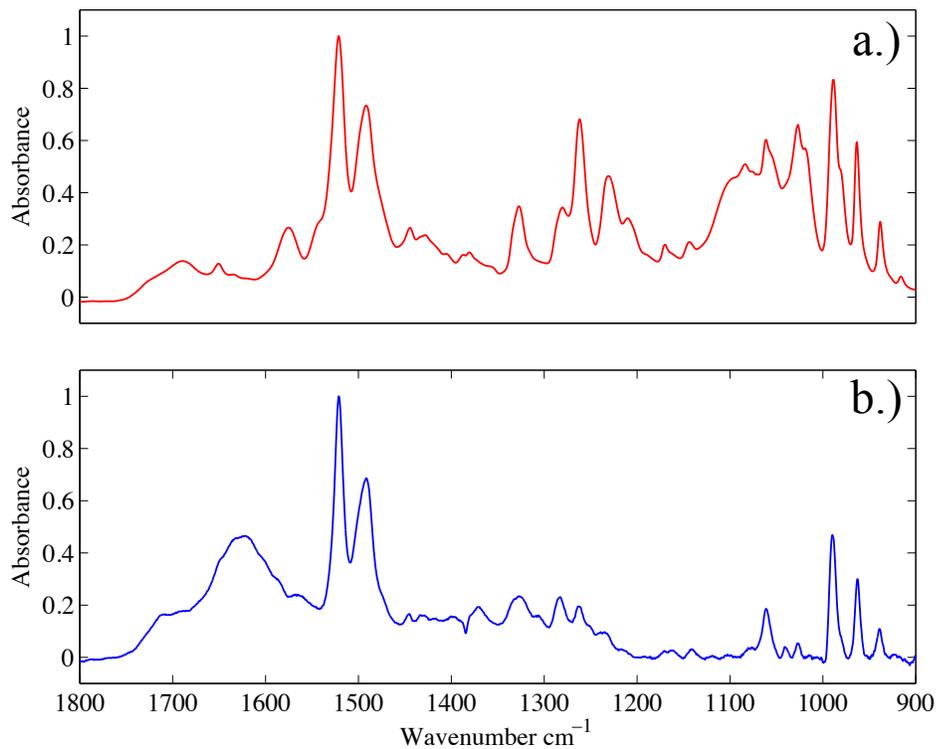
Figure 3.19. FT-IR spectra of Ga-tpfc-CH-(COOH)$_2$ a.) in dry, powdered form, and b.) adsorbed onto TiO$_2$.

Ga-tpfc-(SO$_3$H)$_2$
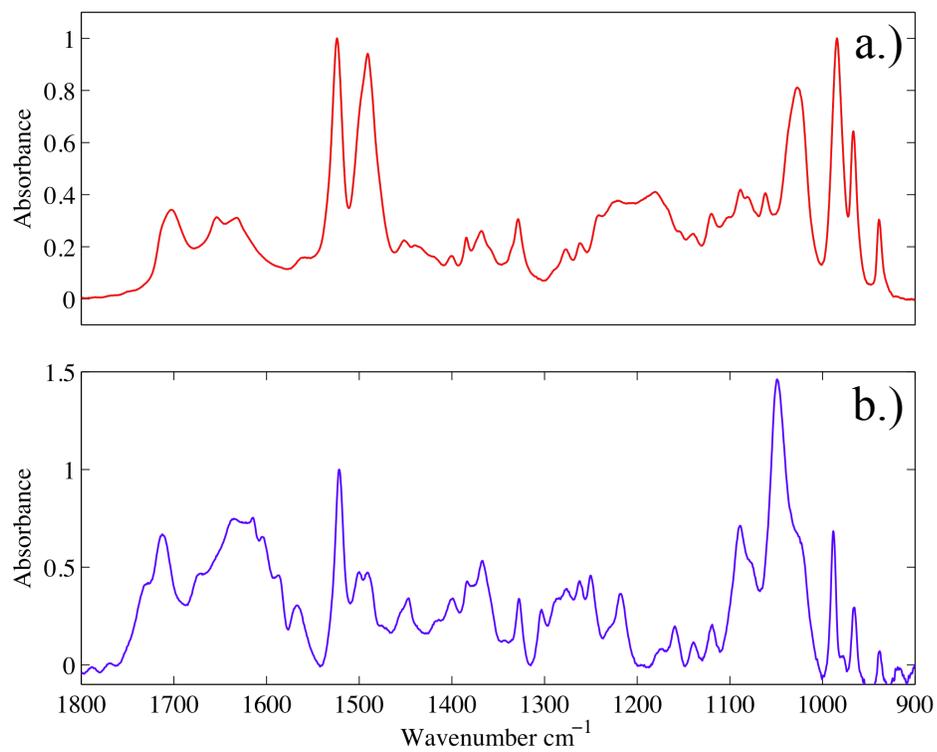
Figure 3.20. FT-IR spectra of Ga-tpfc-(SO$_3$H)$_2$ a.) in dry, powdered form, and b.) adsorbed onto TiO$_2$.

Electrochemistry

Table 3.1 displays all the redox potentials for several gallium and aluminum corroles. All the gallium corroles, except Ga-tpfc-$(COOH)_2$, displayed three oxidation peaks (Figures 3.21 – 3.26). This is in stark contrast to non-substituted gallium corrole which exhibits only one reversible oxidation peak at 0.75V vs. SCE.[83] The most negative oxidation peak seamed irreversible by cyclic voltammetry, but the peaks observed in the differential pulse voltammograms were symmetric and thus indicated the peaks were reversible (Figures 3.21-3.26). The most negative peaks are assigned to the corrole macrocyclic oxidation of acetonitrile ligated gallium corroles. This is because the 2nd oxidation peak is close to the potential of non-substituted gallium corrole. Also, such quasireversible and reversible waves were seen in similar manganese corroles in the presence and absence of axially ligated ligands.[96, 97] Ga-tpfc-$(COOH)_2$ most likely did not display a third oxidation peak in the differential pulse voltammogram because it did not have an axially ligated acetonitrile. Also, when the peak heights of the two most negative peaks of the gallium corroles are compared, Ga-tpfc-COOH, Ga-tpfc-$(COOH)_2$, and Ga-CH-$(COOH)_2$ corrole's two most negative peaks are of the same height. The Ga-CN-COOH corrole's most negative peak is half the height of the next most positive peak which most likely indicated a disproportionate amount of axially ligated corrole to non-axially ligated corrole.

All the aluminum corroles exhibited two reversible one-electron oxidations (Figures 3.27 – 3.30). The absence of a third oxidation peak and because the electrochemistry was conducted in acetonitrile indicates that the axially ligated pyridine on the aluminum corroles is less labile than the pyridine axially ligated to the gallium.[89]

The Al-tpfc-COOH, Al-tpfc-CN-COOH, and Al-tpfc-CH-(COOH)$_2$ corrole's first oxidation was almost exactly at the same potential as their gallium analogues. For the Al-tpfc-COOH, Al-tpfc-CN-COOH, and Al-tpfc-CH-(COOH)$_2$, the second oxidation peak was approximately 200mV more negative than their gallium analogues. The shift to more negative potential of the second oxidation peak is similar to observations in other metalloporphyrins and corroles in which the electronegativity of the metal correlates to the shifts in redox potential of the corrole macrocycle (Sn^{IV}>Ga^{III}>Al^{III}>Mn^{III}).[98] The less electronegative the metal is; the more negative the redox potential for the porphyrin macrocycle. When comparing the different redox potential of corroles with different binding groups, it is interesting to note that the binding group does not significantly affect the redox properties as seen in osmium and ruthenium polypyridyl compounds (Table 1.1) where the addition of more carboxylic acid groups to ruthenium polypyridyl compounds can significantly shift their redox potentials.[20]

Because the second oxidation shifts to more negative potential with the metal, it is believed that the highest one electron oxidation of the gallium and aluminum corroles is from the macrocycle and not the metal. Also, because the first oxidations of the aluminum and gallium corrole analogues were similar, this would indicate that the first oxidation is determined by the β-substituent and not the metal. Further evidence that the oxidations of the gallium and aluminum corroles are from the macrocycle is that the EPR spectra of oxidized non-substituted gallium corrole shows no evidence of Ga^{IV}. Oxidation to Al^{IV} is very unlikely due to its high ionization energy (120eV). The 1st oxidation peak of the corroles can be considered the electrochemical HOMO. It is from

this 1st oxidation that an electron would be excited from and injected into TiO_2. Also the

1st oxidation of the corroles are similar to ground state redox potential of N3.[55]

	1st	2nd	3rd
Ga-tpfc-(SO$_3$H)$_2$	0.640	0.750	1.275
Ga-tpfc-COOH	0.620	0.765	1.210
Ga-tpfc-(COOH)$_2$	0.680	1.305	
Ga-tpfc-CN-COOH	0.650	0.820	1.305
Ga-tpfc-CH-(COOH)$_2$	0.590	0.750	1.255
Al-tpfc-SO$_3$H	0.560	1.060	
Al-tpfc-COOH	0.615	1.120	
Al-tpfc-CN-COOH	0.575	1.055	
Al-tpfc-CH-(COOH)$_2$	0.600	1.115	

Table 3.1. Tabulated 1st, 2nd, and 3rd oxidation peaks as determined by differential pulse

voltammetry. All potentials are referenced to a standard calomel electrode.
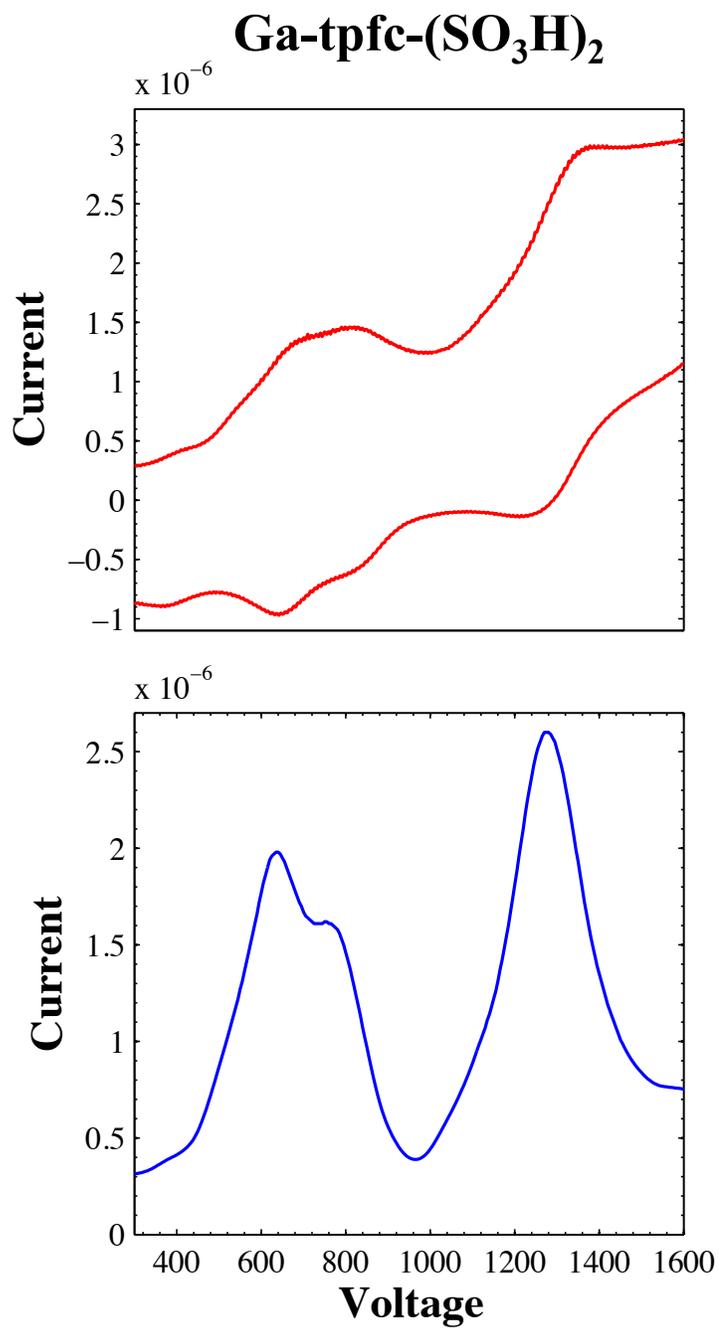
Ga-tpfc-(SO$_3$H)$_2$

Figure 3.21. Cyclic voltammetry (red) and differential pulse voltammetry (blue) of Ga-tpfc-(SO$_3$H)$_2$.

Ga-tpfc-COOH
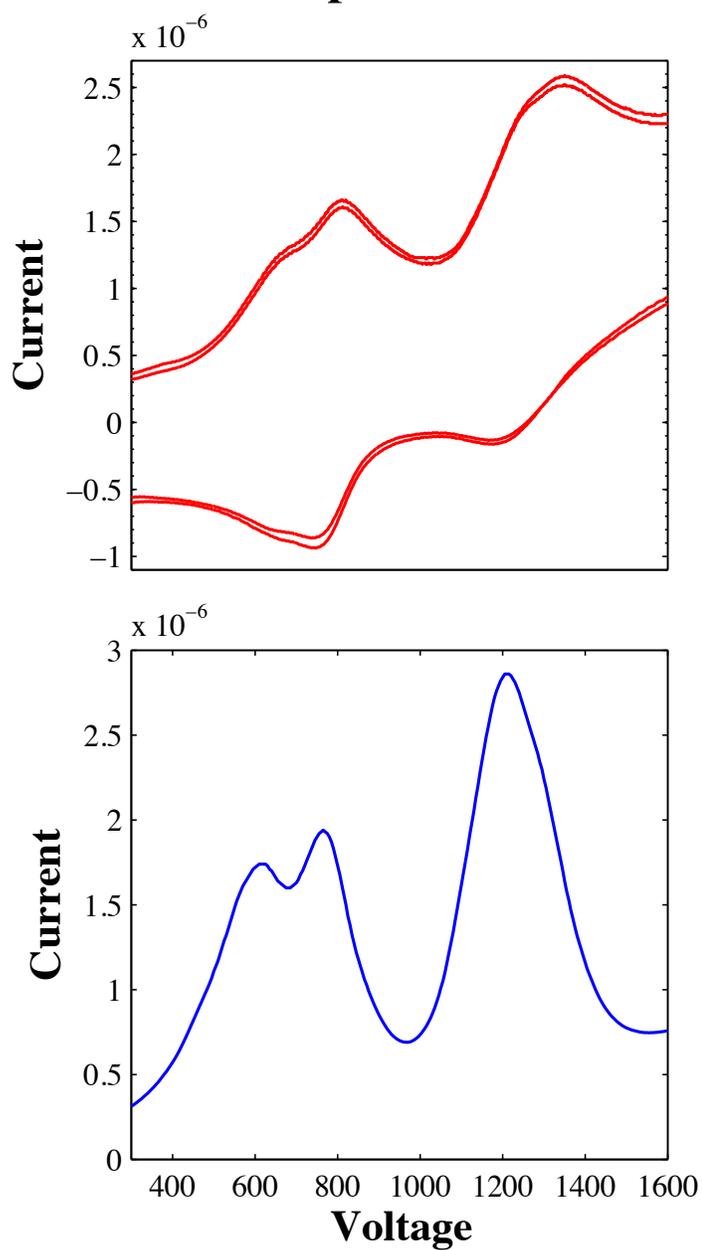
Figure 3.22. Cyclic voltammetry (red) and differential pulse voltammetry (blue) of Ga-tpfc-COOH.
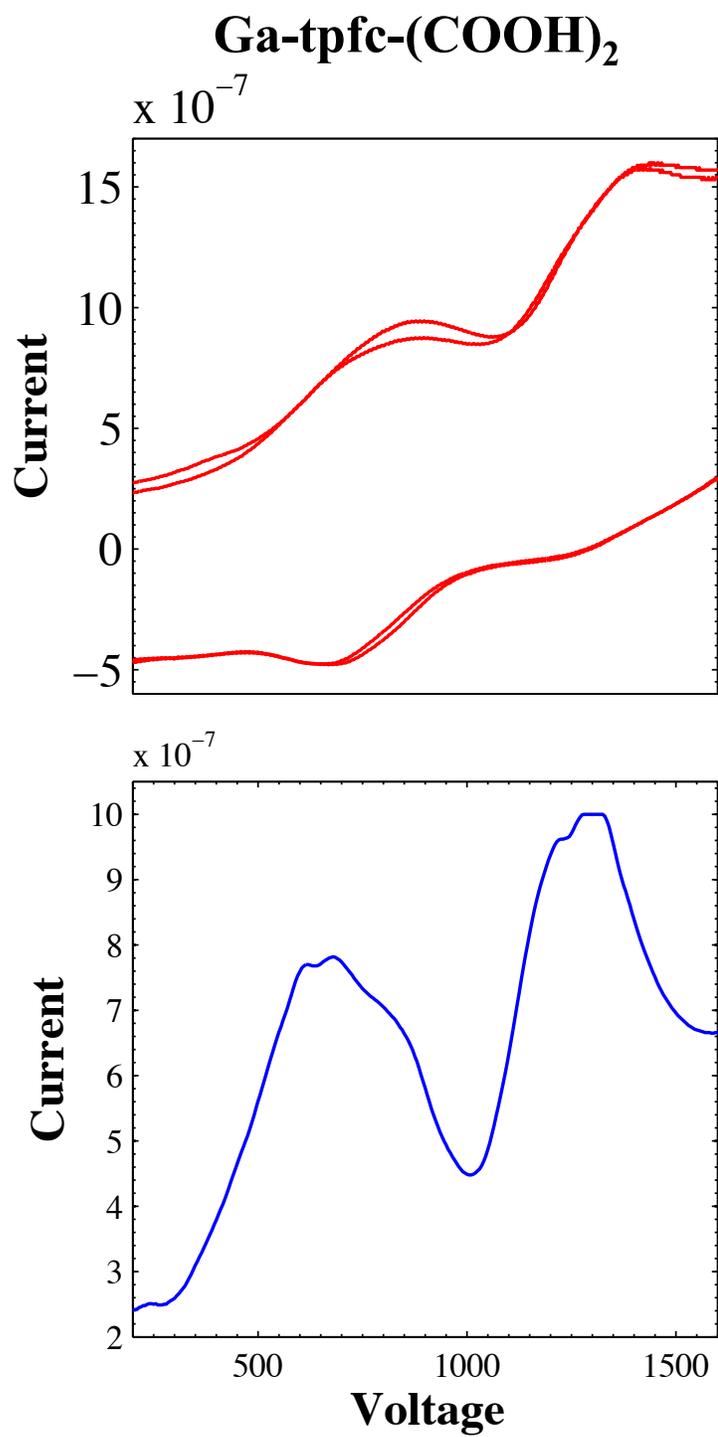
Ga-tpfc-(COOH)$_2$

Figure 3.23. Cyclic voltammetry (red) and differential pulse voltammetry (blue) of

Ga-tpfc-(COOH)$_2$.

Ga-tpfc-CN-COOH
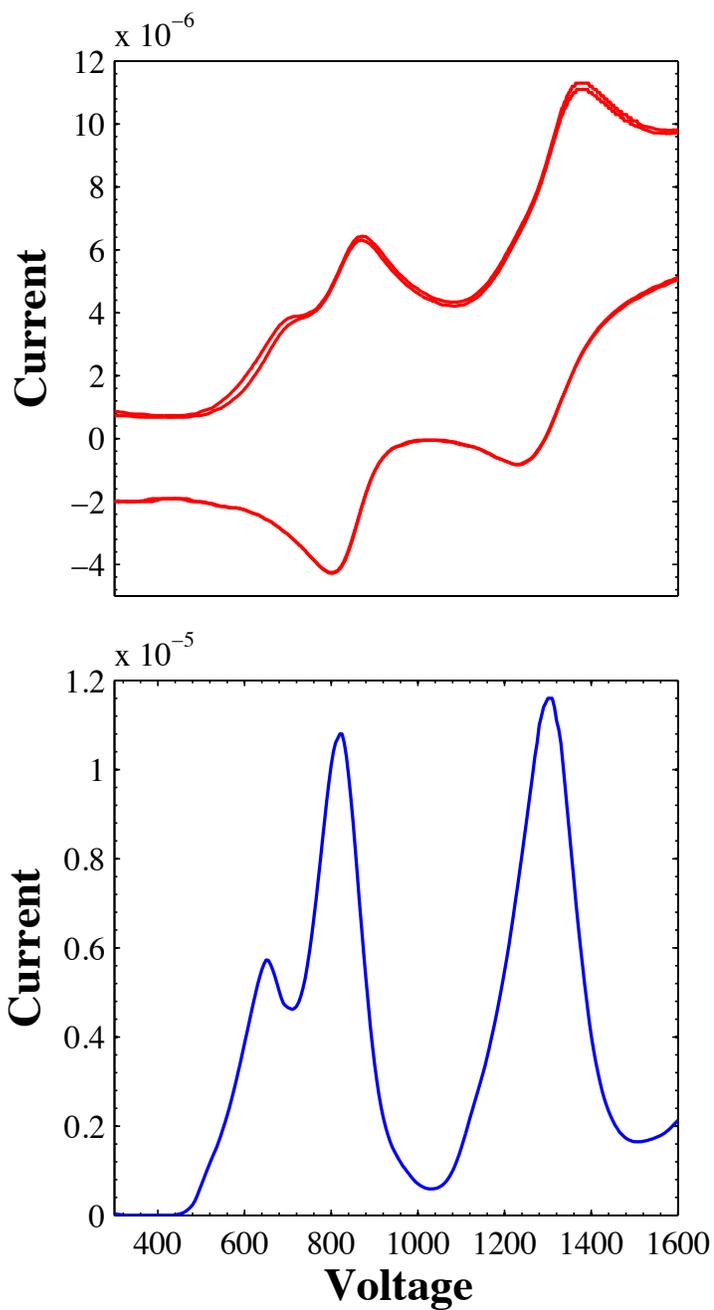
Figure 3.24. Cyclic voltammetry (red) and differential pulse voltammetry (blue) of Ga-tpfc-CN-COOH.
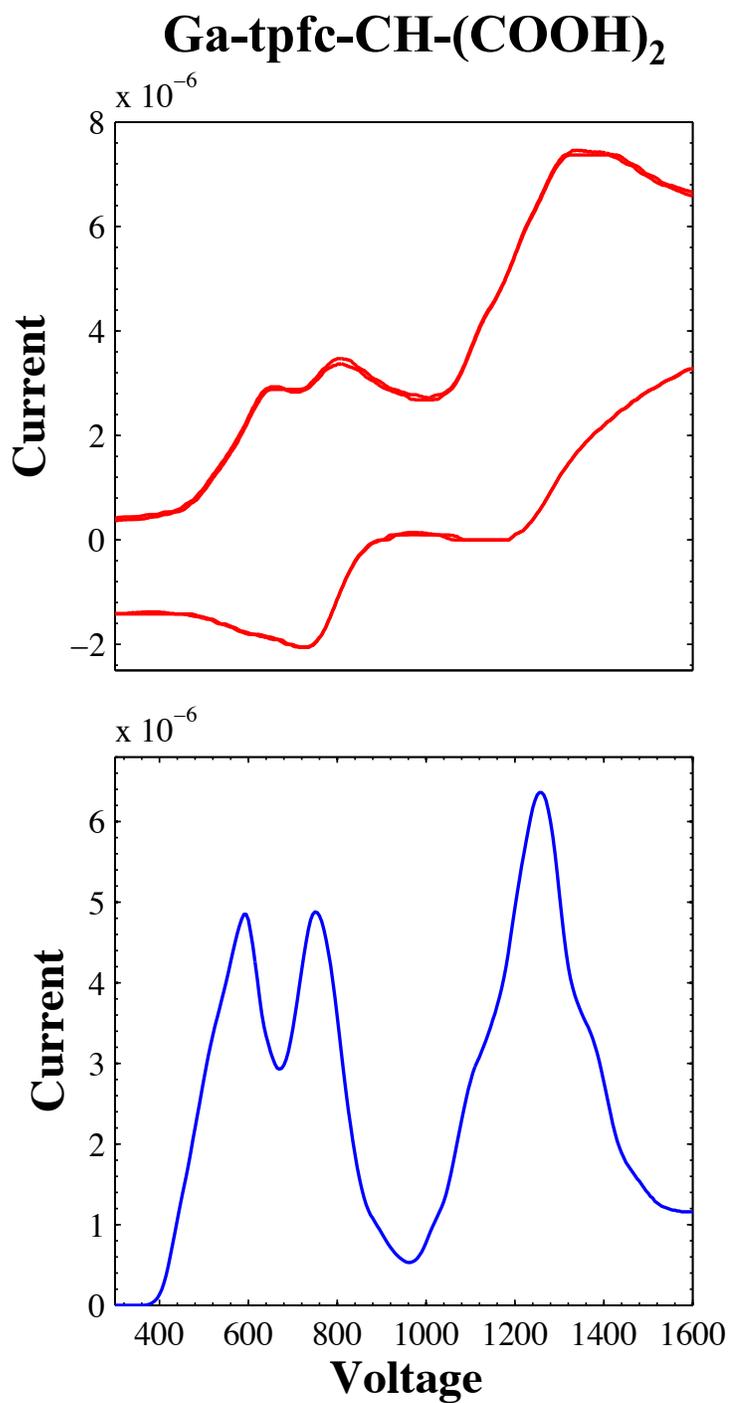
Ga-tpfc-CH-(COOH)$_2$

Figure 3.25. Cyclic voltammetry (red) and differential pulse voltammetry (blue) of Ga-tpfc-CH-(COOH)$_2$.

Al-tpfc-SO$_3$H
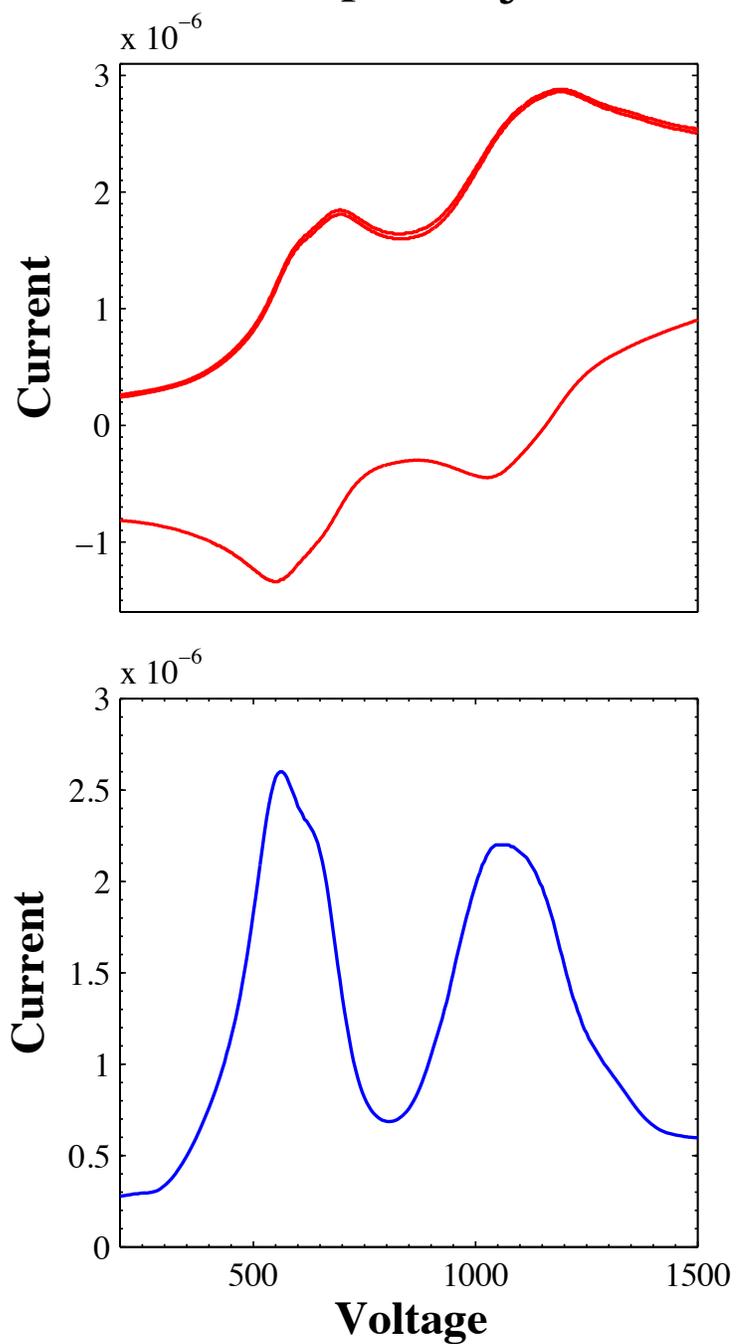
Figure 3.26. Cyclic voltammetry (red) and differential pulse voltammetry (blue) of Ga-tpfc-(SO$_3$H)$_2$.

Al-tpfc-COOH
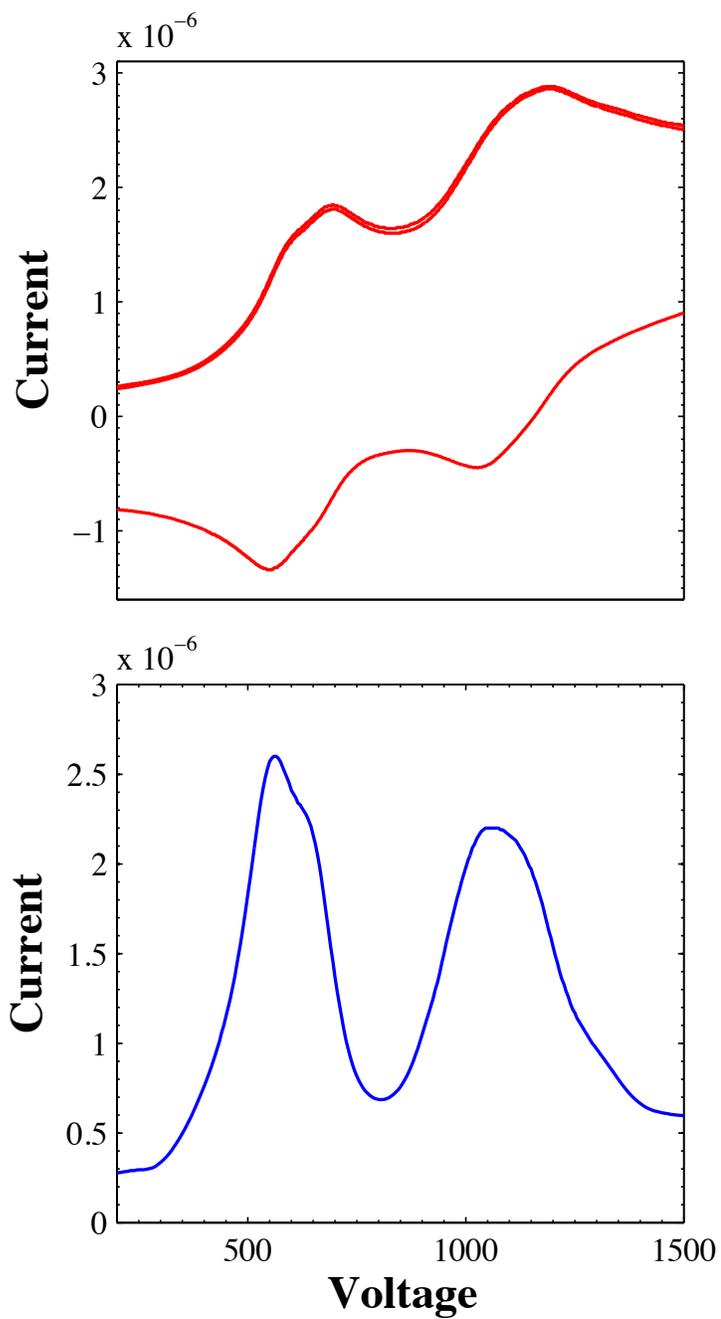
Figure 3.27. Cyclic voltammetry (red) and differential pulse voltammetry (blue) of Al-tpfc-COOH.
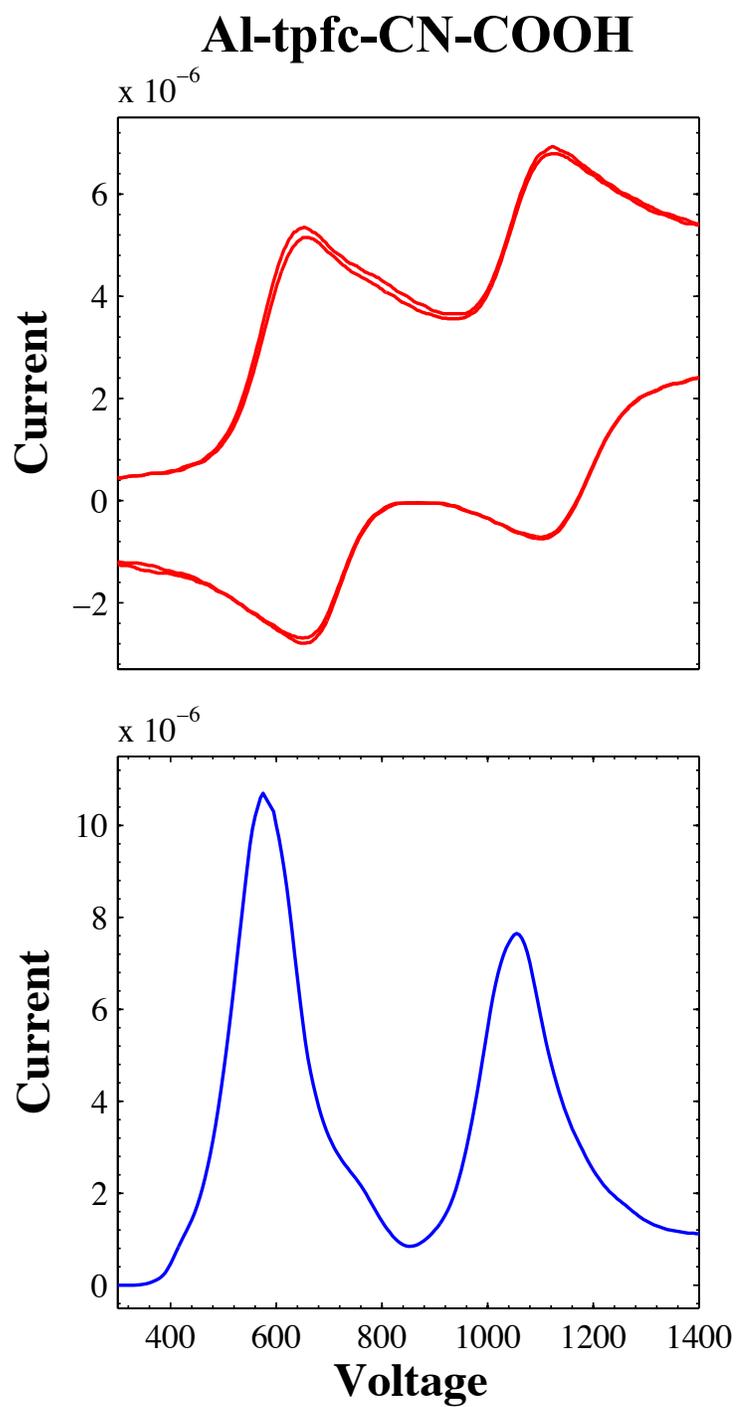
Al-tpfc-CN-COOH

Figure 3.28. Cyclic voltammetry (red) and differential pulse voltammetry (blue) of Al-tpfc-CN-COOH.
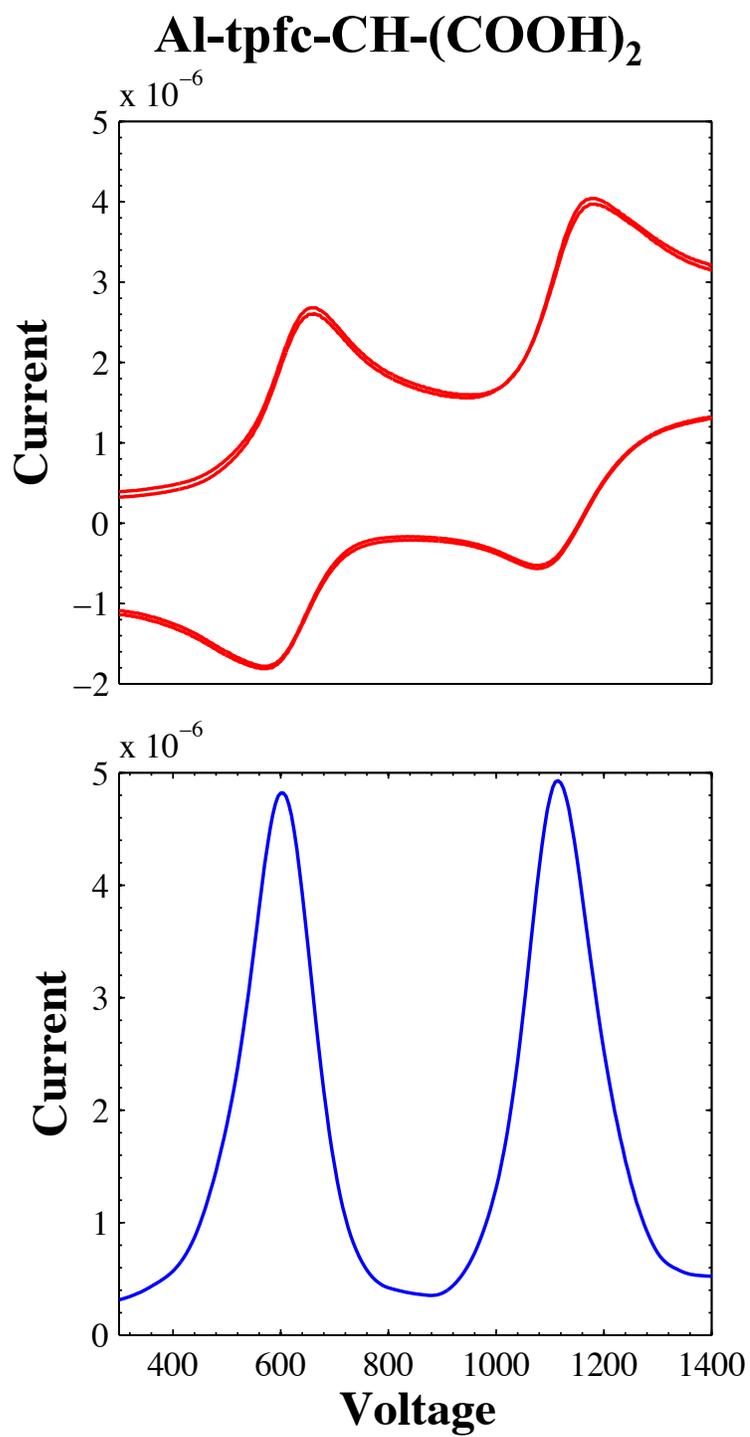
Al-tpfc-CH-(COOH)$_2$

Figure 3.29. Cyclic voltammetry (red) and differential pulse voltammetry (blue) of Al-tpfc-CH-COOH.

Conclusions

Electronic spectroscopy, IR spectroscopy, and electrochemistry further elucidated the effects caused by β-substitution and metal substitution. UV-Vis indicated that an increase in the absorption of red photons is increased by the addition of π-conjugated linkers. For corroles with –CN groups the extinction coefficients were approximately doubled when compared to corroles with non π-conjugated linkers. Electronic spectra of gallium corroles were more red shifted than aluminum corroles. Also, by adsorbing the corroles to TiO_2 no significant changes were observed in the UV-Vis. The increased red absorbance of corroles with π-conjugated linkers was conserved.

IR spectroscopy yielded information into the nature of chemisorption of the corroles to TiO_2. All corroles with carboxylic acid displayed free carboxylic acid groups at approximately $1700cm^{-1}$. When the corroles were chemisorbed to TiO_2 they all displayed a large band at approximately $1610cm^{-1}$, indicative of asymmetric stretching of bound carboxylic acids, and a smaller band at approximately $1370cm^{-1}$, indicative of symmetric stretching of bound carboxylic acids. Also, the gallium corrole with β-substituted sulfonic acid groups that was unbound from TiO_2 displayed bands between $1750cm^{-1}$ and $1550cm^{-1}$ assigned to free sulfonic acid groups. A large, sharp band appeared at $1049cm^{-1}$ was assigned to a sulfoxide stretch that appeared on the spectra of Ga-tpfc-$(SO_3H)_2$ bound to TiO_2. The appearance of the sulfoxide peak indicated that the Ga-tpfc-$(SO_3H)_2$ is chemisorbed to the TiO_2 through the sulfonic acid groups.

Electrochemistry elucidated that the oxidations of the corroles were centered on the macrocycle and not the metal. A shift to negative potential of the aluminum corroles was seen in comparison to the more electronegative gallium corrole. Also, aluminum and

gallium corrole β-substituted analogues displayed similar first oxidation potentials. Some gallium corroles had three oxidation potentials, while aluminum corroles only displayed two oxidation potentials. The difference in the number of oxidation potentials was believed to be due the presence of axially ligated pyridine or solvent. Also, the addition of binding groups did not significantly affect the redox potentials of the corroles.

When comparing the UV-Vis spectra with the first oxidation of the corroles, it can be concluded that β-substitution of corroles does not effect the HOMO of the corroles. It stands to reason the red shift of the absorption spectra is most likely due to a decrease in the LUMO level of the corroles.

Chapter 4

Photoelectrochemistry of Corroles

Introduction

In Chapter 3 characterization of the β-substituted gallium and aluminum corroles indicates they are viable candidates for dye sensitization of TiO_2. β-substituted porphyrins have already been demonstrated to be highly efficient in DSSCs with efficiencies as high as 7.1%.[72, 79, 81] Several key factors are needed for a dye to produce an efficient DSSC. The dye must match the visible solar spectrum, have linkers and binding groups that facilitate efficient electron transfer, and have a sufficient enough ground state redox potential to be efficiently regenerated by the redox couple. As seen in Chapter 3, corroles exhibit all of these characteristics. The corroles have carboxylic as well as sulfonic acid groups. Also the binding groups are located on the β-position of the corroles. The β-position of porphyrins has been shown to facilitate electron transfer more readily than the meso-position of porphyrins.[77] Some of the corroles in Chapter 3 also have π-conjugated linkers to the binding groups that are attached to the β-position of the corroles. The π-conjugation at the β-position of porphyrins has been demonstrated to increase the red absorption of nickel porphyrins significantly.[78] The attachment of effective binding groups and linkers at the β-position of the corroles not only increased the red absorption of the corroles, but may also facilitate efficient electron transfer. The IR spectra of the corroles indicated that corroles readily chemisorbed to TiO_2 in much the same fashion as the N3 dye and other carboxlyated ruthenium polypyridyl dyes.[92, 94] Corroles with sulfonic acid groups also chemisorbed to TiO_2. The electrochemistry of corroles also shows that their first oxidation occurs at the same potential as N3 dye which indicates that they should be efficiently reduced by the iodide/tri-iodide redox couple. The characterization of the corroles in Chapter 3 has given strong precedence to their

efficacy in DSSCs. The corroles' β-substituted binding groups provide a means to allow the corroles to chemisorb to TiO₂ and the π-conjugated linkers increased the absorption of red photons. Also, the electrochemistry indicates that the corroles have the proper redox potential to be reduced by the iodide/tri-iodide redox couple.

At first glance, the corrole's absorbance spectra indicated a large decrease in absorbance at the maximum of the solar spectrum due to the split between the Q and B bands. Such a loss of absorbance would indicate that the corroles could never absorb as much light as the N3 dye. When the absorbance spectra of corroles are compared to N3 it is observed that the corroles can absorb more red photons than N3. If one were to consider that there are more red photons than blue photons, it would stand to reason that it is possible for the corroles to be as efficient as N3. By using Equation 4.1, the estimated current (J_{est}) that can be produced by an adsorbed dye can be calculated. The number of photons available

$$J_{est} = \int_{\lambda_a}^{\lambda_b} P_\lambda \times A_\lambda \times \left(\frac{1e}{1p}\right) \times C \qquad \text{Eq. 4.1}$$

at given wavelength in the solar spectrum is given by P_λ. P_λ is then multiplied by the A_λ, which is the percent of light absorbed at a given wavelength by a dye sensitizer. Once the total number of absorbed photons is calculated, the assumption that for every one photon absorbed, one electron is produced is then calculated. Next the number of electrons is converted to Coulombs ©. Because the AM 1.5 solar spectrum is given in power density and the number of photons at a given wavelength are given as photons per second, the current density can be calculated (Table 4.1). From Equation 4.1 the estimated short circuit current of Ga-tpfc-CN-COOH and Ga-tpfc-CH-(COOH)₂ are greater than the short circuit current estimated for the N3 dye. Also, several of the

	Est. J_{sc}
N3	10.53
Ga-tpfc-(SO$_3$H)$_2$	6.53
Fb-tpfc-(SO$_3$H)$_2$	6.18
Sn-tpfc-(SO$_3$H)$_2$	4.95
Ga-tpfc-COOH	8.01
Ga-tpfc-(COOH)$_2$	9.67
Ga-tpfc-CN-COOH	11.45
Ga-tpfc-(CN-COOH)$_2$	7.25
Ga-tpfc-CH-(COOH)$_2$	11.90
Al-tpfc-CN-COOH	9.57
Al-tpfc-CH-(COOH)$_2$	9.16
Al-tpfc-SO$_3$H	6.00
Al- tpfc-COOH	5.96

Table 4.1. Short circuit currents estimated by using the absorptions spectra of corroles absorbed to TiO$_2$ and Equation 4.1.

corroles have estimated short circuit currents that approach N3. Calculating the estimated short circuit currents provides precedence that the corroles are viable sensitizers and can possibly perform better than one of the best dyes in DSSCs. Also, because the estimated short circuit currents are based on the absorption spectra of the corroles, it can be concluded that even though they lack a strong absorbance at the solar maximum, their broad absorption in the red end of the solar spectrum makes up for any losses in absorbance between the corroles' Soret and Q-bands. Equation 4.1 gives precedence that dyes that absorb more red photons, despite a lack of absorbance in the blue can still be potential candidates to increase the efficiency of DSSCs.

Even if the corroles absorbed more red photons than N3, it is possible they may not efficiently inject their photoexcited electrons into the conduction band of TiO_2. This is because the more you red shift the spectra of a dye the smaller the HOMO-LUMO gap becomes. Decreasing the HOMO-LUMO gap either decreases the LUMO or increases the HOMO energy levels. In the corroles the HOMO is relatively constant no matter what binding group or linker is used. This is in stark contrast to ruthenium polypyridyl compounds. Because the electrochemically determined HOMO levels are the same for all the corroles, it can be concluded that the LUMO levels of the corroles are lowered for the corroles that are red shifted. Due to the lowered LUMO levels it is possible that these dyes may not have efficient injection. By conducting a combination of photoelectrochemical measurements under AM 1.5 light and monochromatic spectral response measurements we can determine if the corroles are indeed efficient dyes in DSSCs.

Experimental

Materials

Acetonitrile (Sigma-Aldrich, 99.8% anhydrous), ethanol (Decon Laboratories, Inc., 200 proof), titanium tetrachloride (Fluka, ≥99.8%), lithium iodide (99.9% anhydrous beads), and pyridine (Sigma-Aldrich, 99.8% anhydrous) were all used as received. Pyridinium trifluoroacetate (Sigma-Aldrich, 98%) was purified by dissolving and supersaturating it in acetonitrile. The pyridinium trifluoroacetate salt was precipitated by addition of diethyl ether. The precipitate was then filtered through a medium-porosity glass frit, rinsed with diethyl ether, and dried for 24hrs under vacuum. Iodine (Sigma-Aldrich, ≥99.8%, solid, ACS reagent) was sublimed at $40^{o}C$. All materials were stored under a nitrogen atmosphere in a dry box with the exception of I_2 and ethanol. TiO_2 screen printing paste was purchased from Solaronix under the product name Ti-Nanoxide HT/SP (~9nm sized particles) and used as received. Fluorine doped SnO glass slides (4in x 1in) with a resistivity of 15 Ω cm^{-2} were purchased from Hartford Glass Co., Inc.

Dye Coated Electrodes

Fluorine doped SnO glass slides were first cleaned in soapy water and rinsed with 18 MΩ resistivity water. The slides were subsequently rinsed with acetone, 200 proof absolute ethanol, and dried under nitrogen. Special care was taken to assure no residue was left on the slides in form or spotting or other blemishes. TiO_2 screen printing paste was deposited on the F:SnO slides by screen printing with an AMI Inc. HC-53 screen printer with a 156 mesh polyester screen, with 10.2 μm of MX emulsion (Sefar Printing). The printed films were covered to prevent dust from settling on top and left at room temperature for 1hr. The slides were then dried in a furnace $80^{o}C$ for 1hr before being

sintered at 450$^{\text{o}}$C for 30 minutes in air. The thickness of the TiO_2 layer on F:SnO was measured by a Dektak 3030 profilometer and determined to be ~5 μm thick.

TiO_2 slides for photoelectrochemical experiments were prepared by cutting the 4in x 1in slides into 0.5in x 1inch electrodes. TiO_2 electrodes were cleaned by rinsing with 18 MΩ water and 200 proof absolute ethanol. The TiO_2 electrodes were then dried under nitrogen and the surface of the TiO_2 of the electrodes was covered with 3-4 drops of 0.2M $TiCl_4$ and allowed to soak for eight hours. 0.2M $TiCl_4$ is not very air stable as was prepared from a stable stock solution of 2M $TiCl_4$.[55] After soaking for eight hours in 0.2M $TiCl_4$ the electrodes were rinsed with 18 MΩ water and 200 proof absolute ethanol and dried under nitrogen. The slides were sintered at 450$^{\text{o}}$C for thirty minutes and allowed to cool to 120$^{\text{o}}$C over two hours. The 120$^{\text{o}}$C TiO_2 electrodes were immersed in 200 proof absolute ethanolic solutions of corroles with a concentration of approximately 1 x 10^{-4}M. The slides were immersed while still at 120$^{\text{o}}$C and allowed to soak in the dye solution for 12-24 hours in the dark.

Photoelectrochemistry

A custom, three electrode, electrochemical cell was used in all photoelectrochemistry experiments. The three electrodes were a platinum gauze counter electrode, platinum wire reference electrode (referenced to the solution potential), and a dye coated TiO_2 slide was the working electrode. The distance between the working and counter electrodes was 2mm, which was determined by a silicon rubber spacer. Light from a 150 Xe lamp in an Oriel Lamp Research housing was used to illuminate the photoelectrochemical cell from the backside of the TiO_2. Light first passed through the glass, then the F:SnO$_2$, and finally illuminated the dye coated TiO_2. The light from the

xenon lamp was filtered with a long pass 385nm filter to prevent direct excitation of TiO_2 and an AM 1.5 filter to perfectly match the solar spectrum at AM 1.5. A Solarex, Inc. diode was used to calibrate the light intensity to $100mW/cm^2$ The photoelectrochemical cell was placed an appropriate distance from the lamp that allowed for measurements to be taken at a light intensity of $100mW/cm^2$. A 0.5M LiI/ 0.04M I_2 electrolyte in acetonitrile with 20mM pyridine and 20mM pyridinium trifluoroacetic acid was introduced into the custom photoelectrochemical cell from the lower port. Special care was taken to remove any air bubbles in the cell by tapping and flushing the cell while monitoring the top exit port for bubbles. A BAS 100B potentiostat was used to apply a scanning potential of 20mV s^{-1}. Scans were performed from 200mV to 600mV or -800mV depending on the dye and electrolyte used. Scans always began at 0V. Cell resistances were measured with the BAS 100B poteniostat and were determined to be 50Ω. The final current potential (I-V) curves were corrected for cell potential.

Spectral Response

The light from an Oriel 75W Xe arc lamp was passed through a Spex 1681B spectrometer to obtain monochromatic light from 350nm to 800nm. The monochromatic light was split, by using a quartz glass slide, between a silicon reference diode and the sample. Approximately 10% of the split light was used to illuminate the silicon reference diode. Two plano convex lenses that were f-matched to the monochromater were used to collimate and reimage the light onto the DSSC. Two Princeton Applied Research Model 173 potentiostats were used to measure the current of the reference diode and corrole DSSC. In order to calibrate the monochromatic light intensity and correct for changes in light intensity of the 75W Xe arc lamp, the DSSC was replaced by calibrated photodiode

(UDT Sensors, model UV-50). External quantum yields (EQY) were calculated using Equation 4.2. The external quantum yields were calculated for every 10nm from 350nm to 800nm. The currents for the DSSC and calibrated silicon photodiode were I_{DSSC} and I_{calib}. The currents for the ref diode of the calibrated photodiode and the DSSC were $I_{ref\ DSSC}$ and $I_{ref\ calib}$. EQY$_{calib}$ was obtained from the calibration file obtained from UDT for the model of calibrated photodiode we received. The photodiode was calibrated from 200 to 1100 nm every 10nm. I_{DSSC}, I_{calib}, $I_{ref\ DSSC}$, and $I_{ref\ calib}$ were all collected during spectral response measurements and used to calculate the external quantum yield per wavelength for the DSSC (EQY_{DSSC}).

$$\left(EQY_{DSSC} = \frac{I_{DSSC}\ I_{ref\ calib}}{I_{calib}\ I_{ref\ DSSC}} EQY_{calib} \right)_\lambda$$
Eq. 4.2

Internal quantum yield (IQY) measurements were calculated using Equation 4.3. The internal quantum was calculated on a per wavelength basis. Absorbance spectra of corrole sensitized TiO_2 was taken prior to EQY measurements. In order to calculate IQYs the absorbance spectra of the DSSC was converted from absorbance units to the percent of light absorbed. The converted absorbance spectra was then divided into the EQY_{DSSC} to calculate IQY_{DSSC}.

$$\left(IQY_{DSSC} = \frac{EQY_{DSSC}}{1 - 10^{-abs}} \right)_\lambda$$
Eq. 4.3

Results and Discussion

Photoelectrochemistry

All the corroles measured in this study produced measurable amounts of short circuit current and open circuit voltage (Table 4.2 and Figures 4.1 - 4.3). The corroles with gallium produced higher efficiencies than their aluminum analogues. The

Ga-tpfc-CH-(COOH)$_2$ produced a remarkable efficiency of 2.24%, which is 70% of the efficiency of N3. The Ga-tpfc-(SO$_3$H)$_2$ produced an efficiency of 1.56% and is the most efficient DSSC using a sulfonic acid binding group.[99]   Also, the Ga-tpfc-(SO$_3$H)$_2$ produced the highest open circuit voltage of all the corroles. When the Ga-tpfc-(SO$_3$H)$_2$ is compared to its carboxylated analogue, the currents of the Ga-tpfc-(SO$_3$H)$_2$ and Ga-tpfc-(COOH)$_2$ are the same, but the Ga-tpfc-(SO$_3$H)$_2$ has 70mV more open circuit voltage.   This would seem to indicate the functional group has some effect on the open circuit voltage of DSSCs. This can be reasoned by the fact that dye binding to TiO$_2$ deprotonates the TiO$_2$ in much the same way a basic solution would deprotonate the TiO$_2$ surface. The deprotonation of the TiO$_2$ surface typically moves the conduction band edge of TiO$_2$ to more negative potentials, which would in turn increase the open circuit voltage. Because the Ga-tpfc-(SO$_3$H)$_2$ has six total oxygens to potentially bind to TiO$_2$ compared to the four available oxygen of Ga-tpfc-(COOH)$_2$, it is possible that the Ga-tpfc-(SO$_3$H)$_2$ deprotonates the surface more than the Ga-tpfc-(COOH)$_2$ corrole. The free base tpfc-(SO$_3$H)$_2$ produced an efficiency of 0.82%, which is relatively high when compared to the few examples of non-metallated porphyrins used to sensitize DSSCs.[81] The Sn-tpfc-(SO$_3$H)$_2$ produced negligible current, which has been attributed to its lower LUMO level as a result of the heavy atom effect.[91, 99, 100]   The lowered LUMO of Sn-tpfc-(SO$_3$H)$_2$ prevents efficient injection into the conduction band of TiO$_2$, thus reducing the amount of current produced.

The Ga-tpfc-CN-COOH and Ga-tpfc-CH-(COOH)$_2$ both produced significantly more current than the gallium corroles without β-substituted, π-conjugated linkers. This was also true when comparing the Al-tpfc-CN-COOH and Al-tpfc-CH-(COOH)$_2$ to the

	J_{sc} (mA/cm^2)	V_{oc} (mV)	Fill Factor	Efficiency (η%)
N3	9.76	556	0.58	3.14
Gatpfc-(SO$_3$H)$_2$	4.55	524	0.66	1.56
Sntpfc-SO$_3$H	0.58	348	0.60	0.12
tpfc-SO$_3$H	2.83	444	0.65	0.82
Ga-(COOH)	4.26	460	0.61	1.19
Ga-(COOH)$_2$	4.48	454	0.65	1.32
Ga-CN-COOH	6.48	468	0.62	1.88
Ga-(CN-COOH)$_2$	2.63	408	0.66	0.71
Ga-CH-(COOH)$_2$	7.38	502	0.60	2.24
Al-SO$_3$H	1.65	396	0.67	0.43
Al-COOH	2.45	430	0.64	0.67
Al-CN-COOH	5.60	422	0.61	1.44
Al-CH-(COOH)$_2$	5.10	452	0.63	1.44

Table 4.2. J_{sc}, V_{oc}, fill factors, and efficiency of corroles.

aluminum corroles with non-π-conjugated, β-substituted binding groups. The number of β-substituents also seemed to cause a significant decrease in current when comparing the Ga-tpfc-CN-COOH and Ga-tpfc-(CN-COOH)$_2$ corroles. The Ga-tpfc-COOH and Ga-tpfc-(COOH)$_2$ produced similar currents to one another. When comparing the Al-tpfc-CN-COOH to its gallium analogue, Ga-tpfc-CN-COOH, the aluminum corrole performed significantly better with an efficiency that was double the efficiency of Ga-tpfc-CN-COOH. The Ga-tpfc-CH-(COOH)$_2$ outperformed its aluminum analogue, Al-tpfc-CH-(COOH)$_2$, with an efficiency that was one and a half times greater than its aluminum analogue. Ga-tpfc-COOH corrole was twice as efficient as its aluminum analogue, Al-tpfc-COOH.

The differences in performance can most likely be explained by examining Table 4.2. Because the data in Table 4.2 is based upon Equation 4.1, the estimated short circuit currents give insight into the number of photons absorbed. By examining the UV-Vis spectra of corroles absorbed onto TiO$_2$ in conjunction with the estimated short circuit currents, the difference in measured currents produced is most likely due to the amount of dye absorbed by some of the corroles and the extent of the red absorption of photons by some of the corroles. For example, In Figure 3.10 it can be seen that the absorbance of Ga-tpfc-CN-COOH is slightly greater than that of Ga-tpfc-(CN-COOH)$_2$. Also, because of the decreased absorbance of Ga-tpfc-(CN-COOH)$_2$, the estimated current it can produce is approximately 35% less than the estimated current that Ga-tpfc-CN-COOH can produce. Since the absorbance of the Ga-tpfc-(CN-COOH)$_2$ is less than the absorbance of Ga-tpfc-CN-COOH and they have similar extinction coefficients, one can conclude that Ga-tpfc-CN-(COOH)$_2$ corrole produced less current than the
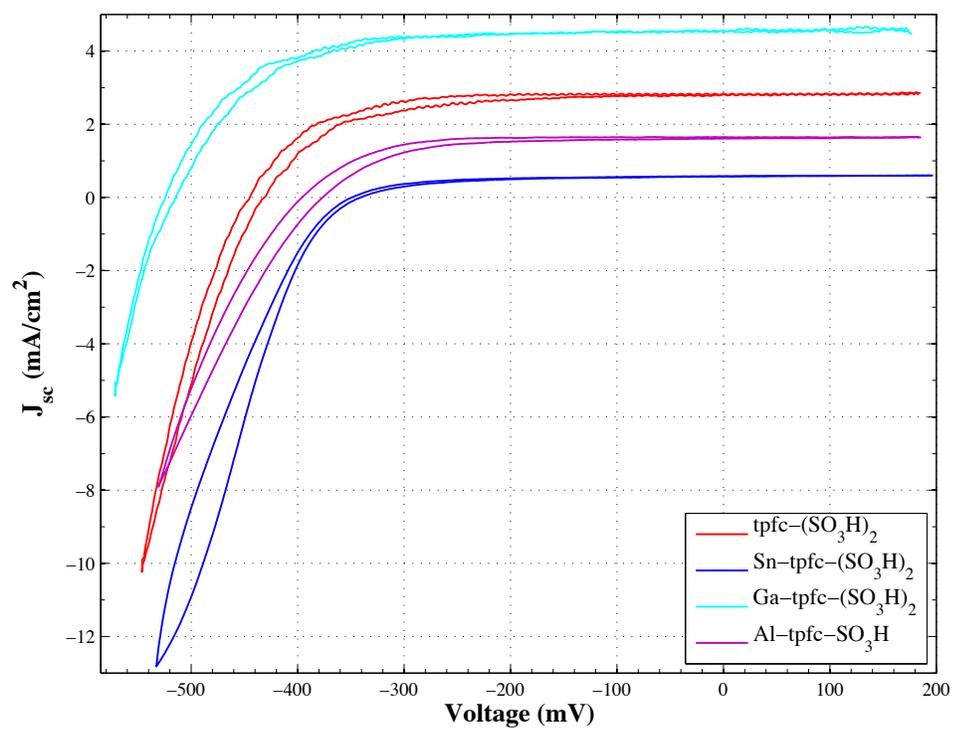
Figure 4.1. Current versus potential characteristics of corroles with sulfonic acid moieties.
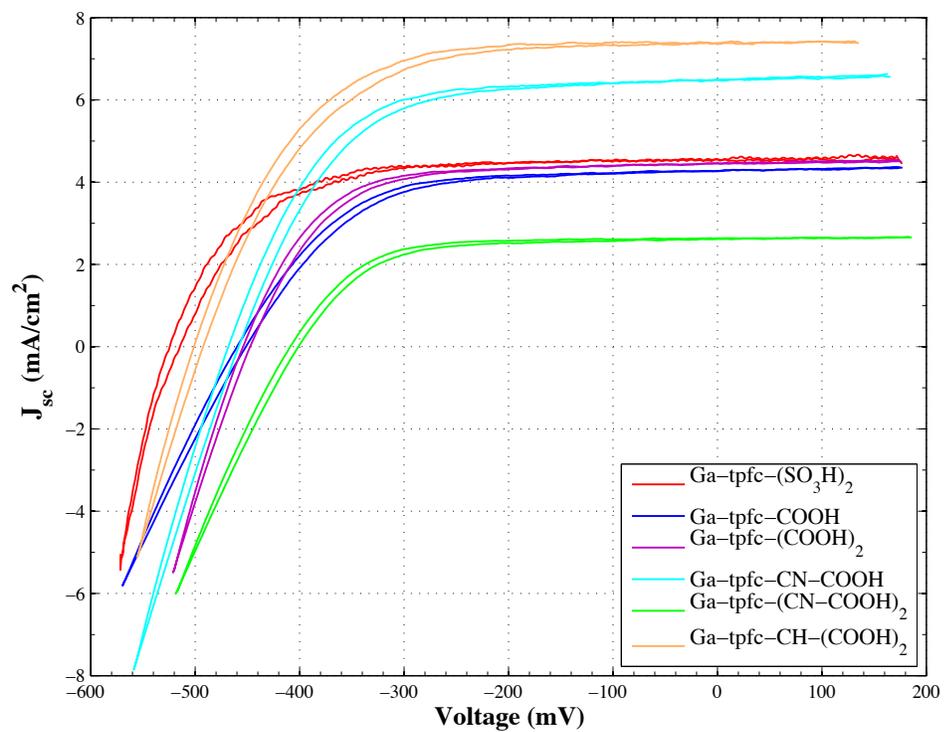
Figure 4.2. Current versus potential characteristics of gallium corroles.
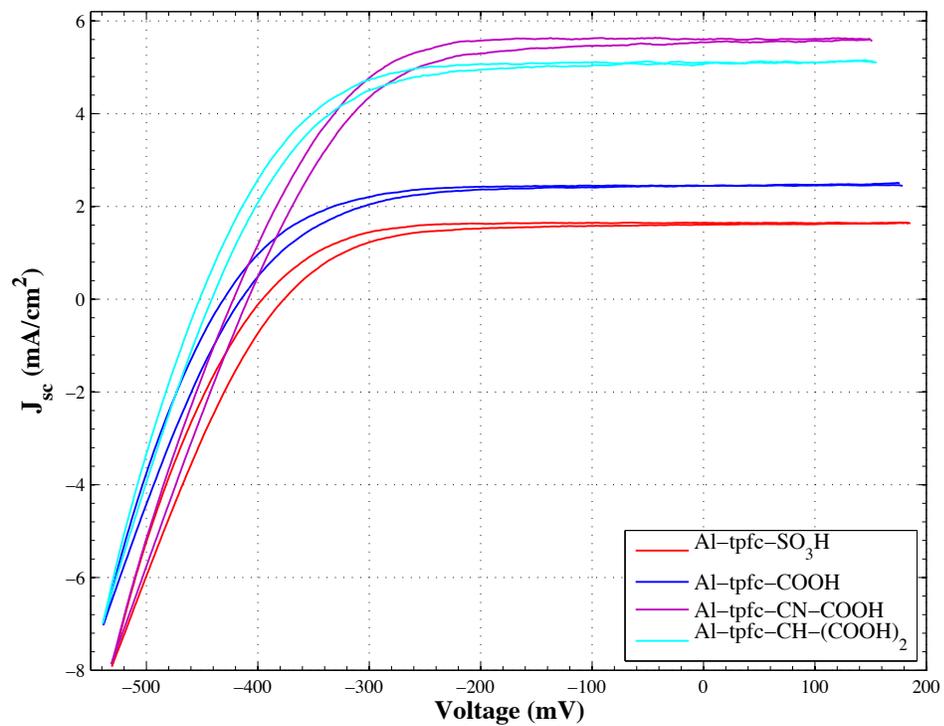
Figure 4.3. Current versus potential characteristics of aluminum corroles.

mono-CN-COOH because less Ga-tpfc-CN-(COOH)$_2$ corrole absorbed onto TiO$_2$. This decreased adsorption of Ga-tpfc-CN-(COOH)$_2$ may have been due to the fact that the addition of an extra -CN-COOH moiety sterically prohibits maximal adsorption of corrole onto TiO$_2$. When comparing the UV-Vis and estimated short circuit current of gallium corroles with their aluminum analogues, the absorption spectra and estimated currents of the aluminum corroles on TiO$_2$ are less than their gallium analogues. This was also true for the measured short circuit currents. The difference in the UV-Vis spectra and estimated short circuit currents indicates that the gallium dyes adsorb more readily to TiO$_2$. This would indicate that the effect the metal has on the macrocycle directly effects the corrole's ability to readily bind to TiO$_2$.

Spectral Response

As mentioned previously, the amount of adsorbed corrole on TiO$_2$ ultimately affects the amount of short circuit current that can be produced. The differences in measured short circuit can also be due to increased or decreased red absorption of photons. Spectral response measurements can give insight on how the corroles absorb monochromatic light at different wavelengths. By examining Figures 4.4 – 4.6, all the corroles were efficient in converting incident light to current in both their Q and Soret bands. As a reference, the EQY of N3 is approximately 70% – 80%. The highest EQY values of the corroles were near 50%. The Soret bands were slightly more efficient than the Q-bands. The free base and gallium sulfonated corroles produced comparable EQY values to their carboxylated analogues. The aluminum corroles were significantly less efficient in converting incident photons to current across all wavelengths. Al-tpfc-CH-(COOH)$_2$ was the only aluminum corrole that had external quantum yield

values near 50%. Even though the aluminum and tin corroles were not as efficient as the gallium and free base corroles, they did produce currents in both their Q and Soret bands. Also, the region between the Soret and Q-bands of the most efficient corroles produced current as well. Ga-tpfc-CH-(COOH)$_2$ converted the most incident photons to current between its Soret and Q-bands. Such a discovery indicates that the absorption spectra of the corrole between the Q and Soret bands can be adjusted so that you do not lose any current.

External quantum yield measurements give insight into the ability of the corroles to convert monochromatic incident light to current, but in order to better understand the corrole's efficiency in converting their absorbed photons to current, the EQY spectra can be normalized by the absorption spectra of the corroles. This would give an internal quantum yield (IQY) and demonstrate how efficient the corroles are at converting absorbed photons to current. By examining Figures 3.7 – 3.9, it can be seen that the corroles convert, on average, 30% - 50% of their absorbed photons to current. As a reference, N3 dye has an internal quantum yield of about 80%. The IQYs of the corroles were significantly less than that of N3 with the greatest IQY being produced was near 60%. The Ga-tpfc-(SO$_3$H)$_2$, Ga-tpfc-CH-(COOH)$_2$, and Al-tpfc-CH-(COOH)$_2$ produced the highest IQY values that were between 50% and 60%. Most of the corroles had IQY values between 30% and 40%. The Sn-tpfc-(SO$_3$H)$_2$, Ga-tpfc-COOH Al-tpfc-SO$_3$H, Al-tpfc-COOH, and Al-tpfc-CN-COOH all had IQY values that were less than 20%. The IQYs indicate that mono substitution of tpfc decreases the corrole's ability to convert its absorbed photons to current, where the addition of a malonic acid group increases IQY values. Also, sulfonic acid binding groups of the gallium corrole and free base corrole

were not detrimental to the IQY. The mono sulfonic acid substituted aluminum corrole had very low IQYs, but so did all the mono substituted corroles with the exception of those with a malonic acid group and Ga-tpfc-CN-COOH. This would indicate that mono substitution at the β-positions is deleterious to a corrole's ability to convert absorbed photons to current, but that mono β-substitution of a malonic acid can enhance IQYs. Also when comparing the IQYs of the Ga-tpfc-CN-COOH and Al-tpfc-CN-COOH corroles it can be seen that the metal has large effect on the IQY when using a –CN-COOH moiety. It is interesting to note that although all the corroles produced different short circuit currents and EQYs, all their IQYs were relatively the same. This would indicate that the differences seen in the EQYs and short circuit currents are mostly due to dye loading. Also, the measured internal quantum yields matched well to the estimated internal quantum yields indicating that the one of the reasons why the corroles don't out-perform N3 is that they are not efficient at converting their absorbed photons to current.

Conclusions

The corroles are efficient dye sensitizers for DSSCs. The corrole Ga-tpfc-CH-(COOH)$_2$ produced a remarkable efficiency of 2.24%, which approaches the efficiency of N3. Ga-tpfc-(SO$_3$H)$_2$ has proven to be the most efficient dye sensitizer with sulfonic acid groups. Also, the Ga-tpfc-(SO$_3$H)$_2$ corrole produced the highest open circuit voltage of all the corroles. When examining the EQYs of the corroles, all the corroles were efficient in their Soret and Q-bands. This indicates the addition of β-substituted, π-conjugated linkers to red shift the absorption spectra does not decrease the EQY of the corroles in the red. One can conclude that the red shifting of the corroles spectra does not decrease the efficiency of the corroles.

The IQYs were the same for all the corroles and the EQYs and short circuit currents were different. Because the IQYs were the same for all corroles and the EQYs differed for the corroles, it can be concluded that the differences in EQY and short circuit current are due to dye loading. This indicates that the gallium dyes were better able to adsorb onto TiO_2 than aluminum corroles. The reason for this is not clear, but it can be concluded the metal does have an effect on the corrole's ability to adsorb to TiO_2.

The internal quantum yield measurements also indicate that either 60% of the absorb photons are not injected or that regeneration of the oxidized corroles by the electrolyte is inefficient. Because all the IQYs are relatively equal to one another, the reason the corrole's IQYs are not as high as N3 is unanimous for all corroles. This would either mean that injection or regeneration may be due to inefficiencies of the base corrole macrocycle. Further investigation into the injection and regeneration dynamics would be needed to better understand the reason for the low IQYs. Because the N3 dye has an IQY of 80%, this indicates that almost all of its absorbed photons are converted current. The corroles only convert 40% of their absorbed photons to current indicating that there is still the possibility to increase their short circuit currents by 60%.
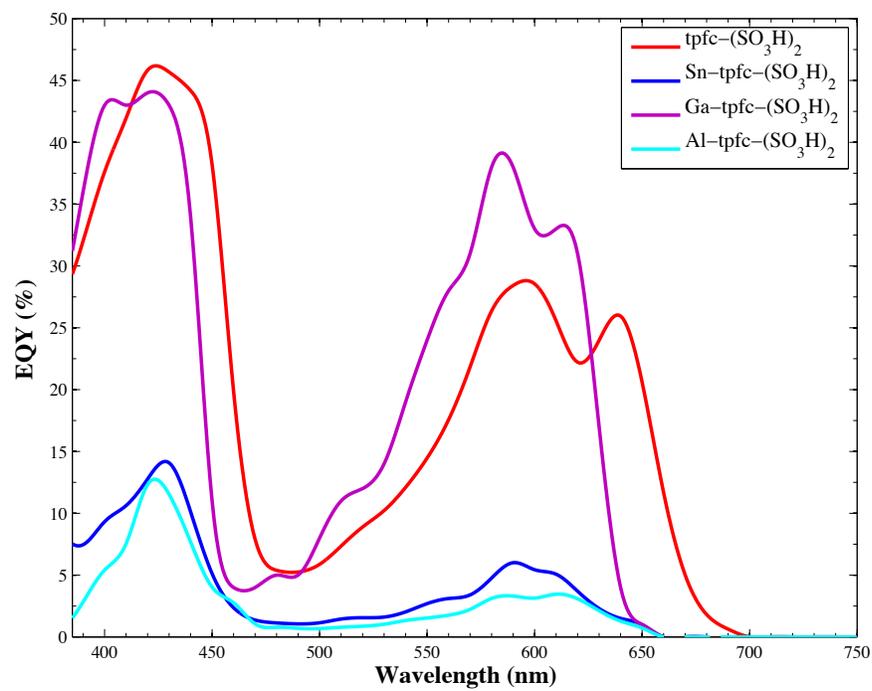
Figure 4.4.   Incident photon to current conversion efficiency of corroles containing sulfonic acid moieties.
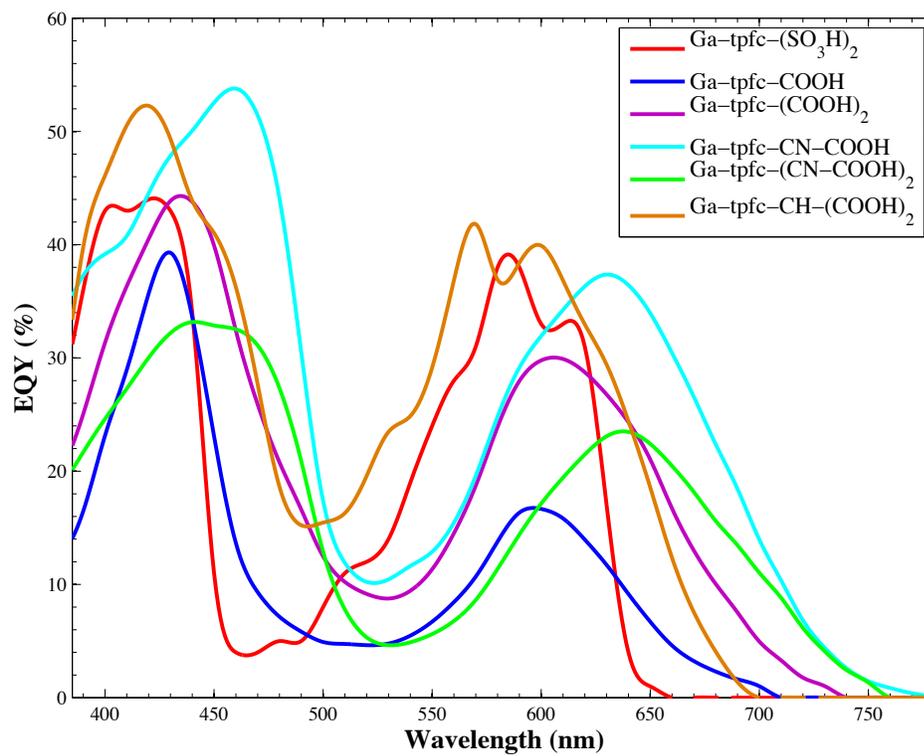
Figure 4.5. Incident photon to current conversion efficiency of gallium corroles.
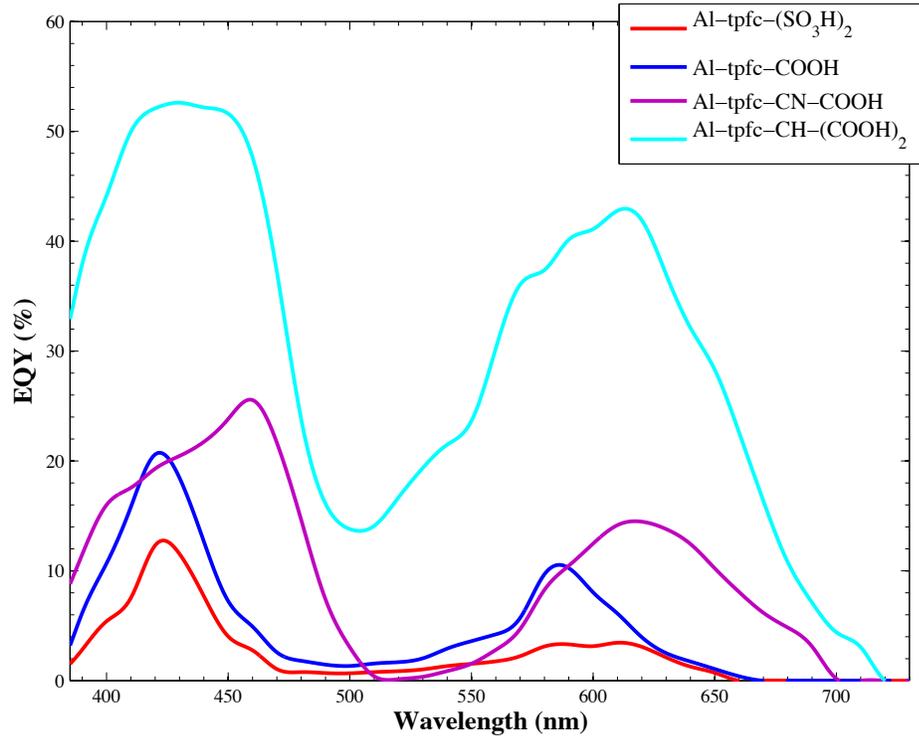
Figure 4.6. Incident photon to current conversion efficiency of aluminum corroles.
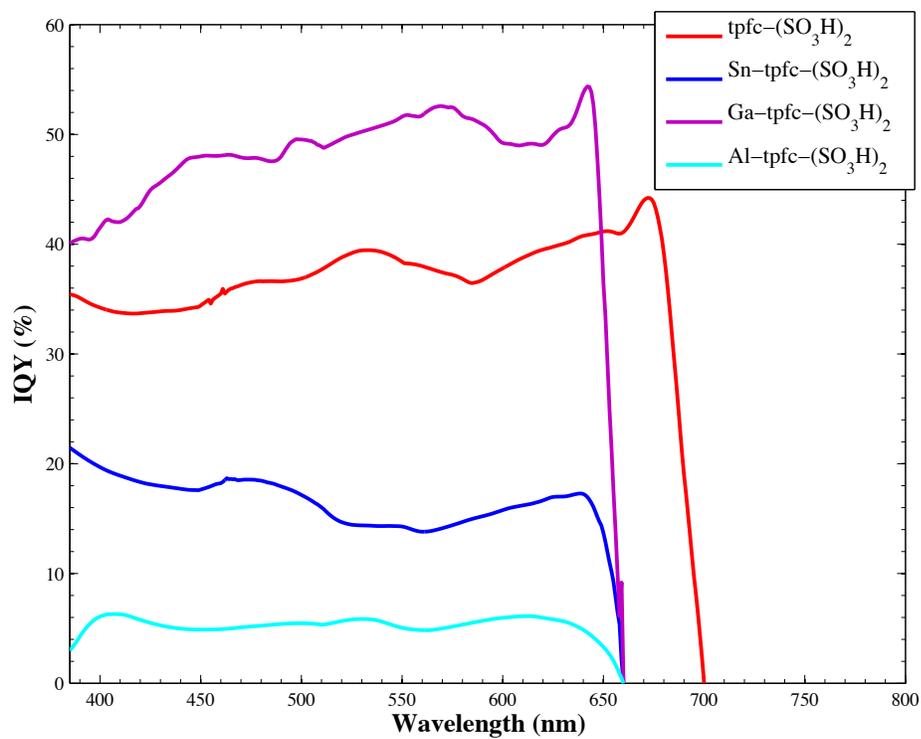
Figure 4.7. Absorbed photon to current efficient of corroles with sulphonic acid moieties.
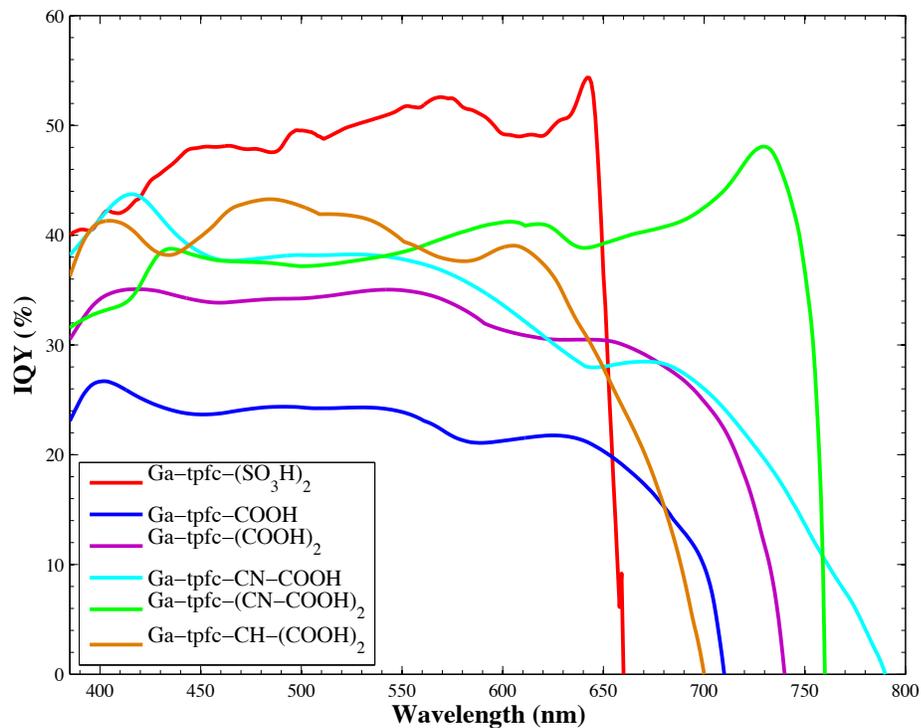
Figure 4.8. Absorbed photon to current conversion efficiency of gallium corroles.
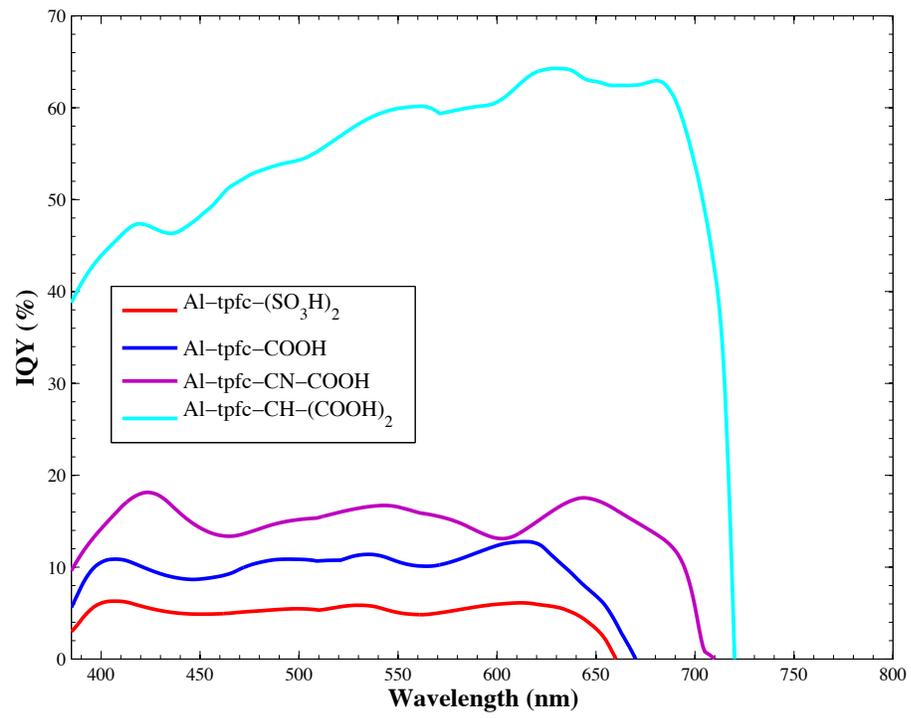
Figure 4.9. Absorbed photon to current conversion efficiency of aluminum corroles.

Chapter 5

Thesis Summary and Future Work

The work in this thesis sought to better understand and demonstrate the necessary steps needed to make solar energy as economically viable as fossil fuels. The chosen system to study was the dye sensitized solar cell. DSSCs have the potential to be cheaper than other solar cells and just as efficient. Despite having been around for over 30 years, DSSCs have only reached an efficiency of 11.2% although their theoretical maximum is near 20%. The current approach as seen in the literature is to continually try various dyes with very little understanding into what makes a good dye, a good dye. Even less investigation into the use and understanding of the redox couple has been carried. The focus of this thesis was to better understand what little is understood about DSSCs in an effort to provide the scientific community a means and direction to investigate DSSCs.

For example, this thesis and Elizabeth Mayo's thesis demonstrated that by using a bromide based electrolyte the open circuit voltage of a DSSC can be greatly increased. For some dyes the current did decrease, but could be raised by introducing more bromide. Based on the work conducted in this thesis, it may be possible to increase the currents of DSSCs with bromide electrolytes even more by using an ionic liquid containing bromide. The ionic liquid 1,2-dimethyl-3-propylimidazolium has been used in the most efficient DSSCs in concentrations greater than 0.5M in an effort to increase the currents of DSSCs.[6] Another advantage to using an ionic liquid is that the concentration of lithium cations can be controlled. In this thesis the lithium was the counter ion to the reductant, bromide. The lithium concentration was 1.0M in this thesis. High concentrations of lithium cations have been known to decrease the efficiency of a DSSC; therefore, by using an ionic liquid, the lithium concentration can be lowered to more optimum levels. You get the best of both worlds. Chapter 2 has given precedence that increasing the

bromide concentration can increase the current of DSSCs with bromide electrolytes; therefore, the next step would be to use a bromide ionic liquid to increase the current and optimize the lithium concentration to maximize DSSC performance.

In Chapters 3 and 4 the efficacy of corrole dyes as efficient light absorbers for DSSCs was investigated. Precedence in the literature has demonstrated that some of the most promising class of molecules to use as light absorbers in DSSCs are porphyrins. Also, β-substitution of porphyrins with electron withdrawing groups have proven to increase the efficiency and spectral overlap of porphyrins. Because corroles are so similar to porphyrins it is expected that they should perform as well as similar pophyrins. The most efficient porphyrins have been based upon zinc porphyrins. Corroles offer a unique system to study, with metals such as gallium and aluminum. The work in this thesis demonstrated that corroles are indeed efficient light absorbers for DSSCs. The corrole Ga-tpfc-CH-(COOH)$_2$ almost approached the efficient of N3. Ga-tpfc-(SO$_3$H)$_2$, to this author's knowledge, has been demonstrated to be the most efficient dye with sulfonic acid groups for DSSCs.

Two of the primary reasons why the corroles worked so well were because of their ground state redox potentials being similar to N3 and also their spectral overlap. The corroles all had similar electrochemical HOMO levels, despite having a variety of functional groups. When changes to the binding group of inorganic polypyridyl compounds are made, large changes in the ground state redox potential are subsequently changed. This makes it difficult to tune the spectral properties of inorganic polypyridyl dyes. The spectral properties of corroles could be tuned by the addition of a variety of β-substituents without effecting the ground state redox properties.

The spectral overlap of the corroles were tuned through using several different binding groups and π-conjugated linkers. The spectra of corroles red shifted depending on the strength of electron withdrawing nature of the β-substituent. This increased red shift was carried into the performance of the solar cells as can be seen in the IQY data. The most profound conclusion of Chapter 4 is that corroles can be improved. Their IQY data indicated that the corroles are only converting approximately half of their absorbed photons to current. From the Chapter 4 it was concluded that two best β-substituents are the malonic acid moiety and sulfonic acid group. One can conclude the next dye to synthesize would be a β-substituted (Ga/Al)-tpfc-CH-$(SO_3H)_2$. The sulfonic acids would provide an efficient bridge to transfer electrons between the dye and TiO_2, possibly increase the open circuit voltage, and the π-conjugated linker would increase the spectral overlap and increase the EQY of the region between the Soret and Q-bands. Chapter 3 and 4 have set the precedence to investigate dyes with binding groups other than carboxylic acid groups. One interesting study to carry out would be to measure the electron injection and recombination rate of the carboxylated corroles with the sulfonated corroles. The determination of the injection and recombination rates could give insight into the effect the binding group has on the electron transfer. To this author's knowledge there has been no investigation into the effect of the binding group on the injection and recombination. Prior to the work in this thesis such a study would not have been feasible. As mentioned before, changing binding groups greatly affects the redox potential of the molecule, but in the case of the corroles the redox potentials remain relatively constant between the sulfonated corroles and their carboxylated analogues. The sulfonated and

carboxylated corroles provide a unique scaffold to better understand the effect the binding group has on electron injection and recombination in DSSCs.

Chapter 4 primarily focused on determining whether or not the corroles could possibly be efficient sensitizers for DSSCs. They were not optimized to maximize efficiency. It is possible to increase the efficiency of corrole DSSCs by using thicker films of TiO_2 to increase the amount of dye adsorbed. Also, a layer TiO_2 nanoparticles with diameters greater than 300nm could be used to scatter any light that was not absorbed back into the DSSC. Instead of using the custom three-electrode photoelectrochemical cell used in this study, a thin solar cell could be constructed with a "mirror like" platinum as the counter electron. The "mirror like" platinum counter electrode would reflect any light that was not scattered by the TiO_2 scattering layer back into the dye coated TiO_2 electrode. Although, the construction of such a cell would lead to greater efficiencies, they still would perform as well as the best dyes for DSSCs. This is because they have lower IQYs. More work must be conducted to optimize the IQYs of the corroles. As can be seen in Chapter 4, possibly using sulfonic acid groups in conjunction with π-conjugated linkers could increase IQYs.

The main goal of this thesis was to lend precedence to pursuing research pathways that could reduce the cost of solar energy. By investigating DSSCs, I hoped to find some potential pathways to improve DSSCs to perform better. I hope my investigation into DSSCs provides a starting point to greatly improve solar technology. The conclusions in this thesis, hopefully, have placed one more brick in the path to better performing DSSCs and ultimately provide energy for the world.

Bibliography

1.   Goldemberg, J.; Johansson, T. B., Eds. World Energy Assessment:; Overview 2004 Update 1992, U. N. D. P., 2004., 2004.

2.   Klein, J., Comparative Costs of California Central Station Electricity Generation Technologies. Commission, C. E., Ed. 2009.

3.   BP Statistical Review of World Energy June 2009. (accessed July 26, 2010).

4.   Zhao, J. H.; Wang, A. H.; Green, M. A.; Ferrazza, F., *Appl. Phys. Lett.* 1998, *73* (14), 1991-1993.

5.   King, R. R.; Law, D. C.; Edmondson, K. M.; Fetzer, C. M.; Kinsey, G. S.; Yoon, H.; Sherif, R. A.; Karam, N. H., *Appl. Phys. Lett.* 2007, *90* (18).

6.   Chiba, Y.; Islam, A.; Watanabe, Y.; Komiya, R.; Koide, N.; Han, L. Y., *Jpn. J. Appl. Phys. Part 2 - Lett. Express Lett.* 2006, *45* (24-28), L638-L640.

7.   Shockley, W.; Queisser, H. J., *J. Appl. Phys.* 1961, *32* (3), 510.

8.   Ross, R. T.; Nozik, A. J., *J. Appl. Phys.* 1982, *53* (5), 3813-3818.

9.   Hiskia, A.; Mylonas, A.; Papaconstantinou, E., *Chemical Society Reviews* 2001, *30* (1), 62-69.

10.   Nozik, A. J., *Annual Review of Physical Chemistry* 1978, *29*, 189-222.

11.   Nazeeruddin, M. K.; Kay, A.; Rodicio, I.; Humphrybaker, R.; Muller, E.; Liska, P.; Vlachopoulos, N.; Grätzel, M., *Journal of the American Chemical Society* 1993, *115* (14), 6382-6390.

12.   Nazeeruddin, M. K.; Pechy, P.; Renouard, T.; Zakeeruddin, S. M.; Humphry-Baker, R.; Comte, P.; Liska, P.; Cevey, L.; Costa, E.; Shklover, V.; Spiccia, L.; Deacon, G. B.; Bignozzi, C. A.; Grätzel, M., *Journal of the American Chemical Society* 2001, *123*, 1613-1624.

13. Nazeeruddin, M. K.; Zakeeruddin, S. M.; Lagref, J. J.; Liska, P.; Comte, P.; Barolo, C.; Viscardi, G.; Schenk, K.; Grätzel, M., *Coordination Chemistry Reviews* 2004, *248* (13-14), 1317-1328.

14. Ma, T. L.; Inoue, K.; Yao, K.; Noma, H.; Shuji, T.; Abe, E.; Yu, J. H.; Wang, X. S.; Zhang, B. W., *J. Electroanal. Chem.* 2002, *537* (1-2), 31-38.

15. Koehorst, R. B. M.; Boschloo, G. K.; Savenije, T. J.; Goossens, A.; Schaafsma, T. J., *Journal of Physical Chemistry B* 2000, *104* (10), 2371-2377.

16. Kalyanasundaram, K.; Vlachopoulos, N.; Krishnan, V.; Monnier, A.; Grätzel, M., *J. Phys. Chem.* 1987, *91* (9), 2342-2347.

17. Hara, K.; Kurashige, M.; Dan-oh, Y.; Kasada, C.; Shinpo, A.; Suga, S.; Sayama, K.; Arakawa, H., *New J. Chem.* 2003, *27* (5), 783-785.

18. Dabestani, R.; Bard, A. J.; Campion, A.; Fox, M. A.; Mallouk, T. E.; Webber, S. E.; White, J. M., *J. Phys. Chem.* 1988, *92* (7), 1872-1878.

19. Mayo, E. I.; Kilsa, K.; Tirrell, T.; Djurovich, P. I.; Tamayo, A.; Thompson, M. E.; Lewis, N. S.; Gray, H. B., *Photochemical & Photobiological Sciences* 2006, *5* (10), 871-873.

20. Sauve, G.; Cass, M. E.; Coia, G.; Doig, S. J.; Lauermann, I.; Pomykal, K. E.; Lewis, N. S., *Journal of Physical Chemistry B* 2000, *104* (29), 6821-6836.

21. Galoppini, E., *Coordination Chemistry Reviews* 2004, *248* (13-14), 1283-1297.

22. Schwarz, O.; van Loyen, D.; Jockusch, S.; Turro, N. J.; Durr, H., *J. Photochem. Photobiol. A-Chem.* 2000, *132* (1-2), 91-98.

23.   Pechy, P.; Rotzinger, F. P.; Nazeeruddin, M. K.; Kohle, O.; Zakeeruddin, S. M.; Humphrybaker, R.; Grätzel, M., *Journal of the Chemical Society-Chemical Communications* 1995, (10), 1093-1093.

24.   Asbury, J. B.; Ellingson, R. J.; Ghosh, H. N.; Ferrere, S.; Nozik, A. J.; Lian, T. Q., *Journal of Physical Chemistry B* 1999, *103* (16), 3110-3119.

25.   Hannappel, T.; Burfeindt, B.; Storck, W.; Willig, F., *Journal of Physical Chemistry B* 1997, *101* (35), 6799-6802.

26.   Tachibana, Y.; Moser, J. E.; Grätzel, M.; Klug, D. R.; Durrant, J. R., *Journal of Physical Chemistry* 1996, *100* (51), 20056-20062.

27.   Fitzmaurice, D. J.; Frei, H., *Langmuir* 1991, *7* (6), 1129-1137.

28.   Alebbi, M.; Bignozzi, C. A.; Heimer, T. A.; Hasselmann, G. M.; Meyer, G. J., *The Journal of Physical Chemistry B* 1998, *102* (39), 7577-7581.

29.   Haque, S. A.; Tachibana, Y.; Klug, D. R.; Durrant, J. R., *The Journal of Physical Chemistry B* 1998, *102* (10), 1745-1749.

30.   Heimer, T. A.; Heilweil, E. J.; Bignozzi, C. A.; Meyer, G. J., *The Journal of Physical Chemistry A* 2000, *104* (18), 4256-4262.

31.   Green, A. N. M.; Chandler, R. E.; Haque, S. A.; Nelson, J.; Durrant, J. R., *The Journal of Physical Chemistry B* 2004, *109* (1), 142-150.

32.   Hagfeldt, A.; Grätzel, M., *Accounts of Chemical Research* 2000, *33* (5), 269-277.

33.   Pichot, F.; Gregg, B. A., *The Journal of Physical Chemistry B* 1999, *104* (1), 6-10.

34.   Fujishima, A.; Honda, K., *Nature* 1972, *238* (5358), 37.

35.   Finklea, H. O., *Semiconductor Electrodes*. Elsevier: New York: 1988.

36. Bolts, J. M.; Wrighton, M. S., *The Journal of Physical Chemistry* 1976, *80* (24), 2641-2645.

37. Hara, K.; Dan-oh, Y.; Kasada, C.; Ohga, Y.; Shinpo, A.; Suga, S.; Sayama, K.; Arakawa, H., *Langmuir* 2004, *20* (10), 4205-4210.

38. Schlichthorl, G.; Huang, S. Y.; Sprague, J.; Frank, A. J., *The Journal of Physical Chemistry B* 1997, *101* (41), 8141-8155.

39. Kusama, H.; Kurashige, M.; Arakawa, H., *J. Photochem. Photobiol. A-Chem.* 2005, *169* (2), 169-176.

40. Oskam, G.; Bergeron, B. V.; Meyer, G. J.; Searson, P. C., *Journal of Physical Chemistry B* 2001, *105* (29), 6867-6873.

41. Gregg, B. A.; Pichot, F.; Ferrere, S.; Fields, C. L., *Journal of Physical Chemistry B* 2001, *105* (7), 1422-1429.

42. Tennakone, K.; Senadeera, G. K. R.; De Silva, D.; Kottegoda, I. R. M., *Appl. Phys. Lett.* 2000, *77* (15), 2367-2369.

43. Tennakone, K.; Kumara, G.; Wijayantha, K. G. U.; Kottegoda, I. R. M.; Perera, V. P. S.; Aponsu, G., *J. Photochem. Photobiol. A-Chem.* 1997, *108* (2-3), 175-177.

44. Bach, U.; Lupo, D.; Comte, P.; Moser, J. E.; Weissortel, F.; Salbeck, J.; Spreitzer, H.; Grätzel, M., *Nature* 1998, *395* (6702), 583-585.

45. Kruger, J.; Plass, R.; Cevey, L.; Piccirelli, M.; Grätzel, M.; Bach, U., *Appl. Phys. Lett.* 2001, *79* (13), 2085-2087.

46. Konno, A.; Kumara, G. R. A.; Hata, R.; Tennakone, K., *Electrochemistry* 2002, *70* (6), 432-434.

47.   Kumara, G.; Konno, A.; Senadeera, G. K. R.; Jayaweera, P. V. V.; De Silva, D.; Tennakone, K., *Sol. Energy Mater. Sol. Cells* 2001, *69* (2), 195-199.

48.   Cameron, P. J.; Peter, L. M.; Zakeeruddin, S. M.; Grätzel, M., *Coordination Chemistry Reviews* 2004, *248* (13-14), 1447-1453.

49.   Wang, M.; Chamberland, N.; Breau, L.; Moser, J.-E.; Humphry-Baker, R.; Marsan, B.; Zakeeruddin, S. M.; Grätzel, M., *Nat Chem* 2010, *2* (5), 385-389.

50.   Sapp, S. A.; Elliott, C. M.; Contado, C.; Caramori, S.; Bignozzi, C. A., *Journal of the American Chemical Society* 2002, *124* (37), 11215-11222.

51.   Fisher, A. C.; Peter, L. M.; Ponomarev, E. A.; Walker, A. B.; Wijayantha, K. G. U., *The Journal of Physical Chemistry B* 2000, *104* (5), 949-958.

52.   Nelson, I. V.; Iwamoto, R. T., *J. Electroanal. Chem.* 1964, *7* (3), 218-221.

53.   Wang, Z. S.; Sayama, K.; Sugihara, H., *Journal of Physical Chemistry B* 2005, *109* (47), 22449-22455.

54.   Mayo, E. I. Kinetics and Thermodynamics of Dye (Group Viii Metal)-Sensitized Nanocrystalline Titanium Dioxide Photoelectrodes. California Institute of Technology, Pasadena, 2004.

55.   Sauve, G. Dye Sensitization of Nanocrystalline Titanium Dioxide with Osmium and Ruthenium Polypyridine Complexes. California Institute of Technology, Pasadena, 1999.

56.   Pelet, S.; Moser, J. E.; Grätzel, M., *The Journal of Physical Chemistry B* 2000, *104* (8), 1791-1795.

57.   Boschloo, G.; Hagfeldt, A., *Accounts of Chemical Research* 2009, *42* (11), 1819-1826.

58. Wang, Z.-S.; Kawauchi, H.; Kashima, T.; Arakawa, H., *Coordination Chemistry Reviews* 2004, *248* (13-14), 1381-1389.

59. Benkö, G.; Skårman, B.; Wallenberg, R.; Hagfeldt, A.; Sundström, V.; Yartsev, A. P., *The Journal of Physical Chemistry B* 2003, *107* (6), 1370-1375.

60. Nakade, S.; Saito, Y.; Kubo, W.; Kitamura, T.; Wada, Y.; Yanagida, S., *The Journal of Physical Chemistry B* 2003, *107* (33), 8607-8611.

61. Sodergren, S.; Siegbahn, H.; Rensmo, H.; Lindstrom, H.; Hagfeldt, A.; Lindquist, S. E., *The Journal of Physical Chemistry B* 1997, *101* (16), 3087-3090.

62. Kelly, C. A.; Farzad, F.; Thompson, D. W.; Stipkala, J. M.; Meyer, G. J., *Langmuir* 1999, *15* (20), 7047-7054.

63. Redmond, G.; Fitzmaurice, D., *The Journal of Physical Chemistry* 1993, *97* (7), 1426-1430.

64. Clifford, J. N.; Palomares, E.; Nazeeruddin, M. K.; Grätzel, M.; Durrant, J. R., *The Journal of Physical Chemistry C* 2007, *111* (17), 6561-6567.

65. Privalov, T.; Boschloo, G.; Hagfeldt, A.; Svensson, P. H.; Kloo, L., *The Journal of Physical Chemistry C* 2008, *113* (2), 783-790.

66. Oregan, B.; Grätzel, M., *Nature* 1991, *353* (6346), 737-740.

67. Ma, T.; Inoue, K.; Noma, H.; Yao, K.; Abe, E., *Journal of Materials Science Letters* 2002, *21* (13), 1013-1014.

68. Kalyanasundaram, K.; Vlachopoulos, N.; Krishnan, V.; Monnier, A.; Grätzel, M., *The Journal of Physical Chemistry* 1987, *91* (9), 2342-2347.

69. Dabestani, R.; Bard, A. J.; Campion, A.; Fox, M. A.; Mallouk, T. E.; Webber, S. E.; White, J. M., *The Journal of Physical Chemistry* 1988, *92* (7), 1872-1878.

70. Odobel, F.; Blart, E.; Lagree, M.; Villieras, M.; Boujtita, H.; El Murr, N.; Caramori, S.; Alberto Bignozzi, C., *Journal of Materials Chemistry* 2003, *13* (3), 502-510.

71. Ma, T. L.; Inoue, K.; Noma, H.; Yao, K.; Abe, E., *J. Photochem. Photobiol. A-Chem.* 2002, *152* (1-3), 207-212.

72. Campbell, W. M.; Jolley, K. W.; Wagner, P.; Wagner, K.; Walsh, P. J.; Gordon, K. C.; Schmidt-Mende, L.; Nazeeruddin, M. K.; Wang, Q.; Grätzel, M.; Officer, D. L., *The Journal of Physical Chemistry C* 2007, *111* (32), 11760-11762.

73. Boschloo, G. K.; Goossens, A., *The Journal of Physical Chemistry* 1996, *100* (50), 19489-19494.

74. Cherian, S.; Wamser, C. C., *The Journal of Physical Chemistry B* 2000, *104* (15), 3624-3629.

75. Viseu, T. M. R.; Hungerford, G.; Ferreira, M. I. C., *The Journal of Physical Chemistry B* 2002, *106* (8), 1853-1861.

76. Gouterman, M., *The Porphyrins*. Academic Press: New York, 1978; Vol. III, p.1.

77. Sen, A.; Krishnan, V., *Tetrahedron Letters* 1996, *37* (46), 8437-8438.

78. Chen, C. T.; Yeh, H. C.; Zhang, X. Q.; Yu, J. W., *Organic Letters* 1999, *1* (11), 1767-1770.

79. Wang, Q.; Campbell, W. M.; Bonfantani, E. E.; Jolley, K. W.; Officer, D. L.; Walsh, P. J.; Gordon, K.; Humphry-Baker, R.; Nazeeruddin, M. K.; Grätzel, M., *The Journal of Physical Chemistry B* 2005, *109* (32), 15397-15409.

80. Gouterman, M., *Journal of Chemical Physics* 1959, *30* (5), 1139-1161.

81. Campbell, W. M.; Burrell, A. K.; Officer, D. L.; Jolley, K. W., *Coordination Chemistry Reviews* 2004, *248* (13-14), 1363-1379.

82. Wang, Q.; Carnpbell, W.; Bonfantani, E.; Jolley, K.; Officer, D.; Walsh, P., *The Journal of physical chemistry. B* 2005, *109* (32), 15397-15409.

83. Bendix, J.; Dmochowski, I. J.; Gray, H. B.; Mahammed, A.; Simkhovich, L.; Gross, Z., *Angewandte Chemie-International Edition* 2000, *39* (22), 4048-4051.

84. Johnson, A. W.; Kay, I. T., *Journal of the Chemical Society* 1965, (MAR), 1620-

85. Paolesse, R.; Jaquinod, L.; Nurco, D. J.; Mini, S.; Sagone, F.; Boschi, T.; Smith, K. M., *Chemical Communications* 1999, (14), 1307-1308.

86. Gross, Z.; Galili, N.; Saltsman, I., *Angewandte Chemie-International Edition* 1999, *38* (10), 1427-1429.

87. Aviv, I.; Gross, Z., *Chemical Communications* 2007, (20), 1987-1999.

88. Saltsman, I.; Mahammed, A.; Goldberg, I.; Tkachenko, E.; Botoshansky, M.; Gross, Z., *Journal of the American Chemical Society* 2002, *124* (25), 7411-7420.

89. Sorasaenee, K.; Taqavi, P.; Henling, L. M.; Gray, H. B.; Tkachenko, E.; Mahammed, A.; Gross, Z., *Journal of Porphyrins and Phthalocyanines* 2007, *11* (3-4), 189-197.

90. Gross, Z.; Mahammed, A., *Journal of Porphyrins and Phthalocyanines* 2002, *6* (9-10), 553-555.

91. Weaver, J. J. Corroles. California Institute of Technology, Pasadena, 2005.

92. Kilsa, K.; Mayo, E. I.; Brunschwig, B. S.; Gray, H. B.; Lewis, N. S.; Winkler, J. R., *Journal of Physical Chemistry B* 2004, *108* (40), 15640-15651.

93. Duffy, N. W.; Dobson, K. D.; Gordon, K. C.; Robinson, B. H.; McQuillan, A. J., *Chemical Physics Letters* 1997, *266* (5-6), 451-455.

94. Finnie, K. S.; Bartlett, J. R.; Woolfrey, J. L., *Langmuir* 1998, *14* (10), 2744-2749.

95. Khoudiakov, M.; Parise, A. R.; Brunschwig, B. S., *Journal of the American Chemical Society* 2003, *125* (15), 4637-4642.

96. Ou, Z. P.; Erben, C.; Autret, M.; Will, S.; Rosen, D.; Lex, J.; Vogel, E.; Kadish, K. M., *Journal of Porphyrins and Phthalocyanines* 2005, *9* (6), 398-412.

97. Kadish, K. M.; Will, S.; Adamian, V. A.; Walther, B.; Erben, C.; Ou, Z. P.; Guo, N.; Vogel, E., *Inorganic Chemistry* 1998, *37* (18), 4573-4577.

98. Kadish, K. M., *Progress in Inorganic Chemistry* 1986, *34*, 435-605.

99. Walker, D.; Chappel, S.; Mahammed, A.; Brunschwig, B. S.; Winkler, J. R.; Gray, H. B.; Zaban, A.; Gross, Z., *Journal of Porphyrins and Phthalocyanines* 2006, *10* (11), 1259-1262.

100. Simkhovich, L.; Mahammed, A.; Goldberg, I.; Gross, Z., *Chemistry-a European Journal* 2001, *7* (5), 1041-1055.